



TECHNISCHE
UNIVERSITÄT
WIEN
Vienna | Austria

MASTER THESIS

Ash Chemistry Characterization after DFB Steam Gasification of Waste Feedstock Mixtures Using Quartz, Olivine & Lime Bed Materials

Carried out for the purpose of obtaining the degree of Master of Science (MSc), submitted at
TU Wien, Faculty of Mechanical and Industrial Engineering, by

Thomas Karl HANNL

Mat.Nr.: 01226201
Blindengasse 46A/5
1080 Vienna
Austria

under the supervision of

Univ. Prof. Dipl.-Ing. Dr. techn. Hermann Hofbauer

and co-supervision of

Dipl.-Ing. Katharina Wagner

Institute of Chemical, Environmental and Bioscience Engineering

Vienna, April 2018

Abstract

Knowing about the replacement necessity of fossil fuels as primary energy resource, fluidized bed combustion and gasification of biomass and anthropogenic waste feedstock have the potential to play a major role for the pursuit of this aim. The technology focuses on high thermal energy outputs (combustion) and optimal product gas yields (gasification). The bed material in fluidized bed systems, mainly used for the purpose of heat transfer and catalytic activity, has been found to interact with feedstock-derived ash. The phenomena observed and documented in literature vary from beneficial, catalytically active layer formation to disadvantageous agglomeration and defluidization. The occurrences of layer formation and agglomeration phenomena have been demonstrated to be mainly dependent on the ash composition in conjunction with bed material type.

The objective of this work was the characterization of these layer formation and agglomeration processes during dual fluidized bed (DFB) steam gasification. In addition a bench-scale fluidized bed combustion (FBC) system was evaluated regarding its application as test rig for the analysis of interaction between bed material and ash.

The investigated feedstocks are mainly considered waste fraction of anthropogenic use and agrarian residuals. The used feedstocks are municipal waste fraction, shredder light fraction, sugar cane bagasse, exhausted olive pomace, rice husks, and hazelnut shells. German lignite was used as feedstock additive. For benchmark and run-up operation, softwood was used. For applicability evaluation of the bench-scale fluidized bed combustion system, coniferous bark was used as feedstock.

The bed material types in the DFB steam gasification operation included two different types of lime, a coarse and a fine fraction of olivine, and quartz. For the majority of DFB experiments a mixture of lime with either quartz or olivine was used. For the applicability evaluation of the bench-scale FBC system K-feldspar was applied. It proved to be a valuable test rig for the investigation of layer formation and agglomeration processes. Nevertheless, the necessity for adjustments in the feeding system and flue gas cleaning was detected.

SEM and EDS analysis of different samples extracted after the processes was conducted. By means of analytical tools such as line scans and element mappings, phenomena previously mentioned in corresponding literature were detected and indicators for new phenomena are obtained. Some of the newly discovered phenomena require adjusted and focussed research.

Layer formation tendency of quartz and olivine (but not lime) could be detected and compared with previous research data. The composition of quartz and olivine layers as well as the absence of alkali elements in near-surface areas of olivine are in accordance with literature data. Dominance of Si, Ca, and K in quartz particle layers and Si, Ca, and Mg in olivine particle layers was measured and quantified. The influence of SER processes on layer formation and layer stability was insufficiently detected. Agglomeration mechanisms during DFB steam gasification for quartz and olivine (but not lime) particles have been detected. The dependence of agglomeration tendencies on the produced ash fraction was detected clearly. Operation failure due to alkali-rich ash fraction, which initiated agglomeration, was investigated and driving forces determined. The ash interaction mechanisms dependent on the type of bed material have been found to be different for quartz and olivine.

Neither layer formation nor agglomeration tendency could be detected quantitatively for lime bed materials. Analysis results in conjunction with ash composition data indicates, that lime bed material attrition increases the potential of Ca to interact with other bed material types.

Kurzfassung

Im Bezug auf die Notwendigkeit fossile Brennstoffe als primäre Energiequelle zu ersetzen haben die Wirbelschichtverbrennung und -vergasung von biogenen und anthropogenen Abfallbrennstoffen das Potential eine wichtige Rolle zu spielen. Die Technologie ist fokussiert auf hohe thermische Leistungen (Verbrennung) und maximale Produktgasausbeute (Vergasung). Für das Bettmaterial in Wirbelschichtsystemen, welches hauptsächlich für den Wärmetransport und wegen katalytischer Effekte verwendet wird, wurden Interaktionsmechanismen mit der Asche des Brennstoffes festgestellt. Die entdeckten Phänomene reichen von vorteilhaften, weil katalytisch wirksamen, Schichtbildungen hin zu unvorteilhaften Agglomerations- und Defluidisierungsprozessen. Die Schichtbildungs- und Agglomerationsprozesse waren dabei im Wesentlichen von der Aschezusammensetzung und dem Bettmaterial abhängig.

Ziel dieser Arbeit war die Charakterisierung dieser Schichtbildungs- und Agglomerationsprozesse während der Zweitbett-Wirbelschichtvergasung mit Dampf. Außerdem wurde ein Wirbelschichtverbrennungsreaktor im Labormaßstab in Bezug auf die Anwendbarkeit als Teststand für die Analyse von Wechselwirkungen zwischen Bettmaterial und Asche untersucht.

Die untersuchten Brennstoffe sind größtenteils dem anthropogenen Müll und Reststoffen aus der Agrarindustrie zuzuordnen. Das sind Hausmüllfraktion, Schredder-Leichtfraktion, Zuckerrohrbagasse, Olivenpressrückstände, Reisschalen und Haselnusschalen. Für den Blindlauf und das Anfahren im Reaktor wurde Weichholz verwendet. Für Brennstoffmischungen wurde deutsche Braunkohle verwendet. Für die Anwendbarkeitsstudie des Wirbelschichtverbrennungsreaktors im Labormaßstab wurde Nadelholzrinde als Brennstoff verwendet.

Die verwendeten Bettmaterialien in der Zweitbett-Wirbelschichtvergasung umfassten zwei unterschiedlichen Typen von Kalk (KSW & KS01), eine Grob- und eine Feinfraktion an Olivin, und Quarzsand. Die Mehrheit der Experimente verwendete Mischungen von Kalk mit entweder Quarz oder Olivin. Für die Anwendbarkeitsstudie des Wirbelschichtverbrennungsreaktors im Labormaßstab wurde Kaliumfeldspat verwendet. Der Reaktor erwies sich als nützliches Instrument für die Untersuchung von Schichtbildung und Agglomerationsprozessen. Zusätzlich müssen jedoch die Brennstoffzufuhr sowie die Abgasreinigung adaptiert werden.

Analysen via SEM und EDS der verschiedenen Bettmaterialproben wurden durchgeführt. Die Analyse mittels Linienprofilen und Elementmappings detektierte Phänomene, welche bereits in der einschlägigen Literatur beschrieben wurden. Außerdem wurden Indikatoren für neue Phänomene entdeckt, welche durch angepasste Experimente genauer untersucht werden müssen.

Schichtbildung und Agglomeration von Quarz und Olivin wurden analysiert und verglichen. Die Zusammensetzung der Schichten ebenso wie die Absenz von Alkalielenenten in oberflächennahen Schichten am Olivin deckt sich mit der einschlägigen Literatur. Dominanz von Si, Ca, und K in Quarzpartikelschichten sowie Si, Ca, und Mg in Olivinpartikelschichten wurde gemessen und quantifiziert. Der Einfluss von chemischen Kreislaufprozessen auf Schichtbildung und Schichtstabilität wurde nur unzureichend detektiert. Agglomerationsmechanismen während der Zweitbett-Wirbelschichtvergasung wurden für Quarz und Olivin nachgewiesen. Die Abhängigkeit der Agglomerationstendenz von der produzierten Aschefraktion konnte klar festgestellt werden. Agglomeration, welche von alkalireichen Aschefraktionen initiiert wurde, und daraus folgende Defluidisierung und Betriebsversagen wurden untersucht und Triebkräfte bestimmt. Die unterschiedlichen Interaktionsmechanismen zwischen Asche und Quarz einerseits und Asche und Olivin andererseits konnten detektiert werden.

Für Kalkbettmaterial wurden weder Schichtbildungs- noch Agglomerationstendenzen quantitativ festgestellt. Die Analysenergebnisse in Verbindung mit der Aschezusammensetzung deutete jedoch darauf hin, dass das Ca-Potential für die Interaktion mit anderen Bettmaterialien durch Kalkabrieb erhöht wird.

Acknowledgement

This work is devoted to all those people, who made its making possible.

First I want to thank Prof. Hofbauer for getting me in contact with the topic of fluidized bed systems. When I had no idea in which field of activity I want to express my interest for natural science, he presented me his area of expertise and inspired me. I remember when he took additional time after an personal exam in his office to explain the circumstances of research he is conducting. This thesis is my way to thank him for his encouragement.

Special thanks I owe to my initial supervisor Matthias Kuba. He answered all my initial questions and dispelled my every doubt. In the early stage of my work he was so positive about my work, that he already thought about long term plans and presented incredible opportunities to me. I hope to fulfil those hopes he pinned on me partially with this work and in the years to come.

Very personal thanks I want to send to my main supervisor Katharina Wagner. At every stage of my work she was there to support me and overcome all troubles which came along the way. Her dedication and ingenuity was the key, which lead to the accomplishment of this thesis. I want to thank her especially for the time she took to help me evaluating the results and for the repeated proofreading of this thesis.

Additionally I want to thank the operating team of the gasification group at TU Wien, especially Florian Benedikt, and the contact person at the test laboratory for combustion systems, Sebastian Diem. With every request about the practical part of this thesis I could come to them.

My colleague and around-the-clock working partner Andrea I want to thank in this way as well as I did in direct way many times. Our cooperation and teamwork through the last few months was most prolific and I hope I could contribute as much to her work as she contributed to mine.

Last but definitely not least I want to thank my girlfriend Neea. Although my work compromised our spare time and I was complaining too often about it she always kept my head up and stayed positive. Her way of supporting me was amazing.

Affidavit

I declare in lieu of oath, that I wrote this thesis and performed the associated research myself, using only literature cited in this volume. If text passages from sources are used literally, they are marked as such.

I confirm that this work is original and has not been submitted elsewhere for any examination, nor is it currently under consideration for a thesis elsewhere.

I confirm, that going to press of this thesis needs the confirmation of the examination committee.

Signature: _____

Vienna, April 2018

Contents

1	Introduction	1
2	Background	2
2.1	Fuel Types & Composition	3
2.2	Applied Technologies (Combustion/Gasification)	6
2.2.1	Combustion	6
2.2.2	Gasification	7
2.2.3	Thermochemical Conversion Reactor Systems	8
2.3	Ash Composition	9
2.4	Bed Material Type and Composition	13
2.4.1	Composition and Structure	13
2.4.2	Particle Size & Form Factor	17
2.5	Agglomeration and Layer-Forming Processes	17
2.5.1	Ash Transformation Chemistry	18
2.5.2	Quartz	20
2.5.3	Feldspar	24
2.5.4	Olivine	26
2.5.5	Lime	28
2.6	Aim	29
3	Material and Equipment	30
3.1	Feedstock	30
3.1.1	Composition	30
3.1.2	Pelletizing	31
3.2	Bed Material	32
3.2.1	Composition	32
3.2.2	Particle Size	33
3.3	Reactor Systems	34
3.3.1	Fluidized Bed Combustion Reactor	34
3.3.2	Dual-Fluidized Bed Steam Gasification Reactor	36
3.4	FBC-Operation	38
3.4.1	Requirements & Limitations	38
3.4.2	Process	39
3.5	DFB-Operation	40
3.6	Sampling	41
3.7	Analysis Methodology	42
3.7.1	Scanning Electron Microscopy	42
3.7.2	Energy-Dispersive X-Ray Spectroscopy	43
4	Results & Discussion	47
4.1	FBC - Evaluation	47
4.1.1	Combustion Parameters	47
4.1.2	SEM/EDS Analysis & Discussion	47
4.2	DFB-01 - SW	51
4.2.1	Gasification Parameters	51
4.2.2	SEM/EDS Analysis & Discussion	52
4.3	DFB-02 - MWF, GL	55
4.3.1	Gasification Parameters	55
4.3.2	SEM/EDS Analysis & Discussion	56

4.4	DFB-03 - MWF, SLF, SCB, GL	61
4.4.1	Gasification Parameters	62
4.4.2	SEM/EDS Analysis & Discussion	63
4.5	DFB-04 - HNS	68
4.5.1	Gasification Parameters	69
4.5.2	SEM/EDS Analysis & Discussion	70
4.6	DFB-05 - EOP	72
4.6.1	Gasification Parameters	72
4.6.2	SEM/EDS Analysis & Discussion	73
4.7	DFB-06 - RH	80
4.7.1	Gasification Parameters	80
4.7.2	SEM/EDS Analysis & Discussion	81
4.8	Identified Ash-Bed Material-Interactions	86
4.8.1	Quartz	86
4.8.2	Olivine	87
4.8.3	Lime	89
5	Conclusion	90
6	Outlook	91
	Nomenclature	92
	References	94
	List of Figures	104
	List of Tables	107

1 Introduction

The world as we see it today is kept alive by humanities domestication and exploitation of terrestrial energy potentials. Being cut off those supplies is an unimaginable scenario and not considered an option. The only way to maintain and advance the human way of living on Earth is to use the quantities of energy available.

Earth itself is not an isolated system, there is continuous exchange of energy and matter with the surrounding outer space. Whereas the matter exchange is of negligible magnitude, the energetic exchange is the most important factor for human existence. This energetic exchange is the result of solar radiation. Apart from solar radiation, geothermal energy and tidal energy are the only initial energy flows on earth directly usable. Since geothermal and tidal energy are insignificant in comparison to solar energy it might be claimed, that all the energy available to us is of solar origin [1]. Fossil energy derived from dead plants and animals, wind energy derived from pressure gradients in the atmosphere, hydro energy derived from the natural hydrological cycle and biomass energy derived from plants are each one an example for energy sources originally derived from solar energy.

Since the potential of elements on earth is rather constant, a problem has arisen, which jeopardizes the long-range mostly stable conditions on Earth. The extraction and combustion of fossil fuels transfers the chemical compounds of those fuels from the terrestrial to the atmospheric system. For the agents of N, O and H (mainly as component in H₂O) the reservoir in the atmosphere is not changing significantly. But then for the fuels inherent C (released as CO₂ during combustion) the atmospheric concentration has jumped from 280 ppm to 400 ppm (2017) due to the excessive usage of fossil fuels [2]. Considering the greenhouse effect of CO₂ this has been mentioned to be the greatest hazard for human existence in the following decades.

A possible way of solving the problem of exceeding fossil fuel usage, without compromising the economic and social standards, is the substitution through biomass fuels. Although both those fuel types are (mainly) combusted, the biomass fuel has the advantage of representing a CO₂ neutral fuel. The CO₂ needed for building up its organisms is released during the combustion process, which creates an even balance in terms of CO₂. [1,3]

Another way of partly substituting fossil fuels is the use of anthropogenic waste "products" for energy conversion. Due to the inherent calorific value the method of thermal conversion may be applied for mainly organic waste streams. The thermal process would not only decrease the landfill volume but also create a suitable energy source. [4]

Last but not least, the realization of energy conversion systems with biomass and waste fuel would provide the potential of extracting valuable products from the non-volatilized fraction. In case of biomass this includes major nutrients for plants, in case of the waste fuel this covers mainly end-of-life material which may be reintroduced into the cycle of anthropogenic use [5–8].

The necessity of replacing fossil fuels has triggered technology and society to develop and enhance systems for the conversion of biomass and waste fuels into energy and valuable products. The entity of consequences humanity is already facing and might face in the future makes it necessary to apply a strategy for stabilizing the environmental conditions and inhibiting the exploitation of our planets chemical resources. Supporting the implementation of such a revolution is the objective of this work.

2 Background

Knowing, that biomass and anthropogenic waste from industrial and municipal facilities provide a valuable alternative to fossil fuels, scientific research of recent years has created a broad knowledge about the most efficient energy recovery and resource potential when biomass fuels are thermochemically converted. The major goals using these fuels are the energy generation and/or the production of secondary products of high value via gasification, biochemical processes, pyrolysis or hydrothermal treatment. Books and Papers published mostly deal with the biomass pretreatment necessary for those processes, the details and balancing just as purification of exhaust gases [1,9,10]. The same issues have been discussed for waste-derived fuels, especially municipal solid waste (MSW) [4,11].

An aspect of high interest is omitted usually, namely the ash and especially the bed ash. Taking a closer look on the ash means focussing mainly on processes of thermal treatment, neglecting the focus on biological and microbiological conversions [12]. Considering this essential part of the thermal conversion is of high difficulty, since the potential of bed ash depends on its origin, the process parameters and certainly the post-processing methods which should provide an optimized product (e.g. fertilizer) [13].

So far the different fractions of ash which accumulate during combustion and gasification of biomass and waste fuels are mostly not looked at as a valuable product, a usual way of disposal is landfilling [14]. Direct usage of the ash as fertilizer may not be practised due to low contents of nutrients, which do not even reach the minimum amounts mandatory by law [1]. Other fields of application may be e.g. as additive in adhesive mortars for the bed ash [15] and as additive in building material for the fly ash [16]. In case of the bed ash it is seen as potential substitution of coarse sand [15], for the fly ash use in building materials an additional post-treatment for leaching the chloride, sulphate and chromium was necessary in certain cases [16]. Recycling methods for Fe from the bed ash and several components from exhaust gas purification (e.g. NaCl, HCl, gypsum) are already applied in waste incineration plants [4].

The examples previously mentioned show ways of utilization, which do not embrace fully the chemical potential in the ash fractions. Besides it is mentioned, that the resulting ash may require secondary treatment to be used as adequate product. Those secondary treatments in general are based on the objective to separate the "harmful" from the "beneficial" substances and elements. The definition of harmful and beneficial in particular depends on the field of application. An example is the recirculation of biomass ashes as nutrient on forest soils, which has to focus on both the composition and consequently the leaching activity for the different compounds. [17,18]

Especially the last utilization mentioned is of further interest since it does not only refer to the inorganic mineral property of ash but also to the detailed content of different nutrient elements. Using these potentials for plant nutrition may be the crucial step for closing the cycle of sustainability when combusting or gasifying biomass fuels. Not including the deficiencies of such an idealistically closed cycle, it offers the possibility to not only create a primary product (gas, energy) but also to recycle the essential components as secondary product to guarantee the stock existence of biomass. This opportunity is lost, when the ash is landfilled or used in anthropogenic building material.

For this grand overview of potentials it is now essential to analyse the details which are the key to evaluate possibilities to create this rather utopian idea.

2.1 Fuel Types & Composition

Literature is providing a vast database in almost every book, journal or article written in this field of study. Therefore the sources provided in this chapter will be based upon papers which exclusively deal with chemical properties of biomass and waste. Due to the applicability and the practical realization, the focus within the anthropogenic waste fraction is set on those with high organic content like municipal solid waste (MWF) and shredder light fraction (SLF) from End-of-Life Vehicles.

Biomass and waste used as solid fuel may be separated into two parts which are by far not equally in amount and show a fundamentally different behaviour during combustion: the volatilizing agents, fixed carbon, and the ash. The line separating those two agents can not be drawn explicitly, depending on the conditions of the thermal treatment mainly ash-forming components may be volatilized or matter which should be transferred into gaseous phase may remain in the ash fraction. The main elements in biomass and organic waste are C, H and O, all of them are in general part of the volatilized agent and are the key reactants for energy conversion when combusting/gasifying aforementioned fuels [19–22]. While C is the predominant part of the organic matter, H and O are found in the moisture content as H_2O , the organic matter and the inorganic compounds (e.g. in oxides and hydroxides).

Generally stating the composition of biomass and waste may be difficult, since there are significant variations in moisture, ash yield and inorganic matter. A commonly used order of abundance may be provided for biomass nevertheless, referring to Vassilev et al.: C, O, H, N, Ca, K, Si, Mg, Al, S, Fe, P, Cl, Na, Mn, Ti [23]. This order may be used as a quick overview, for a detailed explanation of specific biomass types it is of little value especially since exact percentage shares and dominance of ash forming agents need to be identified. For MSW and SLF waste this list may be of use as well as XRF-analysis indicates (see Chapter 3.1).

Mentioning the volatilizing elements leaves a large variety of inorganic compounds which are expected to be found in the ash. From this point of investigation ongoing the origin of the biomass and waste is essential. For the type of woody biomass Obernberger et al. offer a detailed list of volatilizing and ash-forming elements with contents in different types of wood (coniferous and deciduous). Within these categories a differentiation is made between wood without bark, bark and logging residues [19]. There was additionally set a sample for short rotation coppice willow (SRCW) which is mainly harvested for the use as energy crop in two to five-years cycles [24–26]. As analysed by Obernberger et al. the ash content is between 0.3 and 5.0 wt% in every sample and dominated by the elements Ca, K and Si [19]. The most relevant results may be seen in Table 1. From this table basic information regarding the contents of elements in

the biomass of woody type may be extracted. Again it is necessary to record that those values may differ significantly, therefore the individual composition of woody biomass used in a specific experimental realization needs to be analysed in advance.

Although the information given in Table 1 may be used as guideline for estimating the composition of woody biomass it does not provide any details about biomass fuels derived from non-woody stocks. However Obernberger et al. also gives detailed data about herbaceous plants and fruit residues which are summarized in Table 2.

This analysis lacks some data, nevertheless the differences between the two general types of biomass (woody and non-woody) may be observed. Similarities are the contents of C, O and H

Parameter	Unit	Wood without bark		Bark		Logging residues		SRCW
		Coniferous	Deciduous	Coniferous	Deciduous	Coniferous	Deciduous	
Ash	wt% DS	0.3	0.3	4.0	5.0	2.0	1.5	2.0
C	wt% daf	51	49	54	55	52	52	49
H	wt% daf	6.3	6.2	6.1	6.1	6.1	6.1	6.2
O	wt% daf	42	44	40	40	41	41	44
N	wt% daf	0.1	0.1	0.5	0.3	0.5	0.5	0.5
Al	g/kg DS	0.10	0.02	0.80	0.05	-	-	-
Ca	g/kg DS	0.9	1.2	5.0	15.0	5.0	4.0	5.0
Fe	g/kg DS	0.025	0.025	0.50	0.10	-	-	0.10
K	g/kg DS	0.4	0.8	2.0	2.0	2.0	1.5	3.0
Mg	g/kg DS	0.15	0.20	1.00	0.50	0.80	0.25	0.50
Mn	g/kg DS	0.147	0.083	0.500	0.190	0.251	0.120	0.097
Na	g/kg DS	0.02	0.05	0.30	0.10	0.20	0.10	-
P	g/kg DS	0.06	0.10	0.40	0.40	0.50	0.30	0.80
Si	g/kg DS	0.15	0.15	2.00	10.00	3.00	0.15	-
Zn	g/kg DS	0.01	0.01	0.10	0.05	-	-	0.07

Table 1: Typical mean values for the elemental composition of woody biomass adapted from [19]

Parameter	Unit	Straw (Wheat, Rye, Barley)	Straw (Oilseed Rape)	Grains (Wheat, Rye, Barley)	Virgin Reed Canary Grass	Grass (in General)
		Ash	wt% DS	5.0	0.3	4.0
C	wt% daf	49	50	46	49	49
H	wt% daf	6.3	6.3	6.6	6.1	6.3
O	wt% daf	43	43	45	43	43
N	wt% daf	0.5	0.8	2	1.4	1.4
Al	g/kg DS	0.05	0.05	-	-	0.2
Ca	g/kg DS	4	15	0.5	3.5	3.5
Fe	g/kg DS	0.1	0.1	-	-	0.6
K	g/kg DS	10	10	5	2	1.5
Mg	g/kg DS	0.7	0.7	1.5	1.3	1.7
Na	g/kg DS	0.5	0.5	-	0.2	1
P	g/kg DS	1	1	4	12	15
Si	g/kg DS	10	1	-	3	0.15
Zn	g/kg DS	0.01	0.01	0.03	-	0.025

Table 2: Typical mean values for the elemental composition of herbaceous and fruity biomass adapted from [19]

with dominance of C, though the overall ash contents of biomass shown in Table 2 are slightly elevated to values between 2 wt% and 7 wt%. The main differences may be observed when focussing on the ash forming elements, here the dominance of Ca only occurs for the straw from oilseed grape. In comparison to the woody type the contents of Si, K and P are elevated significantly stating a dominance of Si and K in the ash matter. This has major influence not only on the composition of the ash which will be discussed in detail in Chapter 2.3 but as well on the thermodynamics of the ash chemistry and the crystallography described in Chapter 2.5.

Previous examples of data bases for the composition of biomass fuels are basically used to visualize similarities and differences between biomass derived from woody and agricultural origin. Furthermore there are various other types like animal biomass (e.g. manure), biomass derived from anthropogenic waste (e.g. sewage sludge) and plant remains from agricultural and industrial processes (e.g. crop husks).

A more detailed listing of volatilizing matter and ash composition for a large variety of biomass types and also anthropogenic waste was summarized by Vassilev et al. [23]. As mentioned by

Vassilev et al. the main factors influencing the composition of natural biomass are plant species, plant part, the growth process, ability of nutrient uptake, growing conditions (sunlight, geographic location, climate, seasons, soil type, water, pH), plant age, fertilizer and pesticides used, surrounding pollution sources, harvesting time and technique and extraneous material uptake during the harvest. This (incompletely cited) list shows the variety of effects influencing the composition, however the biggest leverage for the elemental consistency is the plant species dominating over all the other factors. The influence of non-biomass contaminants may be of high importance for specific cases when using semi-biomass or due to method inaccuracies in the collecting process. [23]

Focusing first on the mainly volatilizing matter (and continuing with the ash compounds in Chapter 2.3) it is possible to set a base for different types of biomass and waste regarding the dominating thermodynamics taking place during thermal conversion [23]:

- The C, H and O contents in the variety of biomass is similar, the value interval and mean values for the elements as well as the biomass type which represents the maximum and minimum are depicted in Table 3.

Element	Min.Value	Max. Value	Mean Value	Biomass (min.)	Biomass (max.)
C	42.2	70.9	51.3	Pepper Plant	Greenhouse Plastic Waste
O	16.4	49.0	41.0	Greenhouse Plastic Waste	Pepper Plant
H	3.2	11.2	6.3	Pepper Plant	Greenhouse Plastic Waste

Table 3: Maxima, minima and mean values of C, O and H in wt% with the representing biomass [23]

The statement of similar C, O and H values may seem bold when identifying the minimum and maximum values. Nevertheless a closer view on the detailed table presented by Vassilev et al. shows that C contents of 76 out of 86 analysed samples, including the entity of woody, herbaceous and agricultural biomass types, are within the interval of 45-55 wt% C [23]. C contents of woody biomass are slightly higher than in herbaceous biomass types [27]. For the N contents 72 out of 86 values are in the interval of 38-48 wt% C including most of the herbaceous and agricultural samples and the woody biomass [23]. For the H values a very narrow interval of 5-7 wt% C for 72 out of 86 samples is shown [23].

The biomass types representing the minima and maxima are greenhouse plastic waste and the pepper plant, high O contents are characteristic for some economic plants like soya, pepper and coffee plants [23]. High C and H contents in greenhouse plastic waste result from the structural difference of plastics to lignocellulosic biomass. As shown in Chapter 3.1 the waste fuels used for the execution of this work contain higher shares of C and H than the biomass-derived fuels as well.

The observations presented in the previous paragraph indicates higher similarities between different types of biomass than the entity of data would depict. Elemental concentrations of C, O and H in the majority of the analysed biomass deviate from the mean value in ranges of ± 10 % of this very mean value. Merely several biomass types are located outside these ranges regarding the C, O and H contents. [23]

- For the contents of N and S the variation between the fuel types is in quite limited intervals, nevertheless the differences are significant since the percentage shares are differing in magnitudes of 10^3 . The set of data is depicted in Table 4.

Element	Min. Value	Max. Value	Mean Value	Biomass (min.)	Biomass (max.)
N	0.1	12.2	1.2	Coconut Shells, Spruce Bark, Oak Sawdust, Fir Mill Residue, Pine Sawdust, Wood	Meat-Bone Meal
S	0.01	2.33	0.19	Greenhouse Plastic Waste, Cotton Husks, Oak Sawdust	Sewage Sludge

Table 4: Maxima, minima and mean values of N and S in wt% with the representing biomass [23]

The N content is highest in the biomass derived from animals (chicken litter, meat-bone meal) and the mean value of 1.2 wt% shows that the majority of biomass types analysed by Vassilev et al. the N content is below 2 wt% [23]. For the S content a very similar behaviour may be observed, the maximum in sewage sludge and animal derived biomass is characteristic. Also the S content in bark and straw fractions is higher than in classic wood types, although wood derived products as pellets and briquettes may contain S-additives as binding agents [27].

2.2 Applied Technologies (Combustion/Gasification)

The two processes of combustion and gasification are the main thermal operations used for biomass fuels. Although having a lot of parameters in common a short description of both may provide clear insight into the crucial steps of those two processes:

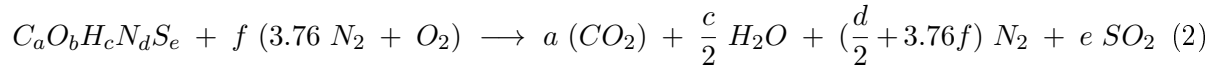
2.2.1 Combustion

Combustion of biomass and waste fuels for conversion of internal chemically bond energy into thermal energy is the method of by far highest importance. This thermal energy is furthermore used directly for heating purposes, coupled with a Rankine cycle to generate electricity via turbines or in combined heat and power plants (CHP), where both aforementioned processes are combined to provide an optimum of efficiency (ca. 90%) [1,28]. The combustion technique may be executed as direct biomass only (or waste only) combustion or co-firing systems (e.g. coal) [3].

During the combustion process the fuel is put in contact with specific amount of air or pure oxygen aiming at the total conversion of organic matter in the biomass into CO_2 and H_2O . For this a minimum air-fuel ratio needs to be maintained. The quotient of air mass and fuel mass participating in the combustion reaction defines the λ -value in Formula 1. The λ -value per definition equals 1 under stoichiometric circumstances [28]. Practical applications are controlled with CO- λ -characteristics to produce a minimum of CO during the combustion and regulating the O_2 -excess via λ sensors, showing the ecological-economic optimum in the range of $\lambda = 1.2-1.4$. [1]

$$f = \frac{\text{Total Provided Air Mass for Combustion}}{\text{Minimum Air Mass for Total Combustion}} \quad (1)$$

The detailed processes taking place during combustion may be investigated through single particle combustion models. Accounted models indicate the principal steps to be in chronological order: drying, devolatilization, recondensation, char gasification and oxidation and gas phase combustion [29]. The overall chemical reaction of combustion processes regarding the mainly volatilized elements is shown in Formula 2 with the stoichiometric air factor defined in Formula 3.



$$f = a - \frac{b}{4} + \frac{c}{2} + e \quad (3)$$

2.2.2 Gasification

Gasification aims on producing a secondary energy source, by name a product gas of high energetic value. The main transformation steps are similar to those of combustion. The main difference is the step of producing an intermediate product, which may be used for energy conversion in various facilities on the one hand but also for the production of other hydrocarbon compounds on the other hand(e.g. methanol synthesis). [1]

During the gasification process the fuel is put in contact with defined amounts of O_2 , H_2O and/or CO_2 . The main goal is to establish an atmosphere where partial combustion delivers energy for an endothermic gasification process [30]. The product gas composition mainly depends on the thermochemical conditions during the gasification and the reactants used, leading to a huge variety of parameters which need to be set to create the desired product. The main constituents of value in this gas are H_2 , CO , and CH_4 [29]. The mass percentage of every component defines the calorific and chemical value of the product gas. The optimization of this value strongly depends on the biomass type, but also the utilized fluid. Through the use of sub-stoichiometric air as reactant, inert N_2 is introduced into the chemical balance, which decreases the calorific value of the product gas significantly compared to the use of CO_2 , H_2O , and O_2 [3].

The performance of gasification facilities may be evaluated through the percentage of carbon conversion which represents the ratio of total carbon in the biomass feed and carbon in the product gas. The ranges for carbon conversion are typically in the range of 60 to 90%. Another important parameter for the gasification is the air-fuel ratio, same as in the combustion process. The major difference between combustion and gasification is shown especially by this value, since the gasification process requires non-total conversion of carbon to CO_2 . The optimum air-fuel molar ratio to be found in literature is approximately 0.26. [29]

The thermochemical conversion processes during gasification may be modelled analogously to the combustion processes with the single particle gasification model. Therefore the steps in chronological order are: heating and drying, pyrolysis, gas-solid reactions and gas-phase reactions [29]. The overall chemical reaction of gasification processes regarding the mainly volatilized elements is shown in Formula 4 without stoichiometric factors [1].



2.2.3 Thermochemical Conversion Reactor Systems

For the thermal conversion of biomass and waste into products of elevated value and/or energy three major systems are applied: grate systems, fluidized bed systems and pulverized fuel systems [31].

- In grate firing (GF) systems the fuel is moved through a boiler on a grate (e.g. reciprocating grate, rocking grate, roller grate; [32]) with air supply for combustion through holes in the grate. This method is the most widespread technique for burning biomass as well as municipal solid waste [31] [4]. For the ash behaviour in grate fired processes it may be stated, that conditions on the grate lead to poor mixing of the ash and reducing conditions, which requires a secondary step of burning for the volatilized matter [33]. Gasification in grate systems is hardly applied and little researched [34]. For the purpose of this thesis the GF systems are of little importance.
- In fluidized bed combustion (FBC) and gasification (FBG) the fuel is normally mixed with a bed material (e.g. quartz sand) and suspended with air injected through the bed. The temperature in the bed then leads to partial gasification of the biomass which leads depending on the atmospheric conditions to full combustion or may produce a product gas [1,31]. The conditions for gasification and combustion depend on the composition of the injected medium, for combustion the inlet normally is air (preferably O₂ enriched), whereas gasification is processed with O₂, H₂O and/or H₂ [35]. The type of FBC/FBG system depends on the relative velocity between injected air and fuel particles, the different conditions are stationary fluidized bed (SFB), circulating fluidized bed (CFB) and entrainment fluidized bed (EFB) [1]:
 - When injecting air at low velocities into the bed without mobilizing the particles the regime is called fixed bed. In this case the bed does not move at all, which makes the use of inert bed material unnecessary. Although a possible regime when using a fluidized bed reactor, this conditions are not part of FBC/FBG since the conditions are non-fluidized. Nevertheless studies for fixed biomass combustion in regards to ignition parameters and emissions have been made [36,37].
 - In the SFB system the pressure drop through the bed increases linear with the air velocity until it reaches the point of disaggregation where the particles are dispersed by the air stream. At this point the pressure drop stabilizes and particles are kept in a floating state. The stationary (or bubbling) fluidized bed shows combustion or gasification of the fuel, which leads to heat and mass transport from the fuel to the bed material and the air stream. The bed material and its inherent heat capacity stabilizes the temperature conditions in the stationary bed to guarantee more homogenous temperature profiles [1]. The bed material normally has initial diameters of 0.5 to 1 mm. Due to ash formation through fuel combustion the bed material may show major interaction with the ash [35].
 - With an increase of gas velocity the particles start to be carried out of the reactor, where they need to be precipitated and recirculated into the reactor. This regime marks the area of a CFB process, the pressure drop stays overall constant until the point of entrainment is reached [1]. The bed surface can not be defined in this regime anymore and the formation of bubbles is also not occurring anymore. In the reactor there are areas formed of higher suspension density in the lower reactor sector and lower suspension density in the upper reactor sector. In general the bed material diameter in circulating fluidized beds is smaller than in stationary fluidized beds (ca. 250 µm in CFB, up to 2 mm in SFB) [35,38]. For the conditions of pneumatic

transport the pressure drop is assumed to be rising when the bed material mass stays constant in the reactor (through precipitation and recirculation) and decreasing if the bed material is entrained and not recirculated [1]. Studies analysing the processing of biomass in circulating fluidized beds show that this method of thermal conversion is of high interest [39–41].

- Reaching the point where all the particles formerly in the bed are carried with the air stream out of the reactor the entrainment condition starts. This mostly is used when the fuel is very fine grained and dry, furthermore inert bed material is not required. Dust separation systems like cyclons need to be installed for the off-gas stream since the dust entrainment is highest in this regime [1].
- Pulverized fuel (PF) systems are mostly used in plants where previously coal was fired [31]. The fuel needs to be pulverized and dried and high temperatures lead to corrosion and slagging problems. Therefore it is often applied as co-firing system with coal [31]. For the purpose of this work the PF systems are of little importance.

Additionally to categorizing the fluidization regime in the reactor a combination of gasification and combustion reactor may be applied, the dual-fluidized bed gasification (DFB) reactor. Here the fuel runs through the mechanisms of drying, pyrolysis and char gasification in the gasification reactor, whereas the remaining char is transported with bed material into the combustion reactor and combusted. This char combustion heats up the bed material which returns into the gasification reactor, providing the energy for the endothermic gasification process. Additional fuel may be combusted to supply sufficient heat. The main improvement is the separation of combustion and gasification zone, which increases the (calorific) value of the gasification product gas [1,35,42].

The variety of systems applicable for the thermal conversion of biomass reflects the large field of research. To evaluate results for a defined system, it is essential to specify the regime of operation. The equipment used for experimental analysis in this work is presented in Chapter 3.

2.3 Ash Composition

Since the proportion of normally volatilizing matter is discussed in chapter 2.1 the focus now needs to be set on the composition of the formed ash through the process of combustion and gasification. The thermal conversion processes will be presented as one set of data regarding the ash composition, due to the fact that ashes are derived from the elemental biomass and waste structure, whereas the atmospheric condition (reducing or oxidizing) does not introduce ash forming compounds [43,44]. In order of importance and abundance in the biomass and waste ash, the major ash forming elements and compounds are:

- Silicon:
One of the major ash forming elements is represented by Si found as little mobile compound SiO_2 , varying in the range of 0.02 wt% (meat-bone meal) to 94.5 wt% (rice husks) [23]. High Si contents are characteristic of biomass fuel derived from grass, straw and husks, being an important factor for the behaviour under mechanical stress [45], especially the Si content in wood stems is significantly lower than in grass components [23]. Silica mineral is absorbed in the plants through silicic acid from soil and precipitated forming organically deposited silica hydrates [46]. In biomass Si functions as structural and protective support [47]. A major part of Si also may be imported into the fuel through soil components [48]. Si may be volatilized during combustion as refractory species [19].

- Calcium:
The range of Ca in form of CaO in ash fractions is found in amounts of 1-83 wt% [23]. Highest amounts may be found in ashes when combusting wood (stems, barks, trunks, large branches) [49] as well as in animal biomass [50]. In soils Ca rarely is abundant, therefore the uptake through plants is not considered a problematic issue [47]. Mostly it is a compound of cell walls and organelles [51]. Concentration of Ca-cations in the cytoplasm may be indicator for metal toxicity and tolerance, due to the finding that Ca^{2+} may be an instrument to extenuate toxic effects of high metal levels [52]. Ca is found to be a limiting factor for the ash melting behaviour, contents of lower than 15 wt% in combination with concentrations of K higher than 7 wt% are mentioned as problematic conditions for the melting by Obernberger et al. [19].
- Potassium:
Varying in the intervall of 0.2 wt% (mixed waste paper) and 63.9 wt% (almond hulls) K in the compound K_2O is found in biomass ash fractions [23]. High K contents are characteristic for grasses, husks, hulls and shells [23]. K is to be found in abundance in plants and parts of plants of high annual growth, which coincided with the previously mentioned examples [49]. K plays its part in plant nutrition as enzyme activator, is a key element for osmotic transport processes and charge neutralizer in e.g. membrane processes [53]. Growth experiments on barley demonstrated a potential K-substitution by Ru [54]. As mentioned the K content (in combination with the Ca concentration) refers to the potential for agglomeration [19] as well as for vaporization and condensation (15 % to 40 % of K volatilizes during combustion) which may lead to greater corrosion problems [49].
- Phosphorus:
For the content of P as oxide P_2O_5 the data provides the large range of 0.2 wt% (mixed waste paper) to 40.9 wt% (meat bone meal) [23]. The maximum P contents in biomass ash are found in fractions derived from animals, anthropogenic wastes and seed-bearing structures of plants. This correlates with the knowledge, that P is a main component in DNA- and RNA-bearing organisms as well as the major frame substance in bones and teeth [55]. Due to the importance of P in the energy cycle of plants and organisms, P-deficiency causes accumulation symptoms of sugars and starch and hinders the transport mechanism [47]. The availability of P for plants and organisms is a critical limitation for growth, whereas decomposition of the organic matter provides P in the available form [47].
- Aluminium:
Al as oxide, forming Al_2O_3 , is to be identified in biomass in the range of 0.1 wt% (Alfalfa straw) to 53.5 wt% (Mixed waste paper) [23]. Higher Al contents are characteristic for contaminated biomass fractions, where the introduction of Al is mainly caused by non-biomass additives or soil inclusions since oxides and hydroxides of Al are main soil minerals [23,46]. The maximum value of mixed waste paper is caused by the addition of kaolinite [23]. The Al uptake of plants is correlated to the pH value of the soil, acidic conditions may lead to improved mobilization of Al cations into the plants and therefore more Al may be found [56,57]. Investigations demonstrated Al to be a strong limitation factor on the growth of plants (especially the roots), therefore low Al levels may be a benefit for the growth of plants (e.g. up to 5 mg/l in corn) [58]. In soils P may be immobilized by presence of high amounts of Al, which may cause deficiency in P [47].
- Magnesium:
The content of MgO in biomass ash varies in the range of 0.2 wt% (rice husks) to 16.2 wt% (walnut hulls and blows) [23]. Mg in plants is an important compound of chlorophyll (2.7 wt%), for various seeds and fruits. High Mg contents lead to dedicated anthropogenic

usage since human organisms require Mg as well [47]. Mg deficiency in plants may provoke reduced chlorophyll concentrations in leaves and higher H_2O_2 concentrations, it has been also demonstrated that Mg contents decrease chronologically in leaves [59].

- **Iron:**
Fe may be found in biomass ashes as Fe_2O_3 in magnitudes of 0.2 wt% (rice husks) to 36.3 wt% (Pistachio shells) [23]. High Fe contents usually may be caused by contamination with hydroxides, whereas the Fe content in sewage sludge mainly correlates with the precipitation method [23]. For plants and organisms Fe plays an important role in the synthesis of chlorophyll [53] and the immobilization of trace and pollutant elements in the soil (e.g. Co, Cu, Zn, Ni, Pb) [60].
- **Sodium:**
 Na_2O forms the oxide component containing Na to be found in biomass ashes in the interval from 0.01 wt% (bamboo whole) to 29.8 wt% (fir mill residue) [23]. High Na contents are characteristic when incinerating olive residues (pits, husks) and fir mill residue, which may be contaminated significantly by sodium chloride (NaCl) [23]. In general it may be stated, that high Na concentrations in biomass ash are mainly of non-biomass origins such as process additives in industrial facilities and halite water [61]. Although NaCl is an important part of plants and organisms for the nerve systems and the regulation of the water balance, an excess of Na (mainly in form of NaCl) may lead to intoxication phenomena (water loss, membrane malfunction) [47,62].
- **Boron:**
B is mainly taken up by plants in form of H_3BO_3 and takes part in the process of Ca uptake [47,63]. The primary function of B is hard to determine since the amounts of boron are negligible (<100 mg per kg DS) [53].
- **Titanium:** Although not an essential element in plants Ti concentrations on the investigations of [23] reached one peak of 27.6 wt% for shredded currency. In the bulk of biomasses Ti is regarded as trace element, for industrial prepared cellulosic fabrics Ti may be introduced through additives [23]. Although Ti is present in soils in rather high concentrations its uptake is quite low due to poor availability in water insoluble compositions which normally leads to contents of 0.1 - 10 ppm in the plants [64].
- **Selenium:**
Se in form of selenate is taken up and assimilated by plants in analogue form to sulphates and greatly depends on the species and the soil regime [65,66]. High amounts of available Se increase the level in the plant, whereas available S decreases the Se uptake [47]. Hyperaccumulation of Se in plants may lead to concentrations up to 0.5 wt% (e.g. astragalus), though Se excess in plants may lead to toxic corresponding uptakes by animals consuming those [47,67].
- **Copper:**
Cu complexes (in organic compounds and proteins) are integrated in biological compounds for various reasons, one of the most important being part of the disease resistance mechanisms [47] [68]. Cu deficiency and excess may both lead to accumulation of Cu in roots and uptake organisms, whereas the Cu transport is decreased [69]. Typical values for the amount of copper are 5-20 mg Cu per kg in tomato tissue [70], approximately 50 mg Cu per kg dry matter in wheat straw and rather high amounts of around 170 mg Cu per kg dry matter in municipal sewage sludge (MSS) [71].
- **Zinc:**
Zinc as enzyme activator is of essential importance for plants. It is taken up from the roots

as hydrated Zn^{2+} ion (preferably from acidic soils) and easily transported in the interior parts [47]. The actual concentration of Zn in plants mainly depends on vegetation state and age, with chronically decreasing amounts of Zn in ageing plants [72]. Whereas analysed wheat straw and cotton stalk demonstrate rather small amounts of around 30 mg Zn per kg dry matter, the same paper states values of about 800 mg Zn per kg on dry basis for municipal solid waste [71].

- **Molybdenum:**
Mo has its greatest importance as support for reduction of nitrates to avoid accumulation of said nitrates [47]. For this case a minimum of Mo should be provided, whereas excess of Mo does not lead to any observable negative effects [73]. Scientific belief is, that Mo is taken up as molybdate-ion and easily transferred to various parts of the plants. The availability of Mo is benefited by both acidic and alkaline soil regimes [69]. A large variance of Mo concentrations in low absolute magnitudes between different plants has been observed, no matter if the soil circumstances are equal or different [74].
- **Manganese:**
Mn as essential element for plants and organisms is regarded a catalyst for oxidation and reduction processes [75]. It is taken up as Mn^{2+} and deficiencies often correlate with high contents of organic carbon or lime in the soil [47]. The Mn transfer in the plants seems to be way faster than the translocation of P or Fe [76].
- **Cobalt:**
The main use of Co in plants is the fixation of nitrogen, whereby deficiency results in reduced growth and chlorosis of leaves [47, 77]. The Co is present both as cation (in the xylem) and as negative complex (in the phloem) [78]. The concentrations reach from hardly detectable (e.g. beans) to "low" (e.g. leaves) [47].
- **Vanadium:**
V is an important factor in the soil enzyme system, affecting mineralisation and release of nutrients to the plants [47]. Nevertheless, intoxication due to V may occur and is often fought through immobilisation in the root [79]. This immobilisation is reported to take place by fixation as Ca-vanadate, which may not happen when the nutrient base is low in Ca [80,81].
- **Chromium:**
The bioavailability of Cr depends on the oxidation state, since Cr(VI) is way more toxic to plants than Cr(III) the preferred nutrient taken up is Cr(III) [47]. Reduction mechanisms within the roots have been investigated, which may reduce the Cr(VI) to Cr(III) (e.g. garlic) [82]. In general the function of Cr in organisms and plants is a controversial issue, when taken up from plants it mainly stays accumulated in the roots and shows slow transport processes [83,84].
- **Nickel:**
Ni as essential element and micro-nutrient has been shown to be part in enzymes and most plants contain Nickel in the range of 1 to 6 mg Ni per kg [47,85]. Uptake is benefited by low pH values and Ni tolerance same as toxicity has been investigated previously [79,85].
- **Strontium:**
Only little is known about the physiological function of Sr, although there has been research about effects on organisms when substituting Ca for Sr [86]. In plants the uptake behaviour of Sr strongly correlates to the soil regime, there has been found a strong relationship in Sr intake and Sr/Ca-ratio [47,87].

- Arsenic:
As, normally considered to form toxic compounds (arsenite, arsenate), is part of most plants although the levels normally do not reach 1 mg As per kg [47, 79]. It has been stated, that As is taken up passively and transferred within the plants easily [88]. Since plants provide an entry into the food chain As concentrations are of importance and may be extraordinary high due to contamination through foul water or pesticides [47].
- Cadmium:
Since Cd is not an essential element for plants and organisms the major concern is about its toxicity [47]. Cd is taken up only in small amounts under normal circumstances, with increased bioavailability under acidic conditions [89, 90]. Same as As the intrusion of Cd into the overall food needs to be monitored since Cd is also part of fertilizers and pesticides [91]. The highest Cd accumulations have been found in lettuce and spinach samples [90, 92].
- Lead:
Considered not essential, Pb is mostly looked upon because of its toxicity [47]. It is hardly available to plants and most of the absorbed Pb^{2+} is bound in the roots [90, 93]. Nevertheless Pb may be found in leaves and aerial parts due to wet or dry atmospheric deposition. Transfer to inner parts has been researched and found to be comparably small [47, 88].

2.4 Bed Material Type and Composition

To describe the thermodynamics within the fluidized bed (FB) it is of greatest importance to know about the composition and constitution of the bed material. While the fuel input is supposed to be converted to ash and interaction with other particles should be highly favoured, the bed material stays mostly unbroken (but often ground and/or cracked) and in its original form except from agglomeration processes and layer formation. Nevertheless an elevated operational time may lead to frequent crack phenomena.

The mathematical models for estimating the operating conditions in FB systems include physical properties of the fluid (viscosity, density) and of the bed material (density, form factor, particle size, bed height). Therefore some of the most important properties of the bed material may be itemized as follows.

2.4.1 Composition and Structure

In contrast to the fuel used in FB systems, the bed material composition may be defined more clearly. The preparation of bed materials prior to insertion normally leads to high purity of a single compound of known composition. Detailed descriptions of common and less common bed materials have been made previously [94]. To set a more focused overview, three of the most utilized bed materials are briefly mentioned below.

- Quartz:
Quartz, with its chemical formula SiO_2 , is the most commonly used bed material so far. Next to feldspar it is the second most abundant mineral in the Earth's continental crust. The main resources of quartz are high quality industrial sands, including the quality criteria of $>98\%$ SiO_2 . α -Quartz, which in general is called quartz, is the most important modification, composed of $[\text{SiO}_4]^{4-}$ -tetrahedrons forming oxygen bridges. [95, 96]

At a temperature of 573 °C the trigonal α -Quartz is converted to the hexagonal β -Quartz, morphology and structure may be seen in Figure 1. This conversion is a displacive phase transformation, which means it is reversible. This does not apply for every transformation process for the SiO_2 -System, e.g. the change from β -Quartz to Cristobalite. Therefore Cristobalite previously produced through irreversible processes may be used as well as bed material at lower temperatures [95,96]. Considering the crystallography of the (possibly during the FB process formed) quartz modification is a key parameter for the investigation of interaction mechanisms with the ash particles. Especially the availability of Si plays an important role in the layer formation processes which are discussed in chapter 2.5.

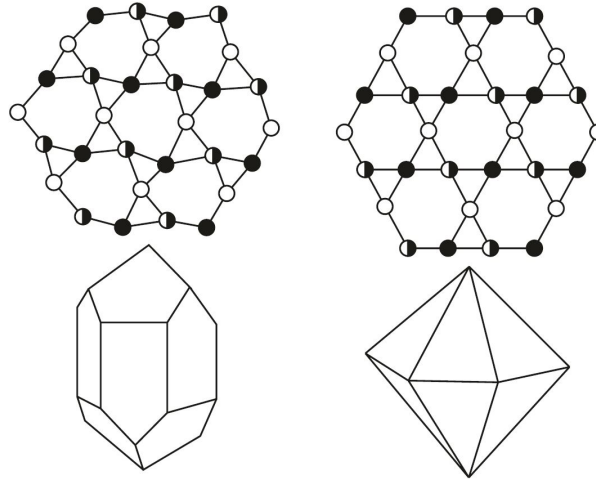


Figure 1: Schematic structures and morphology of α -Quartz (left) and β -Quartz (right) [95]

The SiO_2 -System contains 15 modifications, including high pressure modifications (e.g. Seiferite) and modifications with special requirements for stability (e.g. Tridymite, which needs cation-impurities to stabilize its structure). An analysis of stability areas in terms of temperature and pressure has been implemented previously, demonstrating the 7 phases of naturally occurring SiO_2 minerals are stable at relatively low temperatures. Those naturally occurring minerals are considered to be of high purity and contain few defects, an important fact due to the application of quartz material in applications of maximum sensibility to material (e.g. electronics). [95,96]

For industrial and anthropogenic purposes quartz offers a wide spectrum of applications. Synthetic SiO_2 is mostly used in a monocrystalline solid structure, e.g. in piezoelectric devices. Minerals and stones may be starting material for the generation of metallic Si (e.g. alloying). Quartz sands are mainly used as casting molds and (with high purity) as starting product for glass manufactures. The use as bed material in FB systems is quantitatively insignificant on a global scale. [95]

- Feldspar:

Being the most abundant mineral in the Earth's crust, feldspars are to be found in magmatites (60 %), metamorphic stones (60 %) and sediment stones (10 %). feldspars are monoclinic and triclinic tectosilicates (also called framework silicates) with the general formula $A_x^+ A_{1-x}^{2+} [T_{2-x}^{3+} T_x^{4+} O_8]$. In this formula the elements being displayed by A^+ (K^+ and Na^+) and A^{2+} (Ca^{2+} and Ba^{2+}) define the type of feldspar which is present. These cations are taking the spaces in the hollow formations within the tetrahedron framework, as shown

in Figure 2. Most feldspars are part of the K-Na-Ca system. [95]

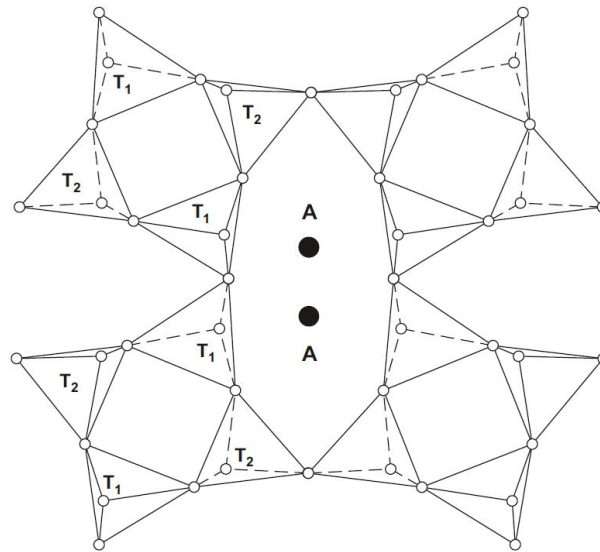


Figure 2: Idealistic structure of Feldspars in a matrix of TO_4 -tetrahedrons with changing orientation and cations (A) in structural hollow spaces [95]

The most important feldspar types are $CaAl_2Si_2O_8$ (Anorthite), $NaAlSi_3O_8$ (Albite) and $KAlSi_3O_8$ (Orthoklas). Alkali-feldspars such as Albite and Orthoklas are changing their modification at high temperatures, transforming a formerly triclinic structure to a monoclinic one. For the K-feldspar those modifications have the names of Microcline (low temperature) and Sanidine (high temperature) [96]. The Microcline-Sanidine transformation temperature has been estimated at $450\text{ }^\circ\text{C}$, due to slow kinetics the experimental evaluation has not been determined [97]. The composition of feldspars also shows the potential of various elements within the structure for interaction with the ash particles in a FB system, especially the cations in the hollow spaces of the structure.

An important criteria for industrial purposes is the ratio $K_2O:Na_2O$. The alkali-feldspars are showing a broad temperature spectrum for refractory deformation, which makes them an easily manageable material for ceramic forming [95]. For the usage as bed material in FB systems these deformation and refraction processes are of great importance, since the inherent thermal energy might tend to create circumstances to enhance these processes.

- Olivine:

Olivine with its chemical formula $(Mg,Fe)_2[SiO_4]$ is an important mineral compound of Peridotites and is to be found as monomineral only as Dunite [95]. It is the most abundant mineral in the outer Earth mantle. In the literature it is also described as mixture of two parts $(Mg,Fe,Mn)O$ and one part SiO_2 , while other sources neglect the Mn modification [96].

Olivine is a Nesosilicate, which means in its orthorhombic structure the SiO_4 tetrahedrons are not linked directly. The O in this structure is arranged as deformed hexagonal close-packing, whereas the Si is filling the tetrahedral gaps and the metals are at the octahedron spaces [96]. The orthorhombic structure is depicted in Figure 3.

Olivine has met its industrial purpose as slag former additive in the iron and steel producing industry. It is also used as fire-resistant construction material in foundries and furnaces. [95]

Olivine is considered a highly suitable bed material for FB systems. The application of olivine proved to have many advantages during the operation including its mechanical durability, high heat capacity, catalytic activity, and tar decomposition. [94,98,99]

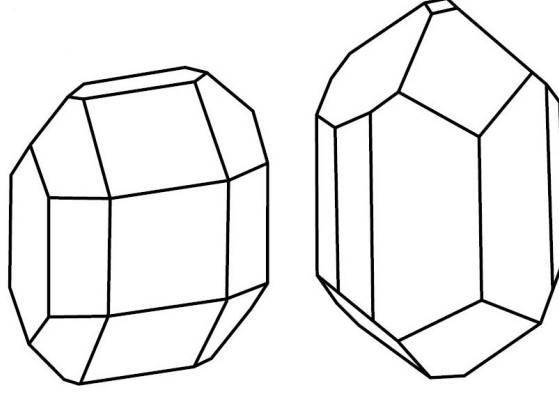


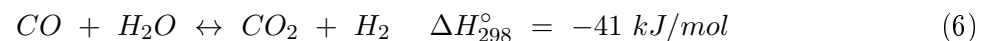
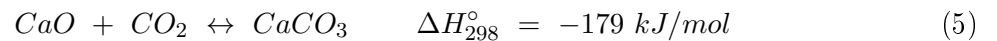
Figure 3: The orthorhombic crystal structure of olivine [96]

- Lime:

Lime in its form as CaCO_3 is one of the most abundant compounds in the outer Earth mantle, mainly occurring in sedimentary rock. Through the calcination of calcite (CaCO_3) at 900°C , gaseous CO_2 is released and CaO is produced. CaO reacts highly exothermic with H_2O to create $\text{Ca}(\text{OH})_2$, which may take up CO_2 and drive out H_2O to create the original CaCO_3 . [100]

The calcite CaCO_3 has a trigonal crystal structure and due to inherent trace elements it is often coloured pink (Co, Mn), green (Cu) or blue (Cu). The calcite form is the most abundant lime fraction and mainly used in the concrete industry. Only through the orthorhombic crystal structure the Argonite is distinguishable. Argonite is stable at high pressures and only occurs metastable under natural conditions. [96]

CaO as bed material component in gasification processes shows beneficial catalytic function for the promotion of H_2 product gas and char reduction. Catalysts of CaO impregnated with Fe not only increased the H_2 yield, but also prevented deactivation of the CaO through tar formation [101]. A comparison between olivine and CaO as bed material during the gasification of wood and lignite proved shifts to higher H_2 yields as well as decreased tar amounts and stabilization of key parameters of gasification [102]. For DFB gasification systems CaO/CaCO_3 may be applied for SER technology and CO_2 capture through the extraction of CO_2 from the gasification zone and calcination in the combustion zone [103]. The principle of SER processes is shown in Formula 5. The effect of the CO_2 extraction from the gasification zone to higher H_2 yields can be obtained from Formula 6.



2.4.2 Particle Size & Form Factor

The particle size of the bed material is the biggest influencing factor for the settings of fluid dynamics and the superficial interactions between particles within the FB. Since the density is a material specification a decision for the separating cut used in the FB needs to be pre-set by the operators.

For the purpose of the research executed in this work it is advantageous to adjust the used bed material to make it comparable. Since the reactor capacity and measurements should be taken into account as well the following list of separating cuts always has to be viewed on with the corresponding FB data:

- Quartz: \varnothing [425, 600] μm (*Reactor- \varnothing* = 400 mm) [104]
- Quartz: \varnothing [250, 355] μm (*Reactor- \varnothing* = 100 mm) [105]
- Quartz, Dolomite: \varnothing_{median} : 350 μm (*Reactor- \varnothing* = 70 mm) [106]
- Quartz: \varnothing [106, 125] μm (*Reactor- \varnothing* = [100, 200] mm) [107]
- Quartz: \varnothing [200, 250] μm (*Reactor- \varnothing* = [100, 200] mm) [108]
- Quartz: \varnothing [200, 250] μm (*Reactor- \varnothing* = [100, 200] mm) [44]
- Olivine: \varnothing [200, 250] μm (*Reactor- \varnothing* = [100, 200] mm) [109]
- K-Feldspar: \varnothing [200, 250] μm (*Reactor- \varnothing* = [100, 200] mm) [94]

Additionally to the diameters provided in the literature an important influence on specific surface and fluid dynamics is the form factor, in this case especially the sphericity. For non-totally spherical particles this factor is needed to compare its surface to a spherical particle of same volume. By definition the sphericity form factor is in the interval from 0 to 1, tending to its upper extremum when the shape resembles a perfect sphere. Since the exact measurement of sphericity has been executed previously and tabled in literature it is possible to obtain approximated values for the sphericity of specific material and particle sizes, e.g. the sphericity of quartz has been found to be in the interval of 0.5 to 1 with a mean value of 0.75. [110–112]

2.5 Agglomeration and Layer-Forming Processes

After presenting properties of all the components and factors of FBC/FBG systems the focus may now be set on the thermodynamics taking place during these processes. Objective is the description and analysis of agglomeration and layer formation processes occurring. It is possible to differentiate between three mechanisms of agglomeration, which have been identified and analysed previously. [44, 107, 113]

- 1 The coating induced agglomeration forms layers on the bed grain through adhesion of alkali silicates from melts and gaseous alkali compounds. Into this alkali silicate melt, Ca may diffuse to react with the alkali silicates to secondary, and furthermore tertiary, compounds. For the combustion of woody biomass this mechanism is proposed the primary one with quartz.

- 2 Direct Attack of alkali gases or liquids on the bed material may create continuous inner reaction layers. This mechanism is suggested to be the primary one when fuel rich in alkali compounds in relation to Si and P are combusted.
- 3 Agglomeration through direct adhesion of molten bed ash on the bed grain followed by formation of agglomerates between different particles has been found to occur at rather low temperatures. The fuel, which demonstrates this mechanism, normally is rich in alkali compounds and involves as well significant levels of Si and P. The relation of alkali to earth alkali compounds in the bed ash, same as the overall ash content of the biomass usually is relatively high when this mechanism occurs.

With the knowledge of these three fundamental mechanisms the focus should be set on the details of ash chemistry during these processes first, followed by a literature research of already undertaken experiments classified in regards to the bed material used.

2.5.1 Ash Transformation Chemistry

Maintaining conditions which guarantee a total volatilization of organic compounds, it is possible to analyse the ash transformation chemistry regarding the most important ash forming elements, being Si, Ca, Mg, K, Na, P, S, Cl, and Al. Those elements are considered most significant for interaction and reaction mechanisms in FB systems, supposed they are present in certain quantities in the utilized fuel. As summarized previously, the quantities of inorganic compounds to expect regarding literature data might differ from the actual values, which makes it inevitable to pre-analyse the ash forming elements to understand the transformation chemistry. The topic on ash transformation chemistry, with a main focus on P-rich fuels, was researched in a cluster of papers being summarized by Boström et al. [114]. The details found in these papers and those of similar objective are summarized and compared in the following chapters.

For the purpose of theoretical description and thermodynamics balancing of ash transformation chemistry Boström et al. give a valuable background [114]. The reaction mechanisms were classified into orders of primary, secondary and ternary reactions which may(!) take place during the combustion of biomass. Although the approach is hypothetical and not experimental, the description of corresponding experiments has been put into agreement with the considerations postulated. [114]

The primary reactions mainly depend on the oxygen affinity of the main ash-forming elements. As described in chapter 2.3 the uptake and accumulation of metals in plants mainly happens in form of cation compounds (neglecting the influence of direct minerals from the soils, which may be added in the harvesting process). Therefore the affinity of metals present in the ash to oxygen during combustion and gasification is of great importance. An Ellingham-diagram of thermodynamic stability for the main ash-forming oxides and main products of combustion as a function of temperature is of use (see Figure 4).

Since more negative values for ΔG^0 correspond with higher stability it may be considered, that Ca and Mg are of highest stability and already present in the biomass as oxides. A release during combustion of those components takes place in form of solid particles. For Si the diagram shows similar behaviour, nevertheless in partially reducing atmospheres within the combustion zone it may be reduced from SiO_2 to SiO and enter the gas phase. [114]

The behaviour of the other main ash-forming metals has to be thought of in a different way. For P the potential of reduction is important to consider. For even less oxygen affine elements like K and Na the volatilization as metal vapour and further reaction with water to alkali hydroxides is especially of importance at higher temperatures. A special position in the diagram

is taken by S, since its affinity to oxygen is lower than the carbon-hydrogen system at any time, therefore the release will mainly be as elemental (S_2) or hydrated (H_2S) S-compound. The same may be predicted for Cl. [114]

In terms of reactivity the present data set by Boström et al. implies high reactivity for the more volatile compounds during combustion, such as P, S, Cl, K and Na. Less volatile and therefore less reactive fractions in the biomass ash are Si, Ca and Mg. However the formed solid refractive compounds of these three elements are of high specific surface and fast to react with other ash components. [114]

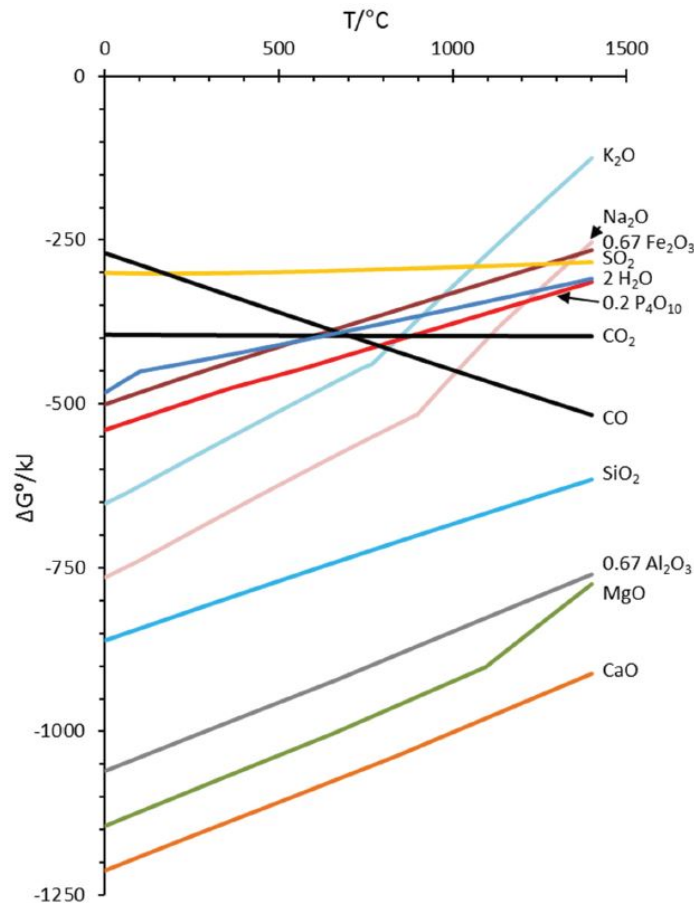


Figure 4: Ellingham-diagram of thermodynamic stability of main oxides and products of combustion systems with 1 mol O_2 [113]

Based on the model of acid-base reactions the primary formed compounds can be divided into acidic and basic compounds and put in order with the highest reactivity on top. The approach made by Boström et al. is depicted in Table 5. It is suggested, that competition between those compounds would lead to favoured reaction mechanisms (e.g. K-phosphates) and reactions of inferior potential (e.g. Ca-silicates). The proposed initial steps for this approach would be the formation of K-compounds, with the tendency for ternary reactions of those compounds (e.g. K-Ca-silicates). Surplus of specific primary formed compounds on the other side may lead to increased release rates (e.g. KCl) or creation of stable non-reacted particles in the ash (e.g. Si as cristoballite at high shares of P in the ash fraction). [114]

To put this theory into practice various experiments have been undertaken with the results in reference to ash transformation chemistry being:

Basic compounds	Acidic compounds
KOH(l,g) (K ₂ O)	P ₂ O ₅ (g)
NaOH(l,g) (Na ₂ O)	SO ₂ (g) SO ₃ (g)
CaO(s)	SiO ₂ (s)
MgO(s)	HCl(g) (Cl ₂)
H ₂ O(g)	CO ₂ (g)
	H ₂ O(g)

Table 5: Simplified classification of primary ash transformation products referring to their reactivity as acidic or basic compound adapted from [114]

- Woody biomass combustion with high ratios of Si:P and Ca:K shows high volatilization tendency of K (as sulfate or chloride) and high presence of earth alkali silicates which decrease the slagging tendency in the ash [114].
- Agricultural crops with its higher contents of K (see Chapter 2.3) and lower contents of Si tend to the formation of K-phosphates rather than K-silicates [114].
- The addition of phosphorus acid to logging residues, whose ash is rich in Ca, Si, and K, decreases the amounts of volatilized K. The K is bound in the coarse ash fraction as K-earth alkali-silicate. When combusting the K-richer wheat straw there is a high fraction of KCl and K₂SO₄ volatilized and the ash to a high degree consists of K-silicates. When adding P to the fuel, K once again was bound in the coarse ash fraction and a significant increase of Ca-K-phosphates was observed, whereas Si in its high temperature modification (cristobalite) was found as well. An abundance of P in the ash may lead to the formation of low melting alkali-phosphates and should be avoided. [115]
- The bed agglomeration affinity of rapeseed cake, which is rich in K and P, could be shifted to higher temperatures through co-combustion with bark. The formation of low melting phosphates sticking on the bed grain and causing agglomeration could be shifted to a Ca-richer environment where layer formation and Ca-diffusion are dominant. [116]
- Through mixed combustion of wheat straw with municipal sewage sludge (MSS) the negative bed agglomeration tendencies of wheat straw combustion could be prevented. Again this procedure shifts the conditions of ash chemistry from the formation of low melting K-compounds (K-silicate in this case) to bed ash of higher melting points. As demonstrated by Grimm et al. the composition of the emitted particles changed from an abundance in alkali chlorides to alkali sulphates [115]. [117]

Various additional papers could be investigated for their accordance with the results obtained in those mentioned in the previous chapter, e.g. [108, 118–121]. Obviously the theory of ash transformation chemistry coincides excellently with the practical research.

2.5.2 Quartz

The utilization of quartz sand as bed material has been previously approached a lot with different process parameters (e.g. feedstock, temperature).

Agglomeration experiments in a FB system under both combustion and gasification conditions have been investigated by Öhman et al. [44]. Five different fuels have been used as feed (bark, Lucerne, reed canary grass, bagasse, olive flesh and cane trash). The resulting data provided

initial agglomeration temperatures (IAT) of more than 660 °C and a comparison between gasification and combustion. Agglomeration could be achieved using every fuel except bagasse in the range of 660 °C to 1020 °C. The differences between gasification and combustion could be obtained, showing a slightly decreasing IAT for bark, olive flesh and cane trash and increasing values for reed canary grass and for Lucerne. Nevertheless the only major difference was obtained for Lucerne, whose IAT decreased from 840 °C to 660 °C when switching from gasification to combustion conditions. [44]

The layer formation in both types of conditions was determined as a homogeneous inner layer and a particle-rich outer layer on the bed grain. The analysis of those layers demonstrated no major differences in the layer formation mechanisms between gasification and combustion. A dominance of Si, K, Ca and O in the inner layers was analysed as well. An exception has been observed when Lucerne was used, where a melt induced agglomeration during combustion due to relatively high S content leads to a significantly decreased IAT. [44]

Similar results have been obtained when using BFB and CFB systems by Brus et al. with wood-based bark, reed canary grass, peat, olive residues, and straw as feedstock [107]. The layers formed on the bed material could be distinguished to consist of an inner layer and an outer layer as well. Energy-dispersive X-Ray spectroscopy (EDS) analysis of both those layers demonstrated high resemblance of layer composition of the inner layer to the bed material composition and of the outer layer to the fuel ash composition. Furthermore the inner layers have been found to grow into the bed grain due to chemical reaction, leading to the formation of Ca-silicates when being directly in contact with ash-dominated outer layer and (K,Na)-silicates when Ca containing matter is not available. [107]

While Ca-silicates formation through diffusion of Ca into the bed grain is described by the coating induced mechanism and creates low melting silicate compounds, the formation of low melting (K,Na)-silicates seems to be not induced directly by the ash matter but through direct attack of alkali compounds in gaseous or aerosol state (see 2.5). The thermodynamics are consistent with those observations, although Ca-silicates are most stable and to be found were (Ca-rich) ash is in interaction with the bed material the formation of (K,Na)-silicates is benefited when interaction of the bed material is not directly with ash but volatilized alkali components. [107]

Scala & Chirone used two different separating cuts of quartz in the intervals of [212,400] μm and [600,850] μm as bed material in a FB system combusting olive husks and pine seeds [122]. As described in Chapter 2.3, these fruits are enriched in K nutrients, which they need for fast, seasonal growth. Major difference between those feedstocks is the Si:Ca ratio.

The influence of these parameters in combination with bed temperature, fluidization velocity and bed particle size have been investigated. In conclusion with thermodynamics, agglomeration is favoured by higher bed temperatures, smaller bed grain and higher ratios of alkali to earth alkali elements in the ash. The initiation of agglomeration in the experiments through combustion of feedstock furthermore created hollow spaces within the agglomerates where feedstock particles had been priorly to being combusted. [122]

A difference of outer and inner layers has been reported by Scala & Chirone as well. The inner layer seems to be embedding the grain fully and continuously, while the outer layer forms an attachment between the particles only consisting of several neck-shaped layers. The molten ash fraction is enriched in lower melting components (K, Na) whereas the deposited ash is enriched in Ca. These observations on one side and the relatively high ratio of K:Ca on the other side would lead to the conclusion, that agglomeration with this type of biomass is dominated by the mechanism of direct adhesion of molten bed ash. [122]

Using a quartz bed in FBC systems with P-rich fuels Grimm et al. established a good data

base [108]. The investigation compares P-lean biomass fuels (bark, willow, logging residues, wheat straw) with P-enriched fuels (distillers dried grain with solubles (DDGS), rapeseed meal) in reference to initial defluidization temperature (IDT), layer formation and composition analysis. Experiments when firing or co-firing fuels with high contents of K demonstrated a high tendency for defluidization at lower temperatures than fuels of woody type. Especially the combustion of DDGS led to total defluidization prior to the planned combustion and process stop. [108]

For logging residues, bark and willow (Ca-rich, K-rich, P-lean) the inner layers on the bed grain were dominated by Si, K, and Ca and agglomeration is initiated by reaction of gaseous or liquid K with superficial Si of the bed material. Furthermore, the Ca-enrichment leads to diffusion of Ca into the melt. In combination with the formed K-silicates this leads to low tendencies of agglomeration at combustion temperatures. Of these three fuels, willow has the highest K:Ca ratio and therefore it demonstrates the relatively low IDT. [108]

Since the ash of wheat straw is enriched in Si and especially K, the layers on the bed grain are dominated by alkali-rich silicates leading to agglomeration due to direct adhesion of molten ash. Due to low melting temperatures of those compounds, agglomeration tendency is rather high at moderate combustion temperatures (IDT: 750 °C). [108]

The addition of phosphoric acid to those biomass fuels shifts the elemental ratios of P:K to higher values. In agreement with the ash transformation chemistry the dominance of K-Ca-silicates in the bed ash is substituted by K-Ca-Mg phosphates. When high contents of P are added (P:K = 0.9) thick non-continuous outer layers of Si, Ca, P, and K could be found, whereas the inner reaction layer was absent. The interpretation provided suggests, that K reaction on the grain was not fully purged at P-low addition, but at P-high concentrations the K may be captured almost totally, eliminating the potential for the formation of inner layers. The synthetically prepared fuels through P-addition therefore show similar behaviour to basically P-rich fuels (DDGS, rapeseed cake). [108]

The comparison of the entity of experiments executed by Grimm et al. demonstrates the dominance of P in the ash melting and agglomeration behaviour. This is in accord with the thermodynamics theory presented in Chapter 2.5.1. [108]

The most recent paper, demonstrating especially the time dependency of layer formation on quartz particles in FB systems, was made by He et al. [119]. The experiments were executed in two different full scale FB systems, one representing a BFB (woody biomass) while the second one was operated as CFB (sawdust). After defined times of operation (1 to 13 resp. 23 days) samples were taken from the bed material and via scanning electron microscopy (SEM) and EDS the formed layers were examined for structure and composition. [119]

The BFB process provided images of cross sections through the quartz particles containing unreacted cores, outer layers resembling the ash and discontinuous inner layers with cracks. Those cracked layers mainly consisted of Si with low amounts of K, Ca and Na and did not vary significantly for different operational times. In comparison to normal inner layer those cracked layers were enriched in K and Si, with lower shares of Ca. The intensity of cracked layers on the surface of bed particles increases for grains of longer dwell durations in the reactor. A comparison of all samples in the time frame may be seen in Figure 5. [119]

The CFB process shows similar structures and composition in reference to cracked layers as the BFB process. Again, the cracked area and at the same the K-share within those areas increases for bed particles of longer hold up. The major difference between the two operational modes is found to be the thickness of the outer layer, which is thinner when CFB conditions are applied. Images of the cross sections may be seen in Figure 6.

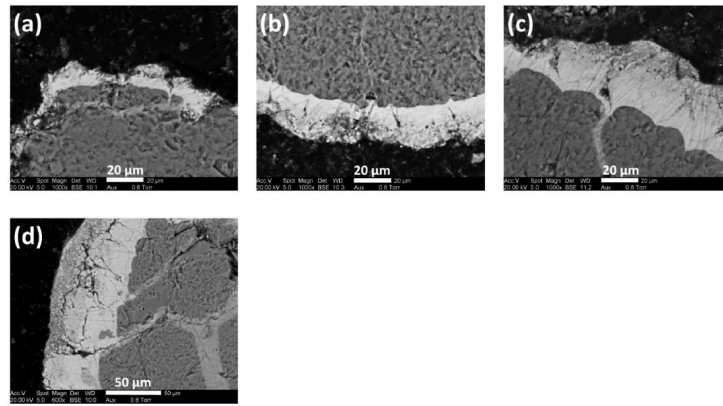


Figure 5: Cross sections of K-feldspar bed grain samples taken from the BFB process after (a) 3 days, (b) 5 days, (c) 13 days, (d) 23 days [119]

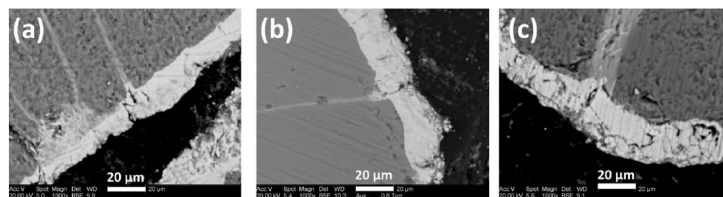


Figure 6: Cross sections of quartz bed grain samples taken from the CFB process after (a) 5 days, (b) 11 days, (c) 13 days [119]

The formation of crack layers seems to be initiated by formation of inner layers and reaction phenomena into the quartz particles. There the mechanism of direct attack of gaseous K-compounds is of high relevance and enhances the formation of cracks. In agreement with ash thermodynamics, a scheme for the formation mechanism has been postulated as shown in Figure 7: [119]

- 1 Formation of the inner layer on the quartz particles through Ca diffusion, therefore Ca-enrichment and creation of Ca-silicates
- 2 Cracks in the formed inner layer initiate tensions on the surface of the bed material, eventually cracking this surface. Through these cracks the surface is exposed to gaseous K-compounds which might diffuse and react into this area, creating K-silicates. This is followed by the reaction and diffusion of Ca.
- 3 The formed cracks are enlarging and the layers on top of the cracked layer may break off, exposing the crack layers to the gaseous phase which leads to additional diffusion of K into the crack layers. Through formation of low melting alkali-silicates the quartz surface is fragmented and the cracks are propagating.

Due to the vast amounts of research in reference to quartz utilization in FB systems it is not possible to cite all of them here. Nevertheless the quantity of presented papers shows the high potential of application and the high degree of knowledge about quartz used as bed material.

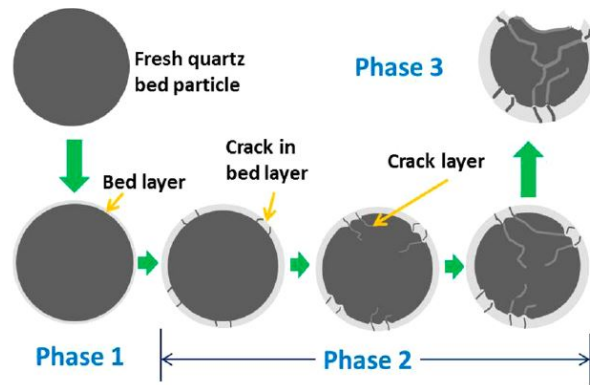


Figure 7: Schematic mechanisms of crack layer formation on quartz particles in FBC of woody biomass fuels [119]

2.5.3 Feldspar

Utilizing feldspar as bed material is an interesting approach for FB systems due to the properties stated in chapter 2.4. There are several options, which cation is taking the place within the tetrahedron silicate structure (mainly K and Na). Therefore research regarding similarities and differences when used as bed material in FB systems between the different types of feldspar are necessary. There have been conducted previous analysis experiments, which provide a large set of data for additional research in this field of study. Apart from layer formation and agglomeration mechanisms it has been proven, that gasification processes using feldspar are benefiting from those layers. The H_2 yield has been increased as well as the tar amounts produced during gasification have been reduced significantly [123].

A detailed study about layer formation in conjunction with time-dependency was made by He et al. [120]. The experiments were executed in two different full scale FB systems, one representing a BFB (woody biomass) while the second one was operated as CFB (sawdust), same as in the study by He et al. with quartz particles [119]. After defined times of operation (1 to 11 resp. 23 days) samples were taken from the bed material and via SEM and EDS. The formed layers were examined for structure and composition. [120]

The bed samples from the BFB process showed inner layers mainly consisting of Ca, Si and Al and outer layers composed of Ca, Si and Mg. Evidently the layer formation mechanism is strongly time dependent, demonstrating two easily distinguishable layers on the bed grain sampled after 23 days but almost no visible layer on the grain sampled after one day. The formation of an outer layer was detectable only when the process time was 3 days or longer. For older particles cracks in the inner layer and irregular interfaces between inner layer and feldspar core could be observed, a comparison of all the samples in the time frame may be seen in Figure 8. [120]

A detailed analysis of the composition as a function of distance from the core particle has been elaborated, the major result being a positive Ca-gradient and negative gradients for Si, K and Al from the inner to the outer layer. Furthermore, a substitution mechanism in the feldspar particle has been indicated, where Ca^{2+} cations take the K^+ place in the hollow gaps in the tetrahedron structure. [120]

For the CFB experiments similar observations could be made. Inner layers consisting of Ca, Si and Al and outer layers of Ca, Si and Mg were visible in the SEM image as well with increasing thickness for particles with longer dwell duration in the reactor. Moreover the longer processing of bed material increases the share of Ca in the inner and outer layers to the disadvantage of Si

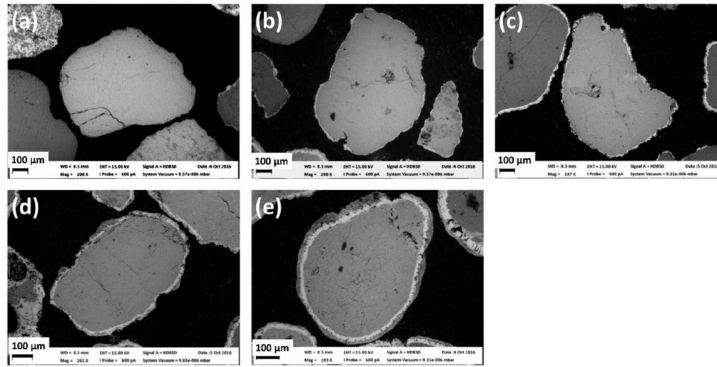


Figure 8: Cross sections of K-feldspar bed grain samples taken from the BFB process after (a) 1 day, (b) 3 days, (c) 5 days, (d) 13 days, (e) 23 days [120]

and Al. Obtaining the elemental compositions of the rather thin layers on particles with only 1 day hold up was impossible. The increase of the Ca share not only on the time scale but from the inner towards the outer layer and Ca^{2+} substitution mechanisms were observed in agreement with the BFB experiment. In comparison to the BFB process, the average layer thickness was decreased in the CFB operation. Images of the cross sections may be seen in Figure 9. [120]

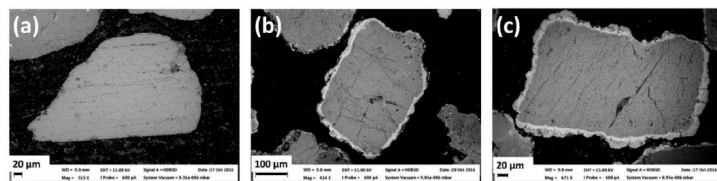


Figure 9: Cross sections of K-feldspar bed grain samples taken from the CFB process after (a) 1 day, (b) 5 days, (c) 11 days [120]

The results of K-feldspar utilization were compared to those of quartz utilization. While the agglomeration and layer formation processes in quartz FB systems are initialized by reaction of gaseous K-components [119], the initial layer formation in K-feldspar systems is due to molten ash of K-silicates, where Ca^{2+} is diffusing into the grain surface and takes part in the described substitution process. Since this occurrence is strongly time-dependent, particles of longer dwell duration in the reactor indicate the formation of Ca-rich layers on the very surface leading to the formation of an additional (outer) layer. Mathematical approaches to this diffusion mechanism are in agreement with the time correlation in the experiments. The formation process of the inner layer therefore seems to be controlled and determined by the diffusion of Ca^{2+} towards the feldspar particle which implements 4 steps shown in Figure 10. The phases can be described as follows: [120]

- 1 Inner layer formation through Ca diffusion into the ash melt; the inner layer grows inwards into the bed particle and creates the inner layer rich in Ca, Si and Al
- 2 Disappearance of the molten phase due to continuous diffusion of Ca^{2+} into the melt and accumulation of the same on the outside of the inner layer (time-dependent; not visible for particles of shortest hold up)
- 3 Layer growth slowed down due to longer diffusion distances (the amounts of new Ca^{2+} reaching the bed particle surface is decreasing)

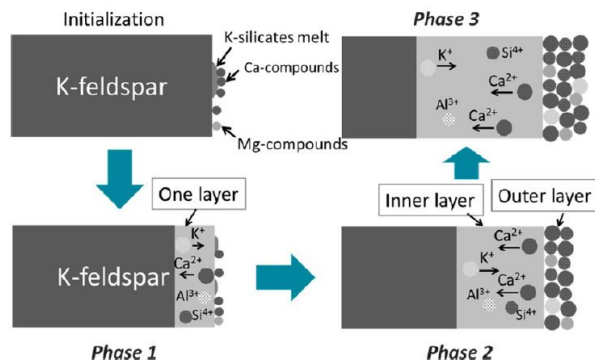


Figure 10: Schematic mechanisms of layer formation on K-feldspar in FBC of woody biomass fuels [120]

Analysis of layers might be aimless, if operation time is kept too short. The operation as CFB and BFB demonstrated differences mainly in the thickness of the outer layer, not so much in composition or thickness of the inner layer. The main difference to the usage of quartz bed is the absence of cracks within the bed material structure, which were proposed to be a consequence of an attack of gaseous K-compounds [119].

2.5.4 Olivine

Olivine bed material in FB systems is used on industrial scale already [124,125]. This is mainly related to its hardness, the high heat capacity and the catalytic function towards gasification processes (e.g. water-gas shift reaction) [98,99]. The catalytic function leads to decreased amounts of tar and interaction with Ca-rich components can improve this function even more [125,126]. Therefore the majority of research has been made in relation with FBG systems so far. Since this work is focussed on the ash chemistry, the improvement of product gas composition with olivine bed material may be obtained via the previously mentioned references.

Typical biomass fuels have been combusted in a bench-scale BFB reactor with olivine bed material by Grimm et al. to identify the bed agglomeration mechanisms [109]. Variation of biomass fuels (willow, logging residues, wheat straw, DDGS) and its influence on the ash chemistry has been researched. The layer formation and agglomeration tendencies were compared with experiments using quartz bed material. [109]

For fuels with K-dominance in the ash fraction (DDGS, wheat straw) the bed agglomeration mechanism was identical for both quartz and olivine bed material. The layer formation and bed agglomeration went through the mechanism of direct adhesion of bed grains via partially molten ash. While the agglomeration process during combustion of wheat straw (rich in Si and K) is initiated by K-silicates, the DDGS agglomeration is driven by K-Mg-phosphates (due to the main ash elements K, P, Mg). The Ca-deficiency and K-enrichment in the ash formed leads to decreased defluidization temperatures of less than 800 °C. The variation of bed material did not shift the IDT significantly. The agglomeration with these two fuels reflects option 3 as described in Chapter 2.5. [109]

For fuels with Ca-dominance (logging residues, willow) an increase of IDT when using olivine bed material could be obtained. During quartz bed combustion mechanism 1, as described for woody biomass in Chapter 2.5, initiated the agglomeration process. Necks and inner reaction layers dominated by Si, K, and Ca are found, which are responsible for the agglomeration process. The IDT was mainly influenced by the Ca:K ratio. Higher shares of Ca led to a decreased

agglomeration tendency of logging residues in comparison to willow. [109]

The main difference when applying olivine bed material is the absence of K in the inner layers, which were dominated by Mg, Si, and Ca. For K the thermodynamics prove higher tendency to be volatilized than to react with the olivine, whereas Ca shows high tendency to form Ca-Mg-silicates on the olivine bed grain. The shift from the K-dominance to the Mg-dominance in the resulting inner reaction layers increases the IDT significantly, since these layers do not agglomerate at FBC temperatures. Agglomeration necks found in the olivine bed showed stronger resemblance to the ash composition than the inner reaction layers. Therefore the agglomeration process during the combustion of woody biomass in an olivine bed is driven by K-silicates derived from the ash particles. [109]

A description of the very specific mechanism of layer formation on olivine bed material during DFB steam gasification was made by Kuba et al. [127]. From a 4 MW biomass gasification plant bed material samples were taken at different operational times and investigated via SEM. Wood chips were used as feedstock and CaO was added during the start-up to increase the initial catalytic activity (see Chapter 2.5.5). [127]

The thickness of formed layers on the olivine was shown to be strongly time dependent, an observation already proven for the aforementioned bed materials. Total coverage of the olivine surface with layers could not be seen before 16 hours of operational time, a distinction of inner and outer layer could not be made for samples extracted before 24 hours of operational times. An increase of operational time did not change the inner layers thickness significantly, whereas the outer layers thickness increased. If the operational time exceeds 180 hours the inner layers demonstrates another discrimination and consists of two zones. After the longer operational times the layers often show cracks between inner and outer layer with the occurrence of broken outer layers. If those cracks are perpendicular to the olivine surface the layers may also penetrate the bed grain. [127]

The first layers created resemble the original olivine particle, the main difference is an increase of Ca, which is introduced through interaction with the ash. Notably, though K is present in significant amounts in the ash (12.3 % K_2O), it does not take part in the layer formation process (as seen in Chapter 2.5.2). For the particles of longest dwell duration (400 hours) three sectors may be identified, since the inner layer consists of two areas. Composition analysis of those 3 areas and the cracks formed within demonstrates the highest Ca shares to be in the inner zone of the inner area, the lowest value is obtained from cracks. The Mg shares then again are highest in the outer zone and the crack area. The mechanism proposed by Kuba et al. describes this phenomenon through a replacement process, where Ca^{2+} takes the place of either Fe^{2+} or Mg^{2+} in the olivine structure and release of MgO. [127]

In initial layers after 4 and 8 hours the enrichment of Ca and absence of K was demonstrated in accordance with aforementioned papers. Therefore the initial step may be described as solid state reaction between CaO and olivine. The presence of low-melting K-silicates, which may promote adhesion processes, is mentioned as well by Kuba et al. and is brought up as an intermediate supportive to Ca^{2+} transport. [127]

The mechanism proposed for the intrusion of Ca into the olivine matrix is a substitution of Fe^{2+} or Mg^{2+} by Ca^{2+} in the matrix and thereby the formation of Mg-Ca-silicates. The substitution is of Fe^{2+} is statistically preferred and may therefore happen at earlier stages. This leads to the conclusion, that short operational times would tend to create Fe-rich melts once the Ca-rich layers have formed. The separation of inner and outer zone within the inner layer is based on the following process of Mg^{2+} substitution, which takes place after longer times of operation. A mechanism scheme for the transformation from olivine Mg-Ca-silicates is depicted in Figure 11. [127]

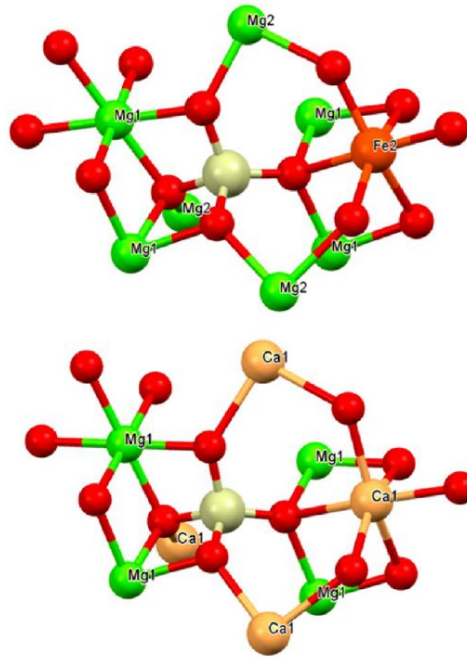


Figure 11: Proposed substitution mechanism to create CaMgSiO_4 from olivine ($\text{Mg}_{1.8}\text{Fe}_{0.2}\text{SiO}_4$) through intrusion of Ca^{+2} [127]

2.5.5 Lime

The use of CaO/CaCO_3 for SER technology and to enhance the H_2 yield in the product gas has been discussed in Chapter 2.4.1. It has been stated, that CaO (as well as MgO and CaO-MgO -mixtures) shows high catalytic activity for H_2 conversion and tar reduction in FBG systems [128]. CaO is the desired component to form layers on other bed materials to provide catalytic potential [125]. The layer formation on CaO/CaCO_3 particles is not studied yet.

A study on DFB steam gasification with CaCO_3 as bed material has been conducted by Benedikt et al. [102]. A comparison was made between olivine and calcite bed materials in a 100 kW DFB steam gasification pilot plant. CaCO_3 was used due to easier handling and lower security standards and the temperatures within the gasification systems guaranteed calcination to CaO . Therefore the actual bed material which came into use was CaO (with small amounts of impurities). [102]

The utilization of calcite as bed material for wood and lignite combustion did not demonstrate any problems concerning agglomeration or layer formation. The increase of H_2 and CO_2 share in the product gas as well as the decrease of CO and C_2H_4 was found to be caused by the catalytic activity of CaO , which is higher than the catalytic activity of other bed materials like quartz. Furthermore the advanced design of the DFB steam gasification reactor, which uses gravity separation units and increases the bed material hold-up, provides higher gas-solid interaction and prevents bed material attrition, which is an important factor when using lime. [102]

The attrition capability of lime has been investigated previously. Attrited lime substance may provide a source within FB systems for potential layer formation and agglomeration mechanisms, if those mechanisms are driven by Ca. Thereby a lot of research regarding the attrition and fragmentation processes of lime in FB processes has been made.

Yao et al. conducted an experimental research of calcite (CaCO_3) attrition and fragmentation in a fluidized bed with quartz bed material. It was observed that fragmentation and attrition

occurred as the limestone was inserted and mainly depended on the limestone type, original size, heating rate, calcination condition and CO_2 concentration. Particles analysed after the fragmentation process had decreased in the range of 10 to 20 %. Additionally the fragmentation process was found to be driven by the calcination process more than by thermal stress. Possible interaction mechanisms between the quartz bed material and the calcite fraction was neglected. [129]

Similar results were obtained by Chen et al. when investigating the attrition behaviour and energy consumption through attrition in a FB system [130]. Attrition was found to decrease for higher temperatures, if calcination is not taking place. For calcined lime particles the highest attrition rates were found, whereas sulfation (creating CaSO_4) decreased the attrition tendency. [130]

These and many additional studies regarding the attrition behaviour of lime suggest, that this phenomena need to be considered for bed material with significant lime ratios. A discussion of obtained results in conjunction with lime attrition is made in Chapter 4.8.

The major effects of CaO has been demonstrated to be as layer forming component on bed materials like feldspar, quartz or olivine [108, 120, 127]. The highly catalytic CaO itself is proven to be a potent catalyst for the water-gas shift reaction [102].

2.6 Aim

The main objective of this thesis is to analyse and compare the influence of key parameters in thermochemical conversion process on the agglomeration and layer formation mechanisms in a bench-scale FBC reactor and a 100 kW DFB gasification reactor. The focus is set on the conformity of theory and practice and the thermodynamics of biomass and waste ashes. Therefore bed material samples from the DFB steam gasification reactor after gasification of defined fuels with specific bed materials are extracted and analysed via SEM & EDS analysis. The objective is analysis and detection of new layer formation and agglomeration mechanisms. For comparative purposes and to evaluate the performance of the bench-scale FBC reactor an experiment with K-feldspar and bark pellets is executed and analysed.

In the long run the research of this thesis should help finding ways of improving the handling of thermochemical conversion processes and possibly identify approaches for the recovery of valuables, which are present in the ashes.

3 Material and Equipment

3.1 Feedstock

The feedstocks used for the experiments in this work are softwood (SW), coniferous bark (CB), German lignite (GL), municipal waste fraction, shredder light fraction, sugar cane bagasse (SCB), exhausted olive pomace (EOP), rice husks (RH) and hazelnut shells (HNS). To estimate the amounts and composition of ash created via thermochemical conversion during the experiments, the feedstock ashes have been analysed. For the feeding system in both applied FB systems the feedstock was pelletized and dried (if not mentioned otherwise).

3.1.1 Composition

The analysis results for ultimate analysis and ash composition analysis are depicted in Table 6 and Table 7 for the used feedstocks. The methodology was carried out according to DIN standard specifications. Two values for water content on total substance (TS) were not measured (EOP, HNS). Therefore they had to be extracted from literature data sets. A comparison of other key parameters between the used feedstock and the one described in the literature source demonstrated high accordance, which minimizes the error possibility. The depicted ash composition includes only ash forming oxides with a share of at least 0.1 wt% dry substance (DS) in at least one of the feedstocks. For the feedstock GL the ash composition data was unavailable, therefore an analysis by Yuanyuan et al. was set as approximation [131].

Parameter	Unit	SW	CB	GL	MWF	SLF	SCB	EOP	RH	HNS
Water Content	wt% TS	7.2	8.2	18.63	1.55	6.29	3.27	10.6 [23]	7.49	7.2 [23]
Ash Content	wt% DS	0.2	8.1	4.23	7.22	12.79	2.3	4.67	15.23	1.52
C	wt% DS	60.7	48.42	65.53	70.13	70.73	47.74	49.35	43.4	51.97
H	wt% DS	5.9	5.57	3.75	10.43	10.67	5.81	5.85	5.14	5.53
N	wt% DS	0.2	0.37	0.84	0.53	0.43	0.4	1.04	0.47	0.36
Cl	wt% DS	0.0	0.03	0.05	1.09	0.22	0.06	0.14	0.09	0.03
S	wt% DS	0.0	0.03	0.38	0.08	1.94	0.05	0.11	0.06	0.03
LHV	kJ/kg DS	18943	18180	19326	31479	31068	17861	18983	15893	19241

Table 6: Ultimate analysis of the feedstocks used for the experiments

The presented data in Table 7 only refers to the pure feedstocks. Since some experiments which are about to be analysed use mixtures of these feedstocks, they need to be categorized further. Table 8 shows the feedstock blends used for every experiment and the corresponding abbreviation for the results data set. The smaller scale of the FBC reactor in comparison to the DFB steam gasification reactor is shown by the big difference in feedstock mass. Information about the feeding system of feedstock mixtures (simultaneous feeding, successive feeding) are described in the regarding section of Chapter 4.

The amounts of thermally converted feedstock and the thereby produced amounts of ash in conjunction with the bed material mass inserted (see Chapter 3.2.1) into the reactor are of major importance. The ratio of bed material mass and theoretically produced ash mass during one experiment should be considered to approximate the influence and probability of ash induced phenomena. The ratio of bed material mass and theoretical ash mass is furthermore mentioned

Oxide	Unit	SW	CB	GL [131]	MWF	SLF	SCB	EOP	RH	HNS
SrO	wt% DS	0.47	0.20	*	0.09	0.11	0.08	-	0.01	1.23
PbO	wt% DS	0.02	0.01	*	0.08	0.26	0.01	-	-	0.01
ZnO	wt% DS	0.59	0.59	*	0.65	3.76	0.09	0.07	0.04	0.09
CuO	wt% DS	0.11	0.17	*	0.53	0.43	0.02	0.57	0.02	0.10
NiO	wt% DS	0.02	0.06	*	0.07	0.06	0.01	0.19	0.03	0.03
Co ₃ O ₄	wt% DS	0.01	-	*	0.01	0.01	-	0.41	-	0.01
Fe ₂ O ₃	wt% DS	0.91	6.21	3.86	3.22	2.59	2.07	1.19	0.47	1.53
MnO	wt% DS	5.44	2.51	*	0.09	0.07	0.26	0.04	0.23	0.51
Cr ₂ O ₃	wt% DS	0.02	0.09	*	0.26	0.20	0.04	0.53	0.02	0.04
TiO ₂	wt% DS	0.12	1.35	0.86	7.61	3.98	0.52	0.08	0.03	0.13
CaO	wt% DS	55.16	20.24	9.91	14.62	20.72	4.48	11.86	0.77	25.51
K ₂ O	wt% DS	13.4	3.29	1.04	0.63	0.37	5.91	42.51	1.57	38.56
Cl	wt% DS	0.01	0.6	*	2.94	4.58	0.03	3.54	0.22	0.34
SO ₃	wt% DS	2.95	2.09	6.09	1.42	3.99	2.92	5.28	0.49	4.94
P ₂ O ₅	wt% DS	3.07	3.08	0.30	1.22	0.75	2.15	8.07	0.80	8.17
SiO ₂	wt% DS	6.62	37.68	49.76	28.36	32.47	70.79	12.92	91.55	6.32
Al ₂ O ₃	wt% DS	1.63	10.76	19.71	30.95	15.00	5.59	2.47	2.07	3.85
MgO	wt% DS	8.35	7.12	2.11	2.41	8.92	4.26	6.08	0.52	7.66
Na ₂ O	wt% DS	1.07	3.81	4.20	4.70	1.55	0.66	4.12	1.16	0.92

Table 7: Ash fraction analysis of the used feedstocks regarding the occurring oxides
- marks values below the detection limit; * marks unmeasured values

Experiment	Unit	SW	CB	GL	MWF	SLF	SCB	EOP	RH	HNS
FBC	kg TS	-	1.63	-	-	-	-	-	-	-
DFB-01	kg TS	106.50	-	-	-	-	-	-	-	-
DFB-02	kg TS	-	-	17.33	34.67	-	-	-	-	-
DFB-03	kg TS	-	-	20.65	21.02	12.89	24.26	-	-	-
DFB-04	kg TS	-	-	-	-	-	-	-	-	64.28
DFB-05	kg TS	-	-	-	-	-	-	69.41	-	-
DFB-06	kg TS	-	-	-	-	-	-	-	115.20	-

Table 8: Amount of total feedstock mass combusted/gasified in every experiment

as " Theoretical Ash Load". This key parameter is calculated for every experiment in the corresponding section in Chapter 4 and defined in Formula 7.

$$\textit{Theoretical Ash Load} = \frac{\textit{Theoretically Added Ash Mass}}{\textit{Bed Material Mass}} \quad (7)$$

3.1.2 Pelletizing

An operational step of pelletizing had to be undertaken to create aggregates suitable for feeding into the reactor. Therefore the milled feedstock was pelletized in a flat die pelletizer equipped with a hole die of 6 mm diameter. The pelletizing process had to be repeated several times due to high moisture contents in the bark. The used pelletizing machine is depicted in Figure 12.

The output pellets were afterwards dried under atmospheric conditions to harden the structure and decrease the water content. The reference water content in this work (e.g. Table 6) always refers to the pellets after drying. For long term storage the pellets are filled into several labelled plastic barrels.



Figure 12: Flat die pelletizer by Cissonius GmbH [94]

Additionally to the bark material the feedstocks EOP and SCB had to be pelletized with the mentioned pelletizing machine. Details about the pelletizing process and additives are mentioned in the referring section of Chapter 4 (if information is available). The feedstocks MWF, RH and SW are bought and delivered pelletized. The feedstocks GL, SLF, and HNS are inserted into the reactor unpelletized.

3.2 Bed Material

3.2.1 Composition

The bed materials used in the experiments within this work are two types of lime (in the CaCO_3 -calcite-state), olivine and quartz for the DFB experiments and K-feldspar for the FBC experiment. The bed materials data is presented in data sheets delivered by the distributing companies.

A total chemical analysis of oxides content in the bed materials has been made by the distributors and is depicted in Table 9. The tabled data shows the dominance of the main constituents in every bed material type. Nevertheless, analysis results are showing, that impurities can not be neglected for a valuable analysis of the elemental composition via EDS.

Same as the feedstocks, the bed materials are mostly applied in the experiments as mixtures. The bed material mass and mixtures are shown in Table 10. An important factor concerning the calcite is the use as CaCO_3 , which decreases the total mass of bed material significantly after the calcination process. Bed materials which are recycled and used in multiple experiments will be indicated as such in the results section of the concerning experiment.

Oxide	Unit	CaO (KSW)	CaO (KS01)	Olivine	Quartz	K-Feldspar
SiO ₂	wt%	0.5	0.1	39 - 42	99.8	65.7
Al ₂ O ₃	wt%	0.3	0.1	<0.9	0.1	17.9
Fe ₂ O ₃	wt%	0.2	0.1	8.0 - 10.5	<0.1	<0.1
TiO ₂	wt%	-	-	-	-	<0.1
CaO	wt%	54.3	51.7	<0.5	-	<0.1
MgO	wt%	0.7	3.6	48 - 50	-	<0.1
K ₂ O	wt%	-	-	-	-	14.7
Na ₂ O	wt%	-	-	-	-	0.8
P ₂ O ₅	wt%	-	-	-	-	0.1
BaO	wt%	-	-	-	-	0.3
NiO	wt%	-	-	<0.1	-	-
L.O.I.	wt%	44.0	44.4	-	0.1	0.3

Table 9: Chemical composition of the bed materials used, given in oxides

Experiment	Unit	Lime (KSW)	Lime (KS01)	Olivine	Quartz	K-Feldspar
FBC	kg	-	-	-	-	0.05
DFB-01	kg	11.5	-	-	68.5	-
DFB-02	kg	14.7	-	-	65.3	-
DFB-03	kg	-	71.5	5.4	-	-
DFB-04	kg	81.4	-	-	-	-
DFB-05	kg	20	-	65	-	-
DFB-06	kg	28.5	28.5	12.7	-	-

Table 10: Bed material masses and mixtures used for every experiment

3.2.2 Particle Size

To obtain bed material suitable for FB systems the particle size has to be adapted to the available system. Since the parameters of the reactor are fixed, the only way of modification was through finding a separating cut for the bed material size. Therefore a mathematical model for the FBC system was set up, which estimates the regime in the combustion area in dependence of the particle size of the bed material.

The mathematical models for the FBC reactor prove the most suitable separating cut to be in the interval of [315,400] μm . To achieve this cut from the original material it was sieved with a laboratory scale sieving column by Retsch GmbH. Various cycles of sieving were executed and the fraction of [315,400] μm was extracted after every cycle. To get a more accurate separating cut the procedure of sieving was repeated once. The sieved bed material was stored in plastic cans afterwards.

The amount of bed material used for the FBC run was taken in relation to the dimensions of the FBC reactor and the approximate amounts of ash produced during one experiment. As seen in the following Chapter 3.4 the dependence of various parameters among each other needs the operator to choose some parameters by experience. One of these parameters is the mass of bed material used per experiment.

The novel DFB design guaranteed high flexibility for the particle size of the bed materials. Thereby sieving operations and the creation of specific separating cuts was not necessary. Nev-

ertheless, for some experiments the used particle sizes were adjusted. If an adjustment has been made, the referring data is shown in Chapter 4 for every experiment individually. The sieve analysis data of the original bed materials used during DFB steam gasification (lime, olivine, quartz) are shown in Figure 13.

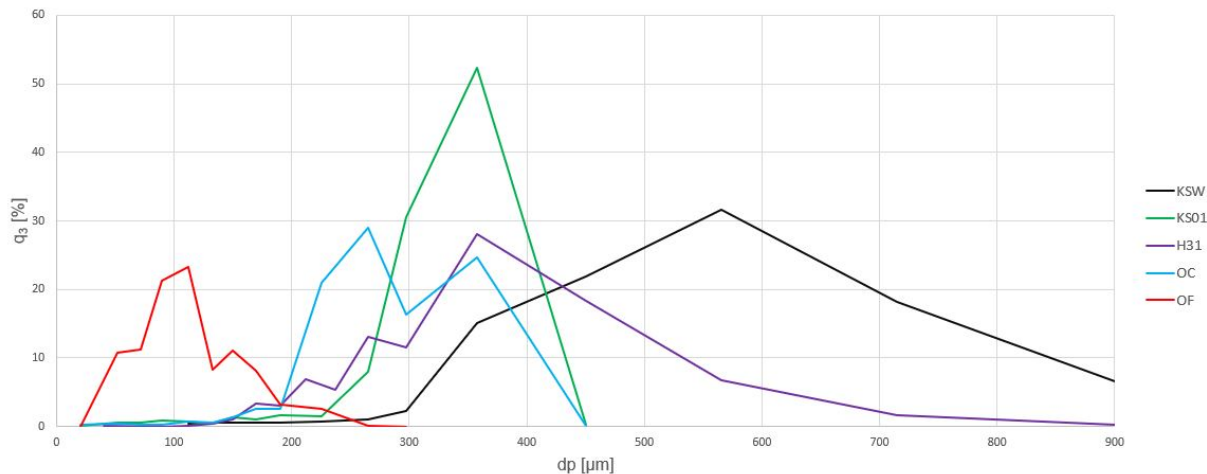


Figure 13: Particle-size distribution of the original bed materials CaO-KSW, CaO-KS01, quartz (H31), olivine coarse (OC), and olivine fine (OF)

3.3 Reactor Systems

3.3.1 Fluidized Bed Combustion Reactor

For research purposes a fluidized bed reactor was designed and constructed at the TU Wien. An initial set of data and parameters of operation was postulated as master thesis recently [132]. A set-up plan may be seen in Figure 14.

The figure depicts the functional schema of the FBC system applied for the purpose of this work. The individual parts are:

1: Fuel Bunker:

For the feed storage a fuel bunker is mounted, allowing process durations of several hours. The biomass may be inserted via filler plug or by taking of the cover plate of the bunker, emptying the bunker requires taking of the cover plate. During the combustion the bunker is purged with N_2 to avoid bunker fire.

2: Spiral Conveyor (Feeding Screw):

For the transportation from the fuel bunker into the reactor a specially for biomass pellets designed feeding screw is applied. The screw rotates and therefore conveys the pellets in a steel tube, the pellets enter the reactor above the reaction zone. A motor operated by a frequency converter regulates the rotation, via frequency modulation the transport rate may be adapted.

3: Sparger Plate:

The fluidization medium (in this work air) enters the reactor through a sparger plate containing 31 holes of 1 mm diameter. This guarantees not only a velocity increase of the

gas stream in these tubes but also prevents trickling bed material into the gas inlet tube. Therefore the bed material to be analysed after every experiment can be extracted from the reactor by dismantling the sparger plate.

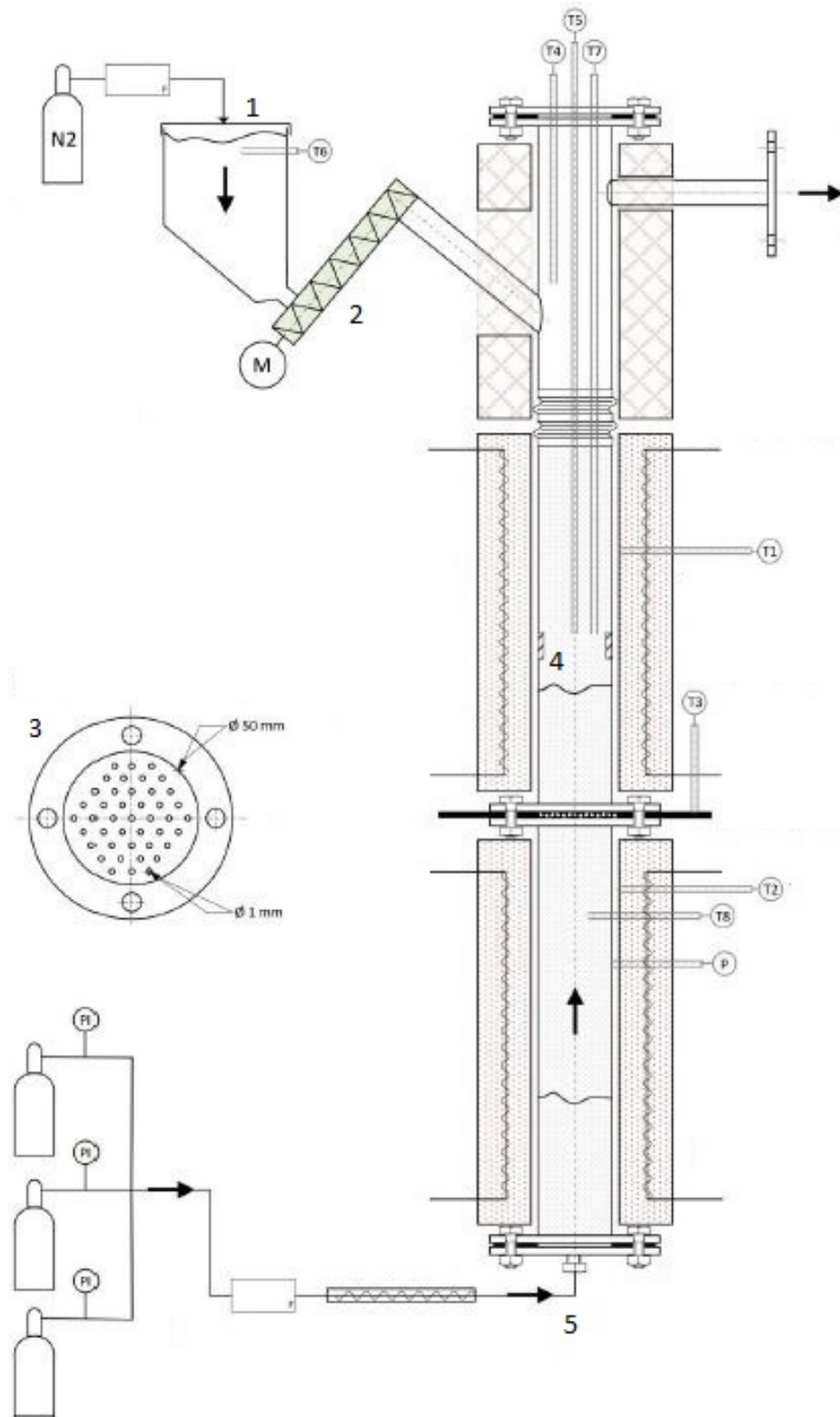


Figure 14: Design of the bench-scale fluidized bed reactor for the conversion of biomass at TU Wien; figure adapted from [132]

4: Combustion Area:

A steel tube with 53.1 mm diameter and 335 mm height is used as combustion area. Theoretical approaches and mathematical evaluation of the processes are built upon the parameters in this zone (e.g. height, diameter, temperature, pressure). All the thermo-chemical conversion of the biomass and the bed-ash interaction processes are taking place in this area. The combustion tube is heated by exterior heating shells.

5: Gas Inlet:

The type and amount of fluidization medium entering the reactor may be controlled by connection valves and a rotameter visible to the operator. The transport line contains various tubes, a preheating coat and the lower steel tube of the reactor, which is heated by a heating shell.

- Measuring Devices:

Process control and adjustment mostly depends on the measured parameters of the measurement units installed. The sensors depicted in Figure 14 do not reflect the installed sensors for the experiments, since one Temperature sensor (T7) was replaced by a pressure sensor. The sensors installed are:

- T1: Temperature sensor for the upper heating shell
- T2: Temperature sensor for the lower heating shell
- T3: Temperature sensor for the flange and the sparger plate
- T4: Not used
- T5: Temperature sensor for the combustion zone
- T6: Temperature sensor for the fuel bunker
- T7: Pressure sensor for the combustion area
- T8: Not used
- P: Pressure sensor for the gas inlet tube

Additionally an off-gas measurement is connected to the gas outlet of the reactor to guarantee combustion conditions within the reactor. The off-gas composition should not only reflect full combustion but also stable conditions for the duration of the experiment.

3.3.2 Dual-Fluidized Bed Steam Gasification Reactor

Based on already existing biomass gasification plants in Austria, cold flow model test runs, and simulation, a 100 kW dual fluidized bed (DFB) steam gasification pilot plant was erected at TU Wien in 2015. The main objective was to improve the gas-solid contact by using a counter-current column instead of the freeboard area. Furthermore the focus was on high system flexibility regarding the combustion of different feedstocks and gasification temperatures. [133]

The detailed setup is presented by Kolbitsch [133]. From an external measuring station all deciding input streams and the main parameters may be adjusted and output parameters may be controlled by the operator. The reactor design is schematically depicted in Figure 15. The main parts and also the sampling position (named coarse ash removal) are illustrated.

Since this work deals only with the bed material samples obtained after the experiments, the information presented will be limited to the following data:

- Schematic recording of main input streams and parameter during the experiments

- Composition and quantities of bed material used for every experiment
- XRF-analysis and quantities of the feedstocks applied for every experiment

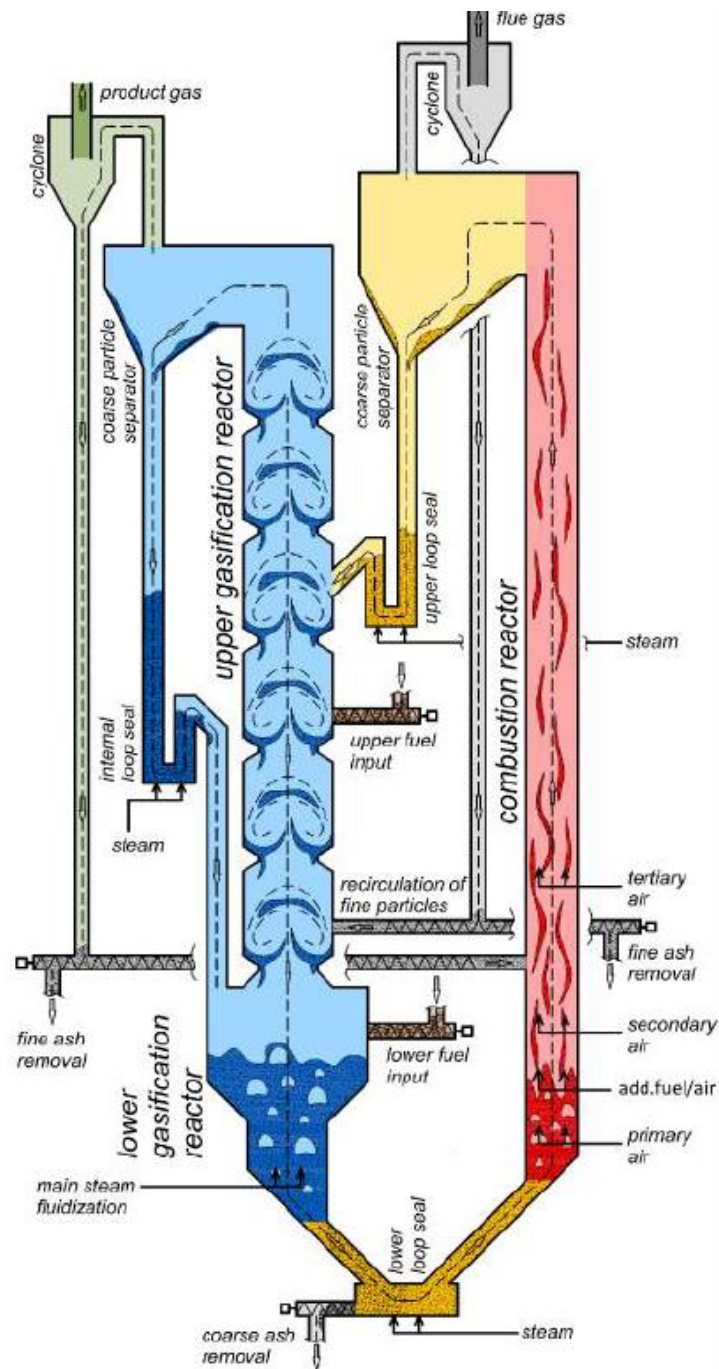


Figure 15: Design of the novel 100kW DFB steam gasification pilot plant at TU Wien [133]

For the purpose of analysis and interpretation of bed material samples and ash chemistry taking place during the DFB-process this set of data covers all the required information. The specified operation and controlling parameters are demonstrated in corresponding literature (e.g. [102,133]). The analysis for every DFB experiment is marked with the abbreviation "DFB" in Chapter 4. The feedstocks and bed materials used for each experiment are given in the Chapters 3.1 and 3.2.

3.4 FBC-Operation

3.4.1 Requirements & Limitations

Subsequent to preparing both feedstock and bed material the characteristic parameters of the FB systems need to be defined. To guarantee high comparability with literature data and within the experiments of this work a maximum of parameter should be set without change. For that reason the following settings and limitations have to be considered:

- Heating shell temperature (T1 & T2):
The maximum heating shell temperature of 1150 °C is defined by the manufacturer. The process requires these heating shell only in the time of preheating the reactor. Since they are deactivated during the combustion process, overheating is an event unlikely to happen. The heating shell temperatures may be recorded digitally for control purposes.
- Flange Temperature (T3):
The flange and its seals are limited by the maximum temperature of 900 °C. Since this value is below the maximum of the heating shells it is the limiting factor regarding the temperature in the FB system. Operational temperatures have to be adapted and may not exceed 900 °C for a long enough time span to overheat the flange. The flange temperature may be recorded digitally for control purposes.
- Combustion zone temperature (T5):
For the temperature in the fluidized bed a maximum temperature is not at hand, since limitation factors are just the occurring temperatures in the constructional elements of the reactor. Nevertheless, temperatures exceeding the limits of the maximum flange temperature (900 °C) should be avoided and handled with caution. Controlled exceedance might be applied for short time ranges and should be executed in the very final stage of the combustion process. The combustion zone temperature may be recorded digitally for control purposes.
- Fuel Bunker temperature (T6):
To avoid bunker fire through ignition of stored feedstock pellets the fuel bunker is purged with N₂. Furthermore the temperature within the bunker is measured and during combustion processing it should not exceed 40 °C. Practical measurements proved the temperature to be quite constant at 37 °C during the combustion experiments [132].
- FB pressure drop (T7 & P):
For the usage as FB reactor the measurements devices were adapted to provide data regarding the pressure drop. The significant value for this analysis is the excess pressure in the gas inlet tube. For constant values of flow stream the excess pressure rises with increasing temperature in the combustion zone (due to air viscosity increase) same as during the combustion process itself (due to the added ash matter in the reactor). The values for the pressure drop are plotted only for qualitative analysis (e.g. to demonstrate agglomeration processes) and are recorded digitally.
The pressure drop, same as the reactor dimensions, determine the amount of bed material used for the experiments. To minimize the probability of failure due to overflowing and to ensure high interaction with the biomass ash, the bed material mass should be kept as low as possible.
- Off-gas composition:
The analysis of the off-gas composition is performed to guarantee combustion conditions in the reactor. The analysed gas components are CO, CO₂, H₂ and O₂. For full combustion

with excess air the analysis should demonstrate absence of CO and H₂ in the off-gas, whereas CO₂ should be the major fraction with significant amounts of O₂ (approximately 8 vol%; see [113]). The off-gas measurement is the most suitable operation analysis during the combustion process for the operator and should be of minimum deviation between all the experiments.

- Operational time:

The amount of feedstock combusted in one experiment depended on both the feed rate and the operational time. To make sure, that high amounts of ash are available for interaction and with the knowledge about ash yields the conclusion was to combust approximately 1.5 kg DS of CB per experiment. The operational time of feeding into the reactor should stay constant for all experiments. With the settings applied within this work the operational time was 212 minutes.

- Feed rate:

Calibration of the feed screw and the motor proved the motor to be too potent for this kind of experiment. The result for the minimum feed rate at 0.5 Hz is 463 g feedstock per hour. To avoid gasification conditions at all time and guarantee full combustion with air excess the minimum air supply was set on 36 NL/min. Since this value for the gas flow rate ensures fluidized conditions without entrainment in the reactor the feed rate was kept at this value for the experiments.

- Gas volume flow:

To provide enough O₂ for full combustion conditions without discharging the bed material an optimum gas flow has to be determined on mathematical models. The minimum flow rate depends mostly on the feed rate, whereas the bed material defines the maximum flow rate. Mathematical evaluation through FB models have been executed and demonstrate a minimum flow rate of approximately 10 NL/min and a maximum flow rate of approximately 50 NL/min due to bed material data. Since the minimum air flow for full combustion has been found to be 35.2 NL/min, the actual range of possible air flow rates is approximately [36,50] NL/min.

3.4.2 Process

The fuel bunker is filled with an excess amount of biomass feedstock, isolated, and purged with N₂. The air flow is set in the range of 38 to 42 NL/min and only adapted within this range during the whole experiment. Through a filler pipe 50 g bed material (K-feldspar) is poured into the combustion zone, where it is instantly fluidized by the air flow. Afterwards all the heating aggregates are activated to heat the combustion zone, the gas inlet tube and the gas inlet line.

When reaching a temperature of approximately 650 °C the feeding screw may be activated to start the process of combustion. Due to endothermic drying processes the heating aggregates should stay activated until the off-gas measurement indicates the start of the exothermic combustion process. Subsequently the heating aggregates are turned off.

The thermal conditions in the reactor are controlled by the combustion process afterwards and the off-gas measurement should demonstrate an excess of O₂. The process needs to be stopped, when the combustion zone reaches a temperature of 900 °C due to the maximum flange temperature. After a short time of cooling the feeding screw is reactivated again and temperature in the combustion zone is controlled in the range of [700,900] °C at all time.

After the feedstock is fully combusted, a short temperature ramp is executed. Therefore the feed is not deactivated upon reaching 900 °C in the combustion zone. If pressure drop and temperature measurements indicate agglomeration processes taking place the feed is stopped and the experiment is completed. If the temperature ramp does not prove any agglomeration processes on short notice (5 to 10 minutes) the feed is stopped as well to avoid overheating of critical components. If agglomeration has occurred previous to the temperature ramp, this last step may be skipped at all. Before emptying the reactor it is cooled down under constant air flow.

3.5 DFB-Operation

The operation of the DFB reactor is discussed in Chapter 4 for every experiment individually, because the data provided for the analysis in this work refers just to overview operational modes. Operation and process control of the DFB experiments is not part of this thesis.

A quick overview for all the executed experiments is given by the following chronology:

- 1 Warm-up phase of approximately 4 hours with electrical heating and without feeding
- 2 Run-up phase with SW feed into the gasification reactor and heating oil into the combustion reactor to stabilize key parameters of importance for the operation
- 3 Steam gasification of the feedstock
- 4 Breaks and pauses when feedstock is changed, if necessary another run-up with softwood
- 5 Shut-down due to planned end or failure (e.g. defluidization)

The run-up phase with softwood is regarded an insignificant factor for the layer formation mechanisms due to the very low ash content. The main gasification process with the particular feedstock was designed regarding the lower heating value (LHV) of the feedstock. Feeding rates mostly were adjusted to guarantee standardized energy input. Details (if available and needed for the analysis) for every experiment are mentioned in the concerning section of Chapter 4.

For promoting the product gas yield and to improve the composition, sorption enhanced reforming (SER) processes are executed occasionally at the end of operation. This process calcines the lime material in the combustion area, which leads to CO₂ release and recycles CaO into the gasification reactor. Dependent on the gasification temperature it may take up CO₂ and releases the CO₂ into the flue gas from the combustion reactor again. This CO₂ removal from the product gas shifts the chemical equilibrium to higher yields of H₂. A schematic illustration of SER processing using lime is depicted in Figure 16.

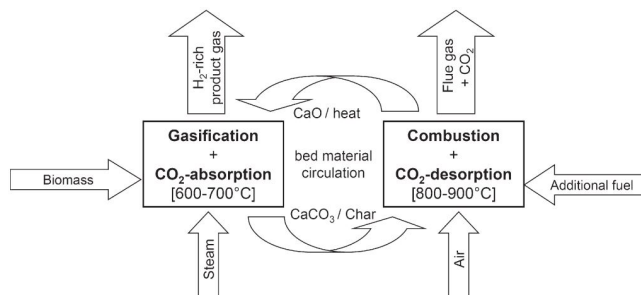


Figure 16: Schematic principle of Sorption Enhanced Reforming (SER) [134]

3.6 Sampling

After every test run the bed material was extracted and stored in glass jars specifically designed for grain samples. To prepare the samples for the following step of analysis via SEM and EDS, the bed material samples need to be stabilized in a solid matrix. Therefore an embedding preparation had to be made, which complies with the following requirements:

- No chemical reaction or physical interaction with the bed material
- Hard, non-brittle embedding material to allow grinding
- High contrast in the SEM and EDS analysis
- Preferably transparent for simplified optical control

Based on experience and on data sheets of different embedding materials, a powder-liquid combination was chosen. The powder:liquid ratio prepared for this mixture is 11:9. The bed material is embedded in plastic forms with the mixture and slowly stirred to avoid the formation of air bubbles in the matrix. Although the minimum hardening time is mentioned to be 20 minutes in the data sheet the samples were hardened more than two hours to avoid complications during the grinding process.

The hardened samples were ground with abrasives papers of different carborundum (SiC) granularities to open the bed material structure. Objective was to create a surface presenting plenty of bed material cross sections. The accomplishment of this task was controlled and verified via optical microscopy.

For bed material samples without lime the grinding method may use water to improve the polishing effect. Lime shows critical behaviour when ground with water supply, because it may react exothermically to create the highly basic $\text{Ca}(\text{OH})_2$. Since only the bed material obtained from the FBC process is free of lime, the main grinding method applied was the dry one. Differences in the resulting SEM and EDS pictures of the polished section are shown in Chapter 4. It may be observed, that wet grinding delivers smoother and steadier surfaces.

Another aspect of the dry grinding method is the blurring effect. Softer particles might gather layers of previously ground down material. This case could be observed for the rather soft lime where C-rich bed material could be found on the polished cross section. Detected C on the particle area was quantitatively unassigned because there are additional possibilities of origin (e.g. carbonated lime). Analysis on C-free and O-free basis made it possible to exclude false conclusions due to this smearing phenomenon. Comparison of wet and dry ground raw bed materials showed that impurities of C on the particle surface are increasing due to the dry grinding method.

For the electron microscopy analysis a preferably continuous layer of electro-conductive material should be coated on the surface to be analysed. Due to the low electric conductivity of the prepared surface, every sample was coated ("sputtered") with an AuPd-coating before inserted into the SEM and EDS analysis system.

3.7 Analysis Methodology

The prepared bed material samples were analysed with a "FEI Quanta 250 FEGSEM" analysis system for characterization of both crystallography and elemental composition. Thereby obtained SEM pictures and EDS analysis data (line scan, mapping) are the main output of this thesis and provide the basis for discussion about different layer formation and agglomeration mechanisms.

3.7.1 Scanning Electron Microscopy

The function of scanning electron microscopy (SEM) is based on the thermionic emission of electrons from a (normally tungsten) filament cathode. These electrons are accelerated through a voltage potential and rastered over the surface of the analysed sample. Through the interaction with the surface the electrons are reflected with specific energies indicating the elemental composition of the surface. The emitted different types of electrons (secondary, backscattered) can be detected and an image is created by the detector in conjunction with the software. [135]

The image created can reflect difference in energy potential of the detected electrons only. Therefore the images reflect different contrasts from black to white (mostly gray). Since the energy potential of the detected electrons depends on the elements with which it interferes, the contrast of a specific point or area gives information about elements occurring there. With increasing atomic number the image depiction gets brighter, excluding the brightness phenomena of edges and shadowing on the sample surface.

SEM analysis is used within this work to depict crystallographic phenomena of agglomeration and layer formation. The approximate identification of different types of areas in the sample may be accomplished with SEM images (ash, bed material, layers). In addition the analysis via EDS needs to be set on certain areas of interest, which are identified with the help of SEM picturing.

For a valuable analysis the following requirements in conjunction with the settings applied were considered:

- The SEM images should depict at least one whole grain to identify phenomena of local and overall occurrence. Therefore the magnification is set to picture an area of minimum 500 μm up to 2 mm in width. This allows to obtain pictures which reflect various particles, which is of greater importance if bed material mixtures are used.
- For focussed and exact pictures the distance between sample and pole piece should be minimized. In agreement with supportive experts a working distance of 10 mm was found to be an approximate objective. This facilitates the EDS analysis since this type of analysis requires a working distance of around 10 mm.
- The contrast between embedding carbon matrix and grains should be maximised to facilitate the identification. The contrast could be increased by using a diaphragm of higher diameter, a higher spot size than usually required for pictures and also through higher acceleration voltage. Although not recommended for pictures with high magnifications, the settings these three parameters were adapted to improve the discrimination of different specimen. The factor of diffusion was neglected because it did not occur significantly at the used magnifications.

- Not only the contrast between different matter has to be considered, but also the contrast and brightness overall. To enable adjustment of images after obtaining them from the SEM software, totally black and white areas have to be avoided. Therefore the images should be maintained in gray levels to allow discrimination but without losing information due to high brightening.
- The possibility of obtaining images via backscattered electrons was neglected due to organisational difficulties with the detector. This would have improved the contrast further. Through adjustments of acceleration voltage, spot size and diaphragm this way of improving the images was found to be not essential. For the purpose of this work only secondary electron detection as applied.
- Secondary electrons originate from the weakly bound valence shells or conduction band electrons. The detection of signals from these low energy electrons tends to show highly irregular behaviour when the secondary electron yield is compared to the atomic number of the sample elements. This effects leads to a contrasting problem, since surfaces of the same composition may be contrasted highly different due to complex interaction of different compounds (e.g. oxides, hydrocarbons). It needs to be considered, that secondary electron signals are generally not predictable and reproducible and a general contrast mechanism is hard to establish. If better correlation of atomic number and contrast is required, the detection of backscattered electrons should be the method of choice. [135]

The settings as they may be inserted via software are shown in Table 11. The values given are meant to be a guideline for the analysis methodology on the one hand, and for reproducibility purposes on the other hand. Nevertheless the exact settings need to be adapted to the analysis device. The settings listed in Table 11 are referring specifically to the "FEI Quanta 250 FEGSEM" at TU Wien.

Setting	Unit	Value
Magnification	-	100x - 400x
Working Distance	mm	10 - 15
Spot Size	-	3.5
Accelerating Voltage	kV	10
Image Resolution	Pixels	1536 x 1024
Diaphragm	-	3

Table 11: Applied settings for the generation of SEM images

3.7.2 Energy-Dispersive X-Ray Spectroscopy

The principle of EDS is based on the uptake of photon energy by inner shell electrons in the interaction volume of the beam. The originally bound inner shell electron is released and an electron from a higher energy level in an outer shell may take its place. The energy difference between the two shells is released in form of an X-Ray. The amount of energy is characteristic for the element and the shell were the electron is ejected and replaced (e.g. K-shell, L-shell). [135]

The EDS-detector is able to measure the charge of the released radiation and construct a spectrum. The spectrum created depicts peaks for every element with the statistical fluctuation in energy of the Gaussian distribution. Peak interference and broadening is likely to happen if data from different shells and elements interfere. Therefore the spectrum increases in complexity

if elements of higher atomic number than 20 or trace elements need to be measured. [135]

The spectrum might be adulterated as well by artificial peaks. One possibility of an artificial peak is the Si-escape peak. Here a Si K-shell X-ray escapes from the detector and decreases the measured charge intensity by its inherent energy (1.74 keV). Therefore a new peak is created, which does not refer to elemental occurrence in the sample. Another possible artificial peak is created through coincidental interaction of two photons, creating an energy level which is the sum of both photons. Artificial peaks occurring in the spectrum need to be identified and eliminated to achieve valuable qualitative and quantitative information. [135]

Another difficulty in EDS-analysis is the detection of the right stoichiometry for the element O. It creates comparably low energy X-rays which are readily absorbed by other elements. Therefore the quantitative detection of O can be misleading because its share may be decreased. This phenomenon was observed especially in lime (CaO) and quartz (SiO₂) particles. The aforementioned limitations of analysis need to be considered to obtain valuable data. [135]

The preparation methodology for the bed material samples requires additional considerations to be taken into account when analysing the elemental composition. First the embedding materials influence on the particles has been investigated. Due to the organic nature of the embedding liquid and powder, the detection of interaction area was facilitated. Nevertheless, interaction and interference phenomena may be neglected because it was unproven in practice. Secondary and more importantly the influence of the grinding process is considered. The used SiC abrasive papers in conjunction with the dry grinding method may lead to intrusion of SiC into the sample surface. This mechanism is of high importance for soft particles especially. Therefore the detection of C and Si on ground particle surfaces needs to be analysed carefully to avoid false conclusions.

EDS analysis of the prepared bed material samples was the most valuable analysis method for the purpose of this work. Areas identified via SEM imaging were inserted into the EDS-software which allows the handling of the EDS detection unit. Various ways of analysis could be applied for this chosen area through the settings of the used TEAM-software. The three applied steps of analysis (area report, line scan, mapping) are as follows (in chronological order):

Area Report:

The elemental composition of manually chosen rectangular areas within the inserted SEM surface images can be obtained with area reports. Multiple areas may be drawn on the shown surface section. The spectrum of every area may be recorded and the elements identified in the spectrum have to be verified and confirmed by the operator. This requires knowledge about the entity of possibly occurring elements in the section. The areas are analysed quantitatively for the elements and through weight and atom percentage the area composition and formed compounds may be identified.

Additional parameters need to be considered to produce valuable output data from the area reports and to support the data input for the line scans and mappings:

- The count rate should be maintained in the range of 10000 to 30000 counts per second, additionally the time lag should take 10 to 30 %. This could be adjusted via input adjustment of spot size and acceleration voltage.
- The area of investigation should not contain more than one identifiable phase. Area reports, which contain multiple particles or include embedding material, are blurring the analysed spectrum and are of little value for the quantification and identification of compounds.

- To facilitate the element input for line scans and mappings one area should cover the whole SEM image. This guarantees there are no unidentified areas left when obtaining the maps and scans.

Line Scan:

To obtain the radial dimension of layers (= thickness) and measure the radial distribution of elements (= composition) in the layers line scans were obtained. The line scans need to be drawn one by one and the elements possibly occurring in the line investigated need to be known in advance. Through counting the detected signals of every element on the line, the software creates a graph which depicts the counts per line section as a function of the distance from the starting point of the line. The output as atomic or weight percentage could not be obtained from the line scans. For valuable and exact line scan data the following criteria should be achieved:

- The count rate should be maintained in the range of 10000 to 30000 counts per second, additionally the time lag should take 10 to 30 %. Same as when doing the area reports this was achieved through modulation of spot size and acceleration voltage.
- To improve the information density of line scans, the step distance should be set on 0.1 μm (instead of 1 μm). This facilitates the analysis of layer thickness and delivers more precise element peaks. A big drawback of this method is the phenomenon of regressional counts. For a single step the detector does not proceed forward but takes one step back. This leads to line points which are counted twice and line points which are skipped. Errors occurring due to this mechanism may be identified easily nevertheless, because the count intensity drops significantly when the detector goes back instead of forward.
- Line scans should at least include 2 phases visible on the SEM image. Since the line scan does not have an output required for compound identification it is just used to measure clear contrasts along the line drawn. Therefore line scans were mostly drawn from the embedding material into the grains. For agglomeration phenomena the line should be drawn between two agglomerated particles or between ash and particle phase. Depicted Line scans refer to the layer and agglomeration areas and extract the key information, neglecting invaluable profile area (e.g. line profile which is drawn far into areas with constant composition). Line scans from the inner particle through the surface into the embedding material are marked as such.
- Line scans use beam intensities which may destroy the superficial structure. This phenomenon is generally observed during EDS analysis, due to the high energy of the beam. If multiple line scans are drawn they should not cross each other or run on the same line profile. The destruction potential of the line scan analysis is best visible on the lines which proceed into the embedding material.
- The element input in advance to obtaining the line scan data has to include every element of potential occurrence on the line. Unknown or unconfirmed elements can neither be detected nor confirmed after the line scan is done. Information about these elements is lost. Confirming the entity of elements detected on the overall image of the area report has proven to be the best method to avoid missing elements. Elements with detected percentage of less than 5 % are not evaluated quantitatively due to the large error intervals.
- Depicted line scans should be easily comparable between each other. Therefore the depicted analysis distances for line scans are standardized to 20 μm . Since the count rate highly depended on the specific condition of the analysed line profile a standardization could not be made.

Mapping:

The mapping takes the whole or a chosen part of the inserted SEM image and analyses the area for occurring elements. The raster drawn on the surface for the mapping may not only show the elemental composition but also the exact position of the elements. Via signal intensity an image for every element is created. There the position and quantity of the regarding element is depicted. The mapping proved to be the most valuable instrument for detection of layers, agglomeration and for particle discrimination. Through parametrization the software also generates atomic and weight percentages of similar areas on the mapping. Since similar areas are analysed as one common area, the error made through assimilation decreases the quantitative accuracy of this data.

To obtain valuable mapping data the following parameters and restrictions need to be taken into account:

- For image improvement the count rate should be set around 30000 counts per second. This may be achieved through an increase in spot size to 5. The disadvantage of this adjustment is, that the analysed area will be severely destroyed by the beam intensity.
- The high potency of the beam and the raster analysis system does allow only one mapping per area. Once a significant mapping has been made, the area (especially the area of embedding material) is severely damaged and another mapping would deliver biased measurement results. Test runs with secondary mappings of the same area showed, that the qualitative element distribution was unchanged, whereas the quantitative amounts (especially of C) were shifted.
- The element input in advance to obtaining the mapping data has to include every element of potential occurrence (and importance) in the area. Unknown or unconfirmed elements can neither be detected nor confirmed after the mapping is done. Information about these elements is lost. Confirming the entity of elements detected on the overall image of the area report has proven to be the best method to avoid missing elements in the mapped area.
- The output maps are getting more exact with every run of analysis. Therefore the software is trying to minimize the error and tries to execute as much runs as it thinks might be needed for highest accuracy. Practice and experience showed that approximately half of the (from the software) proposed runs were enough for the purpose of this work. Further runs did not improve the mapping images significantly.
- The area of investigation should include at least one whole grain. In the optimum way the area reflects every significant phase and component represented in the overall bed material. This is of special importance for the analysis of bed material mixtures.
- The evaluation of received mappings and composition data has to be made in conjunction with the observational error. The values of these errors increase for decreasing share of a specific element in an investigated area. Nevertheless values of less than 1 % might be detected on the mapping as enriched areas in comparison to areas of clear absence. To accommodate these potential misleading data potential, depicted mappings have to be in reference to (approximate) atomic share values. This avoids the possibility of drawing false conclusions from the data sets.

4 Results & Discussion

4.1 FBC - Evaluation

For applicability evaluation of a bench-scale FB reactor, a FBC process with coniferous bark (CB) feedstock and K-feldspar bed material is executed. The process is conducted to obtain information about agglomeration phenomena and layer formation on the used bed material in conjunction with the ash derived from CB. Aim of the experiment is to guarantee and verify process stability and valuable results.

4.1.1 Combustion Parameters

The key parameters of operation as mentioned in Chapter 3.4 are summarized again in Figure 17 again. For the potential classification of ash forming elements the atomic shares of every oxide forming ash component are depicted in Figure 17. The unusually high ash load of 243 % was applied for this experiment, since test runs showed that ash particles are mostly entrained during the process.

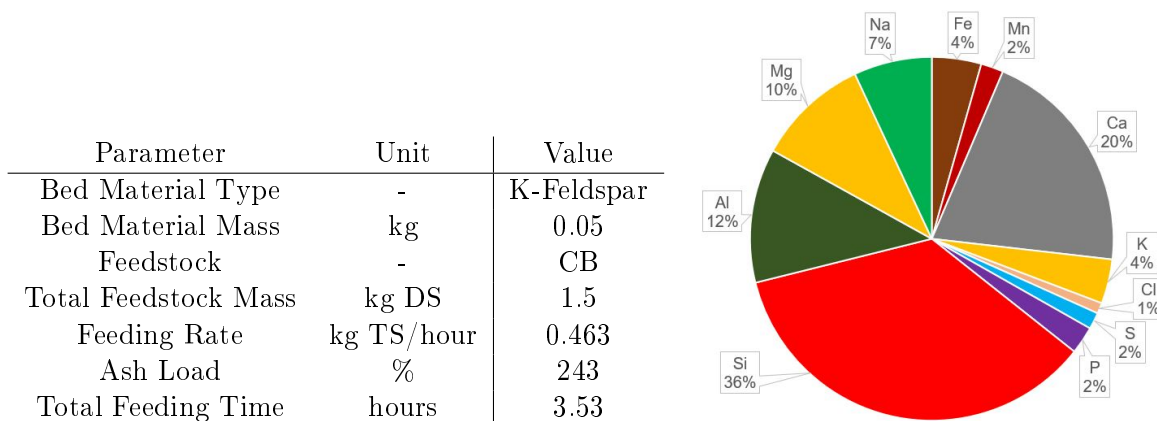


Figure 17: Key parameters for combustion and atomic shares of ash forming elements given in % during experiment FBC

The profiles of temperature and pressure drop in the fluidized bed during the combustion process are depicted in Figure 18. The trends showed increasing pressure drop values over time, which is a usual phenomenon when the amount of fluidized solid in the FB system increases. The sudden drops of temperature and pressure drop which show three times in the graph are due to temperature control. The temperature ramp in the end of the experiment led to an instant pressure drop, although the combustion process was not stopped. This is an occurrence indicating agglomeration processes are taking place, which could be verified when taking samples from the reactor.

4.1.2 SEM/EDS Analysis & Discussion

The analysis executed for the bed material of this operation mainly focusses on the potential of the reactor to perform processes which lead to agglomeration and layer formation. The conduction of FBC-processes in the previously described reactor has to be evaluated in reference to the

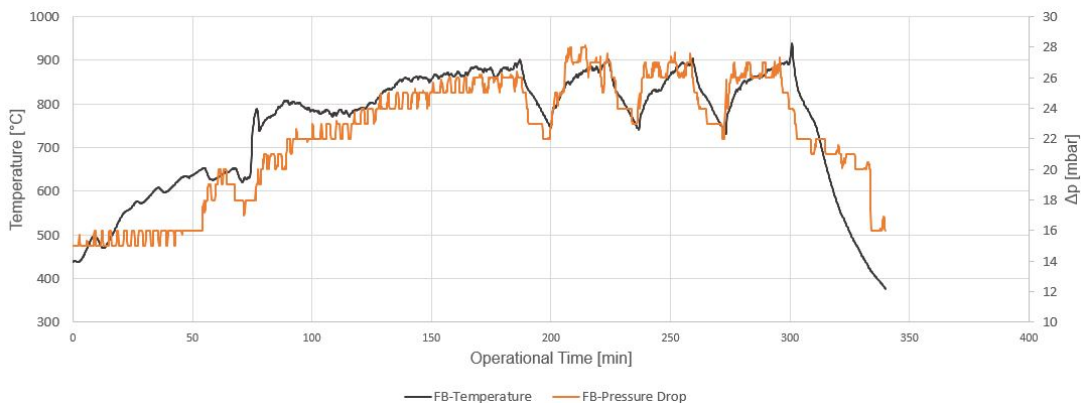


Figure 18: Temperature and pressure drop profile for the FBC experiment in the bench-scale reactor

results obtained. In the optimal case, the bed material analysis shows layer formation, agglomeration and provides information about the main driving forces which lead to this phenomena. A detailed analysis including the investigation of feedstock and bed material mixtures when using K-feldspar based bed materials is executed for the purpose of an additional work. The focus of this thesis is set on the evaluation of the reactor capability to provide valuable output data.

SEM analysis of the bed material sample obtained from the FBC reactor provided a multitude of agglomeration phenomena. The agglomeration mainly took place between K-feldspar particles and quartz impurities. To evaluate the composition and mechanisms which cause the agglomeration and layer formation an area of interest was investigated via EDS. The SEM image of the chosen area with a marked area for the map analysis is depicted in Figure 19.

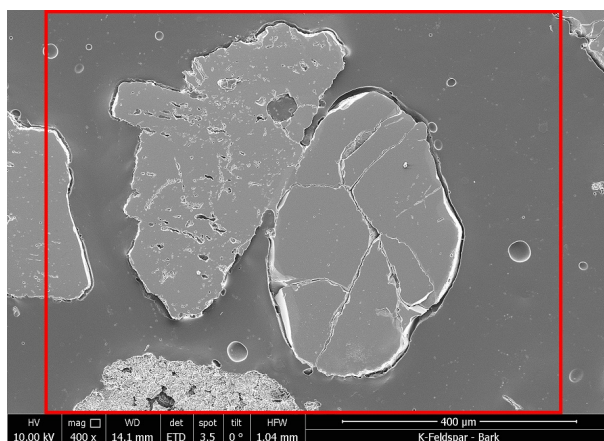


Figure 19: SEM image including the analysed area for mapping of experiment FBC. Visible are K-feldspar (left), quartz (right), and ash fraction (below).

The different nature of the particles in the investigated area is already visible in the SEM image. While the sample surface of the K-feldspar (left) is brighter and demonstrates unsteadiness the quartz particle (right) is smoother on the sample surface although it shows several cracks through the grain. In the lower part of the SEM image an ash derived fraction is visible as well. The surface brightness is increased due to the higher porosity in the particulate structure.

For evaluation of the mapping analysis, all ash forming and bed material elements are inserted

in to the software for detection. The distribution on the sample surface (mapping images) and the composition in specific areas (mapping quantification) were analysed. The whole set of analysed elements by mapping is: C, O, Na, Mg, Al, Si, P, K, Ca, Ba, Mn, and Fe. For reasons of evaluation all the mapping results which presented valuable information are depicted in Figure 20.

The depicted and the additionally obtained mapping results present valuable information for the analysis of layer formation and agglomeration processes. The layers on both analysed particles as well as the agglomerated area reflect clear profiles of the inherent elements. With focus on every elemental composition, a quantitative analysis in conjunction with the mapping images in Figure 20 provides the entity of necessary information and data. The compositional data of the three discriminable areas of K-feldspar, quartz and layer/agglomeration area are described separately.

The Si mapping in section (a) of Figure 20 demonstrates the different nature of the investigated grains. On a C-free and O-free basis the Si atomic share in K-feldspar was quantified to be approximately 59 %, while in the quartz grain it took an atomic share of approximately 99 %. In the layer/agglomeration area the atomic share of Si on a C-free and O-free basis was detected to be approximately 62 %. The available Si may originate in both the bed material or the ash forming fraction, since Si is the main ash forming element.

The Ca mapping in section (b) of Figure 20 demonstrates the layer forming potential of Ca on both grain types. While neither quantitative nor qualitative amounts of Ca are found within the grains, the average atomic share of Ca in the layer/agglomeration area is approximately 19 %. The mapping indicates stronger layer formation tendency on the quartz. For an evaluation of this observation the data output is insufficient.

The K mapping in section (c) of Figure 20 proves the nature of the K-feldspar particle and clearly detects layer formation tendency on the quartz grain and in the agglomeration area. The detected atomic share of K on a C-free and O-free basis in the K-feldspar grain is approximately 22 %, in the layer/agglomeration area it is approximately 12 %.

The Na mapping in section (d) of Figure 20 shows the limited amounts of Na in the K-feldspar and the layer/agglomeration area. Both areas provide only qualitative amounts of Na almost beyond detection limit. The intensity of detected Na peaks was too low to evaluate the shares.

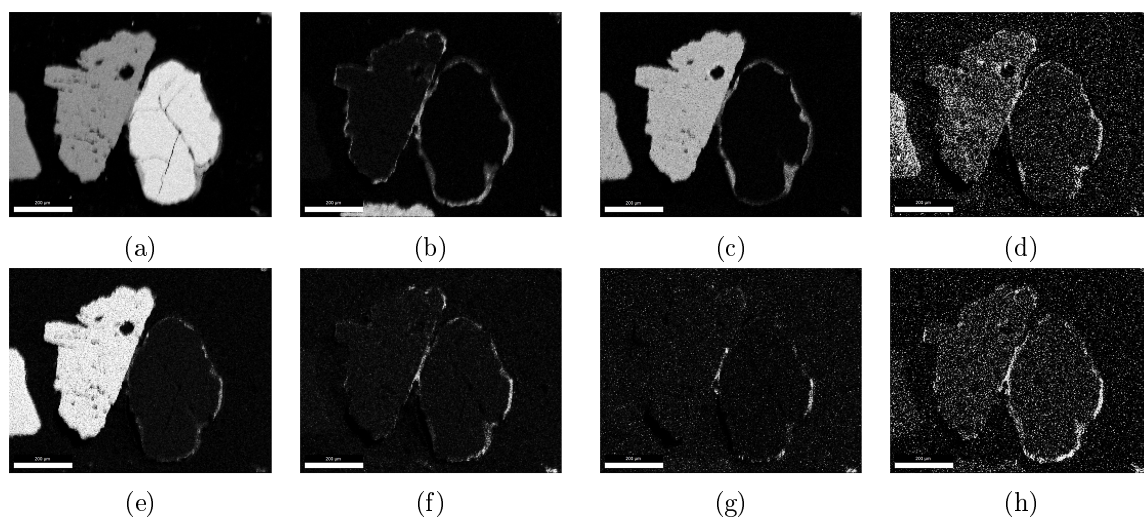


Figure 20: EDS mapping of (a) Si, (b) Ca, (c) K, (d) Na, (e) Al, (f) Mg, (g) P, and (h) Fe, obtained from the red marked area in Figure 19 for experiment FBC

The Al mapping in section (e) of Figure 20 demonstrates the enrichment in the K-feldspar particle and the qualitative detection of Al in the layer/agglomeration area. The atomic share of Al on a C-free and O-free basis in the K-feldspar is approximately 18 %. In the layer/agglomeration area Al can only be detected qualitatively.

The Mg mapping in section (f) of Figure 20 proves both particles to be free of Mg. In the layer agglomeration area the Mg atomic share can only be detected qualitatively.

The P mapping in section (g) of Figure 20 demonstrates the absence of P in the particles. For the layer/agglomeration area the amount of P can only be detected qualitatively.

The Fe mapping in section (h) of Figure 20 demonstrates Fe absence in the particles and qualitative amounts in the layer/agglomeration area.

The mapping results for the FBC sample provide a detailed and plausible data base for the analyses of layer formation agglomeration processes. The elemental composition data of the bed material particles proves them to be K-feldspar and quartz. Furthermore an enrichment of certain elements in the layers can be observed. The analysis results of the FBC process and the EDS analysis method complies with the requirements for the analysis of bed material samples. In terms of every investigated key parameter the following results and issues are of main importance:

- The main issue occurring during FBC operation is the feeding rate. The driving motor in conjunction with the gearing system proved to be too potent for the designed bench-scale FBC reactor. Basic operations like temperature hold and long term processing were unachievable due to the inappropriate feeding rate. Failure of the whole motor system due to interior overheating resulted in operation infeasibility, whereby only one experiment could be fully conducted.
- The operation of heating and temperature stabilization during the FBC process could be conducted without major troubles. Temperature hold at stable combustion temperatures could not be achieved due to unlowerable feeding rates. If these feeding rates could be adapted a temperature operation driven by the exothermic combustion process may be applied. Furthermore, the initiation of defluidization by temperature increase could be conducted easily as well.
- The bench-scale FBC system is qualified for operation over longer terms, if both fluidization and feeding rate can be kept in a steady state. For adapted particle-size distribution through sieving the entrainment of bed material can be minimized, whereas ash fraction is mostly entrained. For long term operation additional flue gas cleaning (e.g. cyclone) should be mounted. The application of additional gas cleaning methods would allow the possibility of creating detailed mass balances.
- High entrainment ratios for the ash fraction proved to be no major problem for the mechanisms of layer formation and agglomeration. Small amounts of bed material inserted and long term processing led to high theoretical ash loads and promoted the interaction of ash and bed material. For upcoming experiments the adaptation of the feeding rate and thereby decreased minimal air volume flow might make this excess of ash unnecessary.
- Enrichment phenomena of several elements in layers and agglomeration zones could be obtained through EDS analysis. The sample provided a multitude of possible research areas. Agglomeration phenomena were visible in high quantities. The presence of Si, Ca, K, Na, Al, Mg, P, and Fe in the layer/agglomeration area reflects the feedstock ash composition. The quantitative detection of Si-Ca-K compounds in the layer areas and adhesion happening through necks formed by these layers indicates, that agglomeration is coating induced by alkali silicates and Ca-diffusion into these melts. This corresponds to mechanism 1 as described in Chapter 2.5, which is expected for woody biomass combustion.

4.2 DFB-01 - SW

This experiment was evaluated as blind run for the following experiments. The influence of the ash fraction on layer formation processes in this experiments is minimized due to low ash yield and low theoretical ash load of the SW feedstock. Therefore the influence of bed material mixtures including quartz and lime on the layer formation should be approximated.

4.2.1 Gasification Parameters

The key parameters of operation are summarized in Table 12. For the results of SEM and EDS analysis of the experiment these key parameters need to be considered. Especially the theoretical ash load of 0.2 % decreases the potential of interaction between produced ash and bed material.

Parameter	Unit	Value
Bed Material	kg	11.5 Lime (KSW) 68.5 Quartz
Feedstock	kg DS	98.8 SW
Feeding Rate	kg TS/hour	21.3
Theoretical Ash Load	kg/kg	0.2
Total Feeding Time	hours	5
Approx. Gasification Temperature	°C	800

Table 12: Key parameters for gasification of experiment DFB-01

The atomic shares of ash forming elements derived from the feedstock are depicted in Figure 21. The dominance of Ca can be seen clearly, additionally the shares of K and Mg should be considered for the analysis. In conjunction with the low ash yield and theoretical ash load the main expected influence from the ash fraction is Ca. For feedstocks with low contents of Ca in the ash fraction the possibility of Ca-enrichment due to the run-up phase with SW can be considered using the atomic ratios depicted in Figure 21.

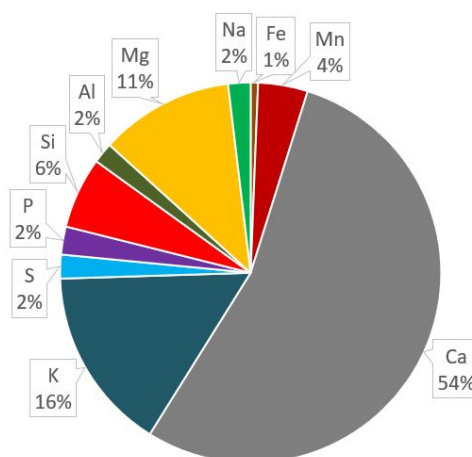


Figure 21: Atomic share of ash forming elements given in % during experiment DFB-01

A schematic timeline for the experimental operation is depicted in Figure 22. The bed material share which is left from a previous run of SW gasification represents a significant part of the

total mass. This fraction needs to be seen as used bed material and extensive layer formation detected during the analysis may be due to the higher operational time in the reactor. The increase of ash load through the re-use of bed material stays unquantified. A run-up phase with SW was not executed since the used feedstock was SW. The execution of the gasification process at approximately 800 °C in the gasification zone could be conducted trouble-free.



Figure 22: Timeline for experiment DFB-01

4.2.2 SEM/EDS Analysis & Discussion

The analysis of this sample was mainly conducted to determine the layer formation tendency when the feedstock is unable to provide enough ash for layer formation and additional potentially ash forming matter (CaO) is used as bed material additive. Studies about the operational time and discharge of ash material stated, that less than 1.5 % of ash in the bed is needed for agglomeration processes [136]. For a theoretical ash load of 0.2 % agglomeration and layer formation mechanisms have not been reported yet.

The chosen area of investigation shows two easily distinguishable types of particles. Through area reports of both represented types they could be identified to be lime (brighter, rough edges, unsteady surface) and quartz (darker, softer edges, smoother surface) edges. The analysis also shows, that contents of C-rich embedding material are ground onto the particle surface. In Figure 23 the SEM image is depicted including the chosen areas for the area reports and the chosen line profiles for the line scan analysis.

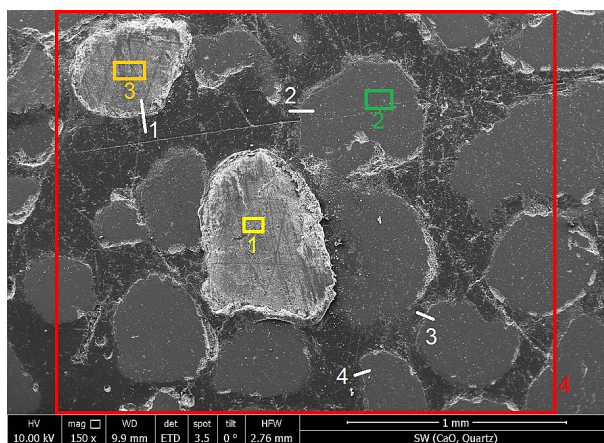


Figure 23: SEM image including the analysed areas for the area report and the line scan profiles of experiment DFB-01. Visible are lime and quartz particles.

The area reports for area 1 and 3 demonstrated the referring particles are CaO with impurities of C and qualitative amounts of Si. No other element was found in significant amounts. Area 2 provided the elemental composition of quartz with no impurities except C. These impurities are mainly accredited to the dry grinding process. The overall area report showed the dominance of C, O, Si and Ca. In terms of the whole area these elements were the only ones occurring in

evaluable quantities.

A line scan profile through the surface of the lime grain delivered little information regarding layer formation. The separating line between embedding matrix and grain was not clearly obtained in the line scans. Along the lines into the lime there is a common area where both lime and embedding material occur. Line Scan 1 in Figure 23 depicts an area of decreasing CaO content with a slight peak of Si in the transition area from embedding material and grain. Other line scans in different areas showed the same phenomenon. The profile of Line Scan 1 is depicted in Figure 24 and is representative for the other line scans.

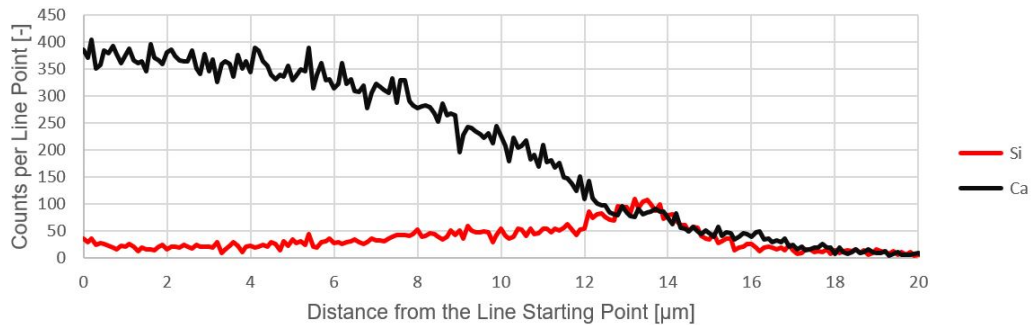


Figure 24: Line Scan 1 profile of Si and Ca as marked in Figure 23 of experiment DFB-01 through a lime particle surface

The profile of the line scan indicates an increase of offset for the Si counts in the lime grain. From the area reports and the limiting factors of EDS-analysis (see Chapter 3.7.2) a highly possible explanation might be the intrusion of abrasive material into the surface of the lime particle. The observation of qualitative amounts of Si on sample surfaces where lime is located was observed several times through all the experiments.

Line scan profiles executed through the surface of quartz particles demonstrated similar phenomena as for the lime particles. Where lime showed a hardly detectable increase of Si in its layer, the quartz had undergone Ca layer formation. The profile of Line Scan 4 marked in Figure 23 is depicted in Figure 25. Other line scans into different quartz particles had similar trends, therefore the depicted example is representative for the entity of line scans executed.

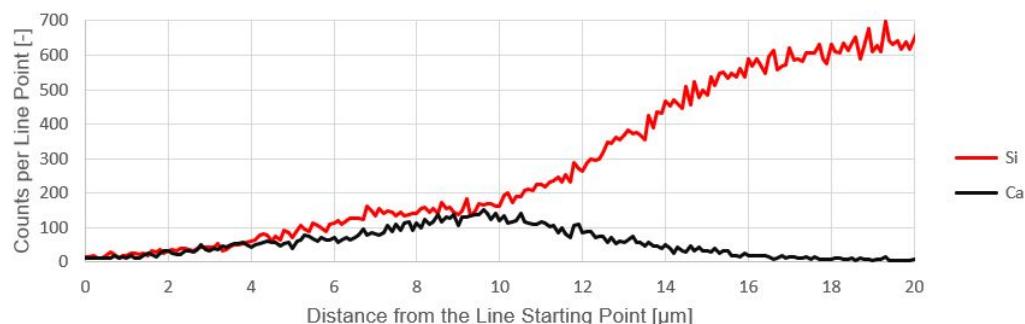


Figure 25: Line Scan 4 profile of Si and Ca as marked in Figure 23 of experiment DFB-01 through a quartz particle surface

The line scan profile indicated a Ca-enriched layer on the surface of the particle. Again a quantification can not be made, for a quantitative approximation the mapping data is required.

In comparison to the total data of line scans through lime particle surfaces, the entity of line scans through the quartz particle surfaces delivered generally higher peaks. Nevertheless the grinding method seems to influence the quartz particles as well, since the rise of particle forming elements is not as steep as for the wet ground particles (see Chapter 4.1).

To verify the observations in the area report and the line scans, a mapping of area 4 (see Figure 23) was made. To avoid information loss the entity of determined elements in area 4 was put to analysis. The whole set of elements is: C, O, Na, Mg, Al, Si, P, K, Ca and Fe. For reasons of manageability only the mapping results which presented valuable information are depicted in Figure 26.

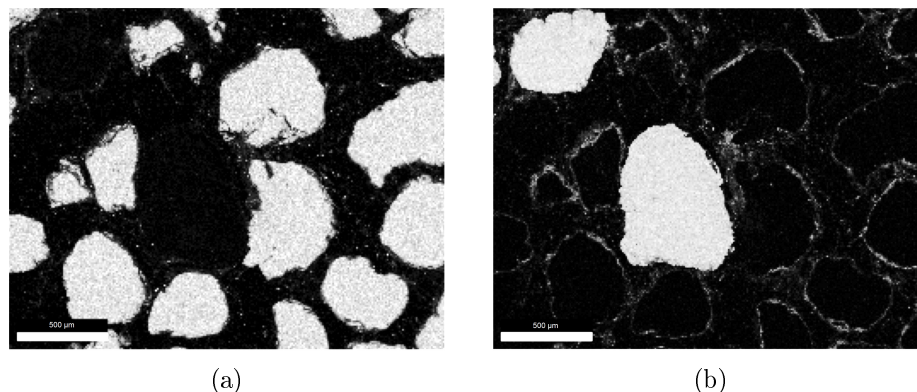


Figure 26: EDS mapping of (a) Si and (b) Ca obtained from area 4 in Figure 23 for experiment DFB-01

As the mappings for Si and Ca demonstrate, the qualitative detectability of Si on lime surface is much lower than the one referring to Ca on quartz surfaces. The layers on the quartz particles may be analysed qualitatively for their Si content. The unidentifiable discontinuity and poor detectability of layers on the lime particles makes quantitative analysis impossible.

Layers formed on the quartz particles were detected to be widened by the grinding process. High contents of embedding material are found in the area where the layers are detected. The high share of embedding material in conjunction with qualitative amounts of Ca indicates, that Ca is discharged from the layers onto the sample surface. This is one possible explanation for the broad but not very high peaks of Ca obtained by the line scans through the quartz surface.

On a C-free and O-free basis the composition of these layers on the quartz particles may be stated. Since all the other elements occurring as trace elements in the layer area do have a measured share of less than 1 % in total, the only elements left after excluding C and O are basically Ca and Si. The atomic ratio of Si:Ca in the area detected to be the layer forming one is 1:1.

Aforementioned results could prove the tendency of layer formation in the present system of wood gasification with quartz and lime as bed material. Main driving force for layer formation was the Ca present in the system in interaction with the quartz particles. If the source of Ca is the produced ash or is made available by abraded lime particles is impossible to determine within this work. The bed material charge with ash of just 0.2 % would suggest, that layer formation mechanisms would be inhibited by unavailability of sufficient ash matter.

4.3 DFB-02 - MWF, GL

The investigation of layer formation and agglomeration processes when using waste and fossil fuel mixtures is aim of this experiment. The quartz and lime bed material mixture contains mostly bed material already used for the blind run.

4.3.1 Gasification Parameters

The key parameters of operation are summarized in Table 13. The theoretical ash load provides high potential for the ash to interact with the bed material. Since most of the bed material has already been used for experiment DFB-01, the effect of long-term operation needs to be considered. The approximate temperature in the gasification zone is comparably high and has to be considered for the expected constitution of lime and possible agglomeration processes.

Parameter	Unit	Value
Bed Material	kg	14.7 Lime (KSW) 65.3 Quartz
Feedstock	kg DS	14.1 GL 34.1 MWF
Feeding Rate	kg TS/hour	15.6
Theoretical Ash Load	kg/kg	3.8
Total Feeding Time	hours	3.33
Approx. Gasification Temperature	°C	850

Table 13: Key parameters for gasification of experiment DFB-02

The atomic shares of ash forming elements derived from the feedstock are depicted in Figure 27. Strong dominance of Al and Si and Ca in the ash fraction needs to be considered for the analysis. The influence of run-up phase SW ash on the overall ash chemistry stays unquantified due to low relevance. Consideration of this ash fraction would only shift the atomic ratios available slightly towards a higher Ca-share.

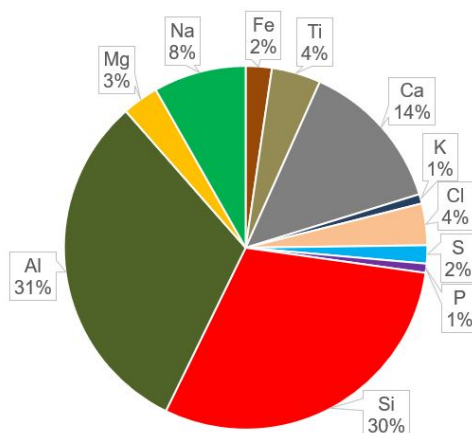


Figure 27: Atomic share of ash forming elements given in % during experiment DFB-02

A schematic timeline for the experimental operation is depicted in Figure 28. The re-use of previous bed material from SW gasification processes makes it necessary to compare the ob-

tained information. The possibility of finding bed material particles showing ageing phenomena is high due to the high share of recycled bed material. Although the ash produced during the run-up phase stays unconsidered, phenomena detected in the previous experiment (see Chapter 4.2) need to be seen in conjunction with phenomena detected in this analysis.



Figure 28: Timeline for experiment DFB-02

4.3.2 SEM/EDS Analysis & Discussion

Layer formation and agglomeration tendency during the combustion of the common fossil lignite fuel mixed with a municipal waste fraction of known composition was investigated in this analysis. Especially the low share of Ca and the high share of Al and their influence on the ash chemistry should be identified. As described in the previous chapter the mixture ash composition resembles the original ash of MWF. For the investigation of layer formation and agglomeration processes two separate areas were analysed, one focussing on the major bed material constituents quartz and lime, the other one demonstrating an agglomeration process in conjunction with an olivine impurity.

The area depicted in Figure 29 presents a multitude of darker quartz particles and one single lime grain in the central area. Compositional reports of the shown rectangular areas verified the nature of the particles. Through those reports the influence of embedding material and grinding method could be obtained as well. C-rich bed material was found on the analysed surface of the grains (on lime more than on quartz) and qualitative amounts of Si could be traced on the lime. Except from Ca, O, C and Si on the lime grain as well as Si, O, and C on the quartz grain no other element could be identified in atomic shares of more than 0.7 %. As the error interval reaches unquantifiable magnitudes for these detected amounts, the presence of other elements than those mentioned stays unconfirmed.

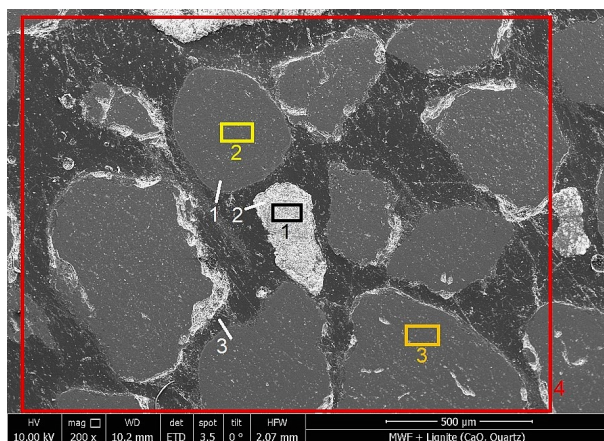


Figure 29: SEM image including the analysed areas for the area report and the line scan profiles for experiment DFB-02. Visible are various quartz particles and one lime particle (center)

Analysis of the overall area 4 depicted in Figure 29 showed the dominance of Si, C, O and Ca

in good agreement with the composition of quartz, lime and the organic embedding material. The remaining elements identified with approximately 1 % each were Na, Mg, Al, P, S, Cl, K, Ti, and Fe. Occurrence of these elements was impossible to quantify, as the error interval was increased again. Therefore these elements need to be considered for the mappings and line scans, but conclusion may only be made qualitatively.

Line Scan 2 in Figure 29 and several additionally executed line scans were unable to detect layer formation mechanisms on lime particles. Although Si shares were slightly increased in the particle area, the formation of layers could not be detected.

Line Scan 1 and 3 in Figure 29 through the quartz particle surfaces are representative for line scan results for quartz. The identification of Ca-rich layers in the line scan profile is indisputable and quantitative analysis by mapping showed the results to be plausible. The entity of line scans also demonstrated the absence of other elements in these layers, significant element signal were only obtained for Si, Ca, C, and O. A representative line scan profile is depicted in Figure 30.

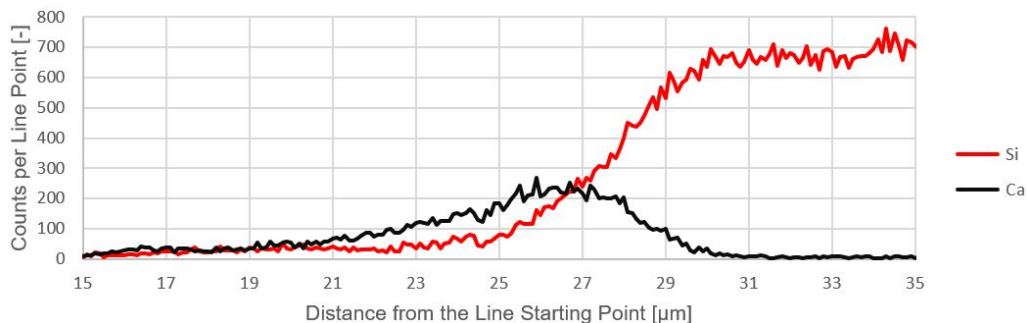


Figure 30: Line Scan 1 profile of Si and Ca as marked in Figure 29 of experiment DFB-02 through a quartz particle surface

The line scans obtained again demonstrated the separating line between embedding material and particles to be blurred. The identified reason for this phenomenon has been found to be the grinding process. Nevertheless the occurrence of Ca in the quartz layer was clear and qualitatively demonstrated by the line scans.

For verification and quantification a mapping of area 4 was made. The loss of information was minimized by doing the analysis in reference to all elements of slightest qualitative occurrence in the elemental report of area 4. The entity of elements analysed via mapping is: C, O, Na, Mg, Al, Si, P, S, Cl, K, Ca, Ti, Fe, and Ni. For reasons of manageability only the mapping results which presented valuable information are depicted in Figure 31.

The mapping proves what line scans already demonstrated before. Layer formation on the lime particles could neither be detected quantitatively nor qualitatively. The result of this mapping was in agreement with four additionally made mappings. A continuous formation of layers on the lime particle, by Si or any other element, was undetected and had to be neglected.

The layers occurring on the quartz particles are clearly visible on the depicted mapping result and quantitative analysis delivered valuable results. Furthermore a identification of two discriminable layers on the quartz particles was possible. On C-free and O-free basis the layers only major constituents are Si and Ca. Qualitative amounts of Mg, Al, Ti, and Fe could be detected, for quantification purposes the shares were too low. The average atomic ratio Si:Ca

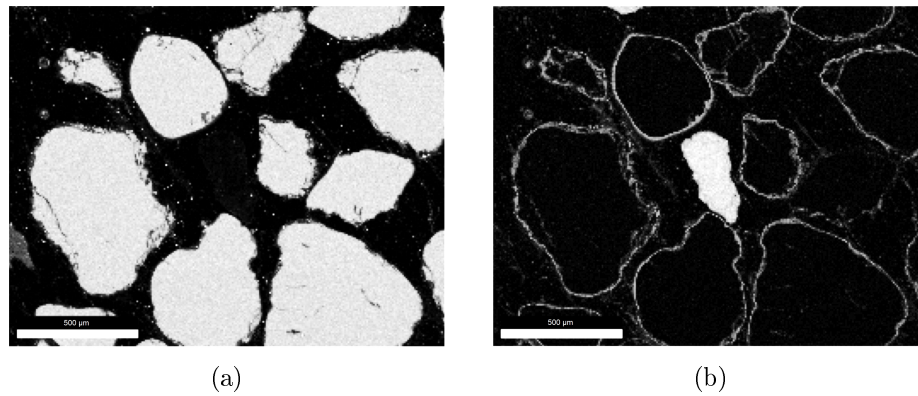


Figure 31: EDS mapping of (a) Si and (b) Ca obtained from area 4 in Figure 29 of experiment DFB-02

in the "outer" layer was found to be in the range from 5:6 to 1:2. In the "inner" Si-rich layer the reversed ratio Si:Ca average atomic ratio identified was in the range of 2:1 to 7:2. The total atomic shares of trace elements Mg, Al, Ti and Fe on a C-free and O-free basis was approximately 5 %. The discrimination of inner and outer layer via mapping was made by approximation. The line scan data for quartz particles shows, that outer and inner layer are not clearly separated. For better discrimination the operational time needs to be increased.

The results obtained from the analysis so far demonstrate the dominance of Ca in the layer formation mechanisms. Although Al (31 %), Si (30 %) and Na (8 %) are present in significant amounts in the ash fraction, the layer formation and composition is most dependent on the Ca share (14 %). Especially the potential interaction of Al (with quartz or lime) and Si (with lime grains) could not be detected at all. The influence of the lime additive in the bed material on the layer formation mechanisms through Ca stays undetected and unquantifiable.

Within the analysis of this sample an especially interesting area has been found and analysed. The mentioned area provided signs of agglomeration between two quartz particles. Therefore the whole procedure of line scanning and mapping has been executed. The analysed area including line scans and mapping are depicted in Figure 32.

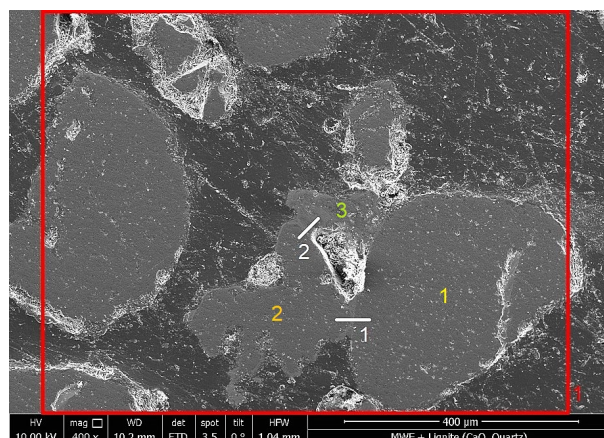


Figure 32: SEM image of agglomerated particles including the line scan profiles, the mapped area and a particle numeration for references for experiment DFB-02. Visible are various quartz particles and one olivine particle (3)

On the depicted SEM image the nature difference between particles 1 and 2 in comparison to particle 3 is hardly visible. Nevertheless the difference in contrast indicates that particle 3 is neither lime nor quartz, the only possibilities left being ash fraction and unclassified impurity in the system.

Excluding the possibility of being an impurity, line scans were conducted to see the profile between quartz particle 1 and 2 in the agglomerated zones. The zones were identified via SEM image through the brighter appearance. Line Scans 1 and 2 provided data for the direct agglomeration between the quartz particles and the profile from particle 2 to particle 3, respectively. The line scan profiles are depicted in Figures 33 and 34.

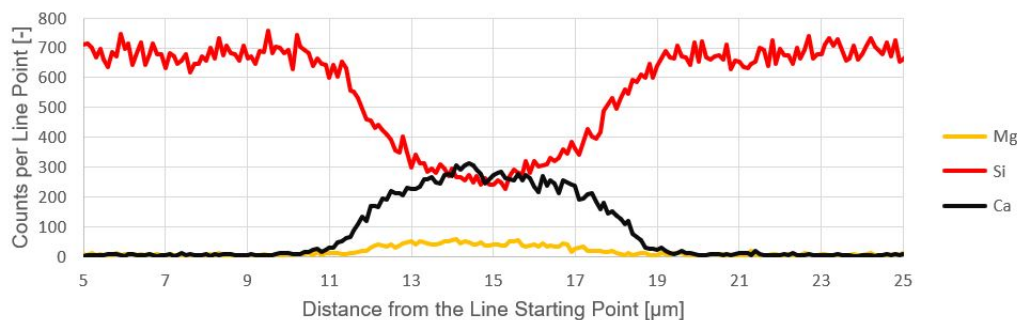


Figure 33: Line Scan 1 profile of Mg, Si and Ca as marked in Figure 32 of experiment DFB-02 between two quartz particles

Line Scan 1, with its starting point in particle 2, through the agglomeration area between the two quartz particles demonstrated dominance of Si and Ca, shares of Mg, and total absence of any other element except O. The qualitative analysis by line scan depicts a Ca trend along the line profile with a clear maximum and strictly monotonic decrease towards the quartz particles. Similar behaviour with lower shares are detected for Mg in the agglomeration zone. The data obtained from line scan 1 proves a perfect basis for quantitative analysis by mapping.

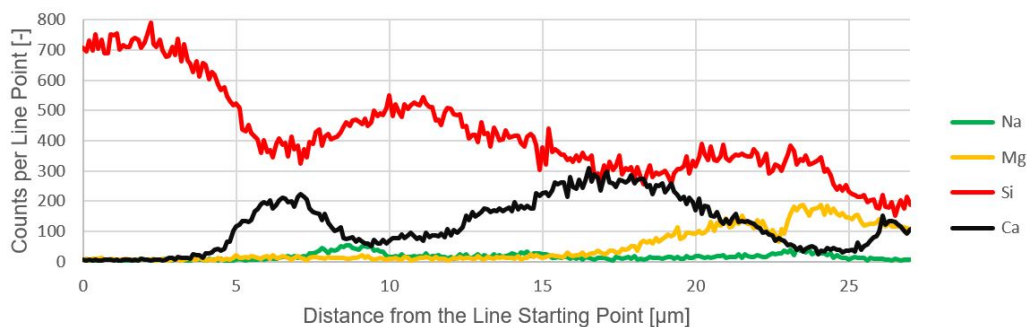


Figure 34: Line Scan 2 profile of Na, Mg, Si, and Ca as marked in Figure 32 of experiment DFB-02 through a quartz particle surface into the agglomerated phase

The profile of Line Scan 2 as depicted in Figure 34 provides a much more complex elemental distribution than Line Scan 1. The line was drawn from quartz particle 2 into the agglomerated fraction. The trends for Si and Ca are detected totally oppositional, whereas Na shows two minor peaks. Both Si and Ca indicated the formation of multiple Ca-rich layers, once between 5 and 10 μm and again between 10 and 25 μm distance from the starting point of the line scan. The nature of the third peak in the end of the line profile stays unidentified due to the length of the analysis line. Since this failure of measurement was observed after the mapping was executed, a

repetition of the line scan was impossible (see Chapter 3.6).

The most interesting trend is made by Mg. At the very end of the line scan profile the Mg establishes a level of counts which indicates the agglomeration area mainly consists of Si, Mg and Ca. The trend further into the particle 3 is unavailable, therefore the mapping is used for additional clarification.

The set of elements applied for the previous mapping was confirmed for the investigation of this mapping as well: C, O, Na, Mg, Al, Si, P, S, Cl, K, Ca, Ti, Fe, and Ni. For reasons of manageability only the mapping results which presented valuable information are depicted in Figure 35.

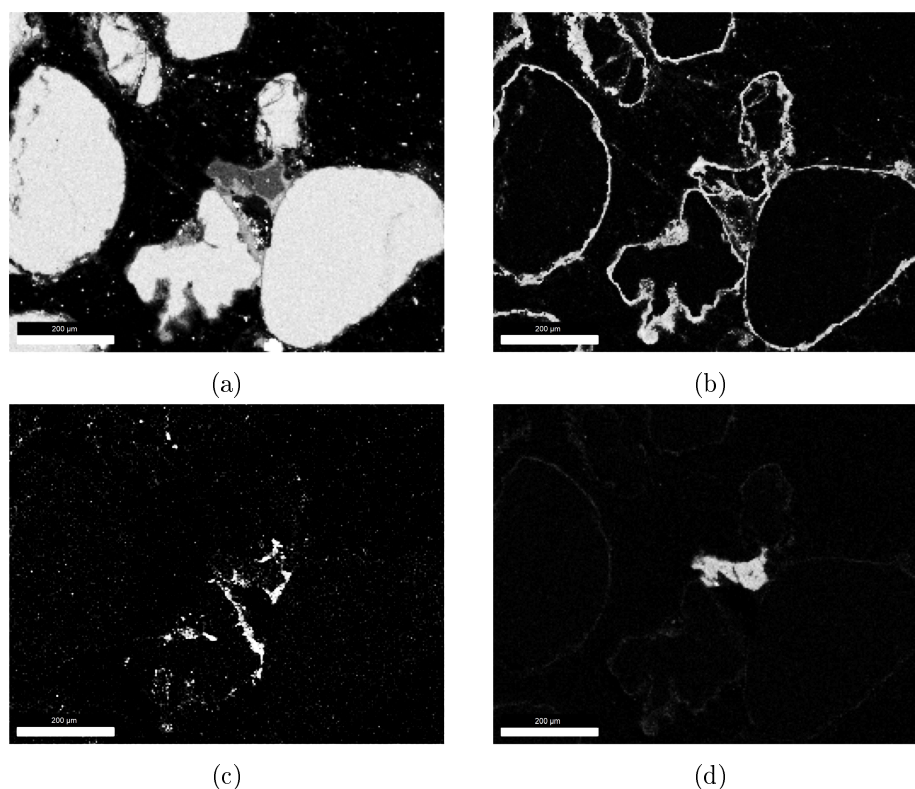


Figure 35: EDS mapping of (a) Si, (b) Ca, (c) Na and (d) Mg obtained from area 1 in Figure 32 of experiment DFB-02

The mapping results of this area contain a lot of information regarding the four main elements. The intensity contrasts shown in Figure 35 in conjunction with the quantitative analysis of the different areas may lead to the identification of the exact details regarding the unidentified agglomeration area. Particle 3, which is incorporated in the agglomeration area, can be identified as olivine grain. An individual interpretation for the depicted element distributions should thereby be approached.

The distribution of Si over the whole area is in agreement with the nature of most identified particles. For layer zones on the quartz particles the spectrum shows decreased shares of Si. For the agglomeration area the Si detection indicates decreasing distribution from the inner quartz into the layer and further decreasing into the olivine particle whose shape is demonstrated clearly in image (a) of Figure 35. The particle shows decreased intensity (and therefore share) of Si within the grain. Nevertheless a significant amount was detected, which can be seen in the con-

trast to the Si-free embedding material.

The occurrence of Ca in the analysed area complies with the expectation very well. Layers on the quartz particles are clearly identifiable, and also on the olivine particle an explicit Ca-rich layer is detected. When focussing on the agglomeration area between the olivine particle and the quartz particles it is visible, that there is an area of decreased Ca share. The agglomeration process therefore is considered to be not initialized by the Ca-rich layers on the particles. The analysis suggests, that the area of decreased Ca-share is responsible for the agglomeration.

The analysis of Na distribution provides insight into the driving force of the agglomeration mechanism. Except from partially detected layers on quartz the main fraction of Na is situated in the areas of agglomeration between the three particles. The Na rich fraction seems to be the connecting agent between the Ca-rich layers of every particle to initiate agglomeration. Furthermore, the Na-rich layers are detected to be directly attached to the quartz particles, but not the third olivine grain.

The spectrum of Mg now gives clear information about the olivine particle. In conjunction with the (not depicted, but analysed) spectrum of Fe and the quantification the particle is clearly identified to be olivine. The atomic ratio of Mg:Si:Fe detected quantitatively was approximately 10:7:1, which verifies this conclusion. Apart from the olivine particle no major share of Mg was detected in the spectrum.

Drawing primary conclusions from the analysis results obtained for this area provides a multitude of explanations and possibilities. The most obvious ones are discussed in the following itemization:

- The quantitative analysis of layers formed on the quartz particles showed the occurrence of two discriminable types of layers. An inner layer of Si:Ca atomic ratio of approximately 2:1 and an outer layer with Si:Ca atomic ratio approximately 1:2 were identified. The results from both analysed areas agree with each other quite well.
- Layer formation on the olivine particle was shown to undergo a different mechanism. While the layers are Ca-rich the direct adhesion and interaction with Na seems to be less favoured than for quartz. A discrimination between different kinds of layers was hardly possible. In the agglomeration area the layer composition resembles the inner layer identified on the quartz particles, in layers not taking part in the agglomeration the layer composition resembles the Ca-rich outer layers of quartz particles.
- Although being detected in the agglomeration initializing phase, Na can not be measured quantitatively. The amounts of Na detected draw the conclusion, that it is occurring as trace element. Considering, that Na present in the ash is responsible for the agglomeration process the total amount of Na remains unquantifiable.

4.4 DFB-03 - MWF, SLF, SCB, GL

This experiments represents a gasification process with comparably long operation time and successive feeding of different feedstocks. The bed material is mainly consisting of lime with less than a 10 wt% share of olivine. The feedstocks MWF, SLF, SCB and GL are gasified one after another. In the end of the experiment the operation implements SER with GL feedstock. The possible influences of unmixed, successive feeding of different feedstocks and the implemented

SER process are investigated.

4.4.1 Gasification Parameters

The key parameters of operation are summarized in Table 14. The inserted olivine fraction represented a sieved fraction of the fine olivine in the range of 100 to 200 μm . The operational time of almost two days in total and 10 hours of feeding time are of special importance. The approximate gasification temperature is applied for the DFB steam gasification without SER processing. For the SER process the temperature was decreased to approximately 700 $^{\circ}\text{C}$.

Parameter	Unit	Value
Bed Material	kg	71.5 Lime (KS01) 5.4 Olivine
Total Feedstock Mass	kg DS	21.0 MWF 12.9 SLF 24.3 SCB 87.6 GL
Feeding Rate	kg TS/hour	12.2 MWF 12.7 SLF 23.2 SCB 17.7 GL
Theoretical Ash Load	kg/kg	9.7
Total Feeding Time	hours	10
Approx. Gasification Temperature (excl. SER)	$^{\circ}\text{C}$	750 - 850

Table 14: Key parameters for gasification of experiment DFB-03

The atomic shares of ash forming elements derived from the feedstock are depicted in Figure 36. The depicted data refers to the theoretical ash composition including the different feedstocks and the specific inserted mass of every feedstock. The consecutive order of feeding different types of feedstock increases the operational time of certain ash fractions. With the original feedstock data from Table 7 the theoretical ash composition can be determined at any moment during the experiment.

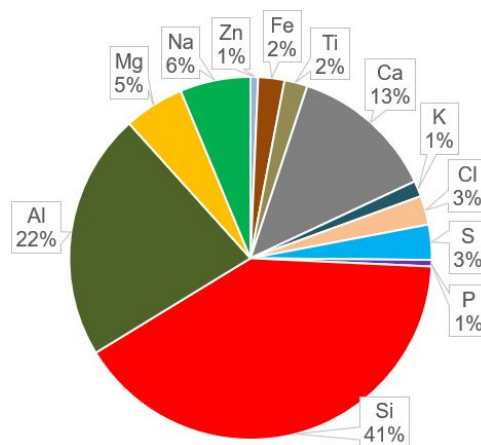


Figure 36: Atomic share of ash forming elements given in % during experiment DFB-03

A schematic timeline for the experimental operation is depicted in Figure 37. The influence of SW input during the run-up phase is neglected. Especially the influence of SER processing in the very end of the operation and its influence on the ash chemistry should be investigated.

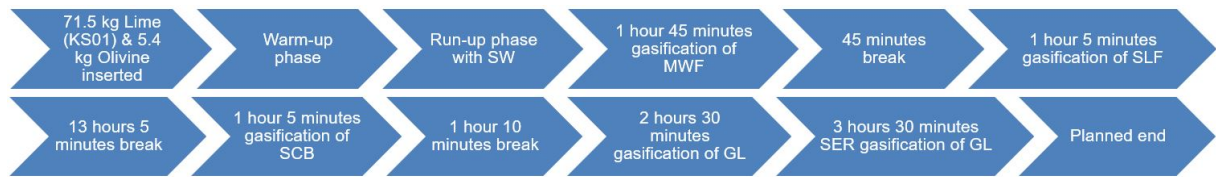


Figure 37: Timeline for experiment DFB-03

4.4.2 SEM/EDS Analysis & Discussion

Focus of this analysis was the ash chemistry when waste and biomass feedstock is gasified successively. The dominating element in every feedstock is Si, with high shares of Al in each feedstock and Ca contents of approximately 20 % maximum. Another key factor is the process duration, within this work the bed material sampled is the one with longest dwell time in the DFB system. In conjunction with the SER process with GL feedstock the influencing parameters on the ash chemistry and thermodynamics are numerous.

The area depicted in Figure 38 reflects the two different bed material types lime and olivine which were analysed for layer formation mechanisms. For the verification of the particle composition reports of the areas 1 to 4 were executed, additionally the entity of occurring elements is measured by report analysis of area 5. The line scan profiles conducted for the referring analysis are depicted and numbered in Figure 38 as well.

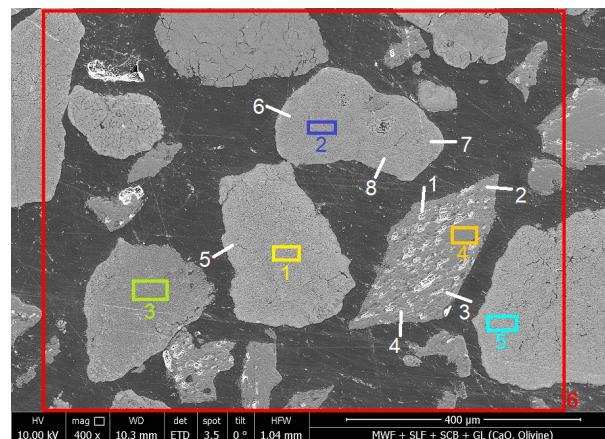


Figure 38: SEM image including the analysed areas for the area reports and the line scan profiles for experiment DFB-03. Visible are lime and olivine particles.

Composition analysis of areas 1, 2, and 5 as marked in Figure 38 proved the marked particles to be pure lime grains. The main impurity found was C. If the elevated C-share is due to embedding material intrusion or carbonation of lime stays undetected. The elevated content of O within the particle structure in comparison to lime grains from other experiments indicates that the lime bed material in this sample is at least partially carbonated. Since carbonation is an essential reaction taking place during SER processing, the occurrence of carbonated lime particles in bed

material samples from the reactor needs to be considered. The entity of impurities on a C-free and O-free basis in the lime grains is unquantifiable individually and below 1 % of atomic share.

The composition analysis of area 3 as marked in Figure 38 proved the particle to be a mixture of C, O, Mg, and Ca with a Ca:Mg ratio of approximately 1:1. The absence of any other elements in the particle and the low potential of the feedstock to form an ash particle with a composition like that leaves the primary conclusion this grain represents a lime bed material with major dolomite impurity. The elevated share of O and C within the structure again suggests, that the particle is at least partially carbonated.

For area 4 the report detects an olivine grain with Mg:Si:Fe atomic ratio of approximately 9:5:1. On a C-free and O-free basis the area represents a composition of more than 99 % in Mg, Si, and Fe.

Area report 6 over the whole sample surface shows the dominance of C, O, Mg, Si, Ca with qualitative detection of Fe and Al. The line scan profiles depicted in Figure 38 were analysed for the aforementioned elements.

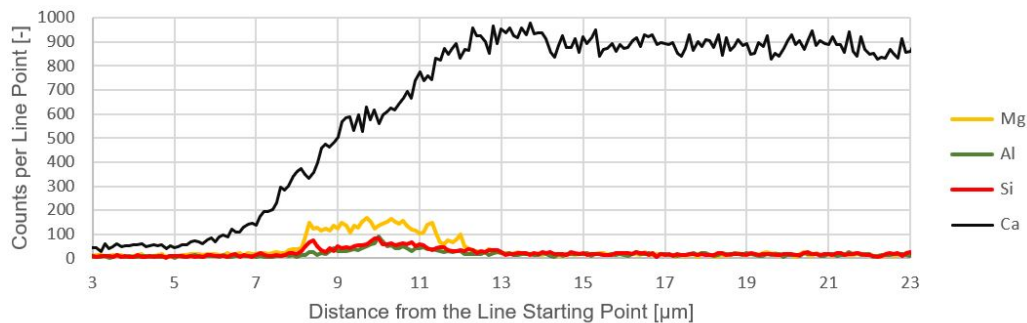


Figure 39: Line Scan 5 profile of Mg, Al, Si, Ca as marked in Figure 38 of experiment DFB-03 through a lime particle surface

Line Scan 5 through the surface of a lime is depicted in Figure 39. Although the dominance of Ca is clearly visible, the detection of trace elements in the transition area between grain and embedding material is possible. Especially the peak of Mg might have the intensity for quantitative detection by mapping. For the Si and Al peaks as shown in Figure 39 a quantitative detection is improbable. Analysis of Line Scans 6, 7, and 8 presented similar results as Line Scan 5, the only major difference being that the peaks of Si varied in intensity. The profile depicted in Figure 39 is chosen because both the intensity of Mg and Si is presented in the mean intensity as detected for the additional line scans. Therefore Figure 39 is a representative for the results obtained by line scans through lime particle surfaces.

Line Scan 1 in Figure 40, as representative for the entity of line scans conducted through the surface of olivine particles in this and other areas, does not reflect any layer formation mechanism by ash induced elements. The profile indicates slight increases of olivine inherent elements (Mg, Si, Fe) in the transition area between grain and embedding material and sharp increases of the Fe content on the surface of the grain, but Ca intensity stays undetected on the whole profile. This observation stands contrary to the expectation that Ca-rich layers are commonly formed on olivine particles if the Ca potential in bed and ash is high. Although the result of Line Scan 1 in Figure 40 is unexpected, additionally executed line scans in different areas on several olivine particles presented similar results. Ca peaks in the line scans through olivine surfaces were either

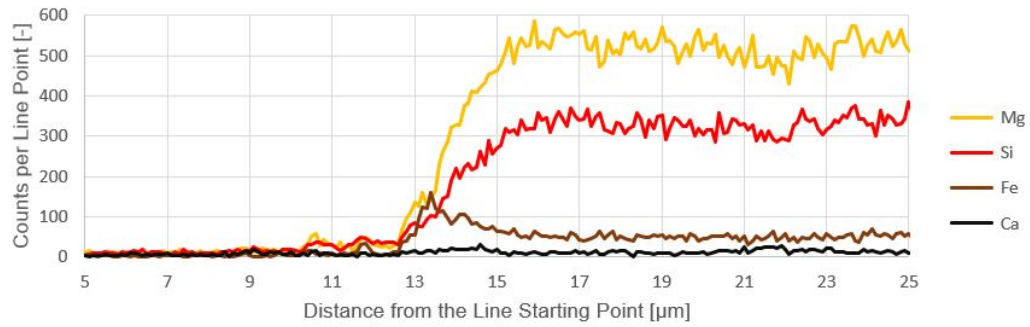


Figure 40: Line Scan 1 profile of Mg, Si, Fe, and Ca as marked in Figure 38 of experiment DFB-03 through a olivine particle surface

undetectable or insignificant for all three executed line scans as marked in Figure 39.

For verification and quantification a mapping of area 6 was made. The loss of information was minimized by doing the analysis in reference to all elements of slightest qualitative occurrence in the elemental report of area 6. The entity of elements analysed via mapping is: C, O, Na, Mg, Al, Si, P, K, Ca, and Fe. For reasons of manageability only the mapping results which presented valuable information are depicted in Figure 41.

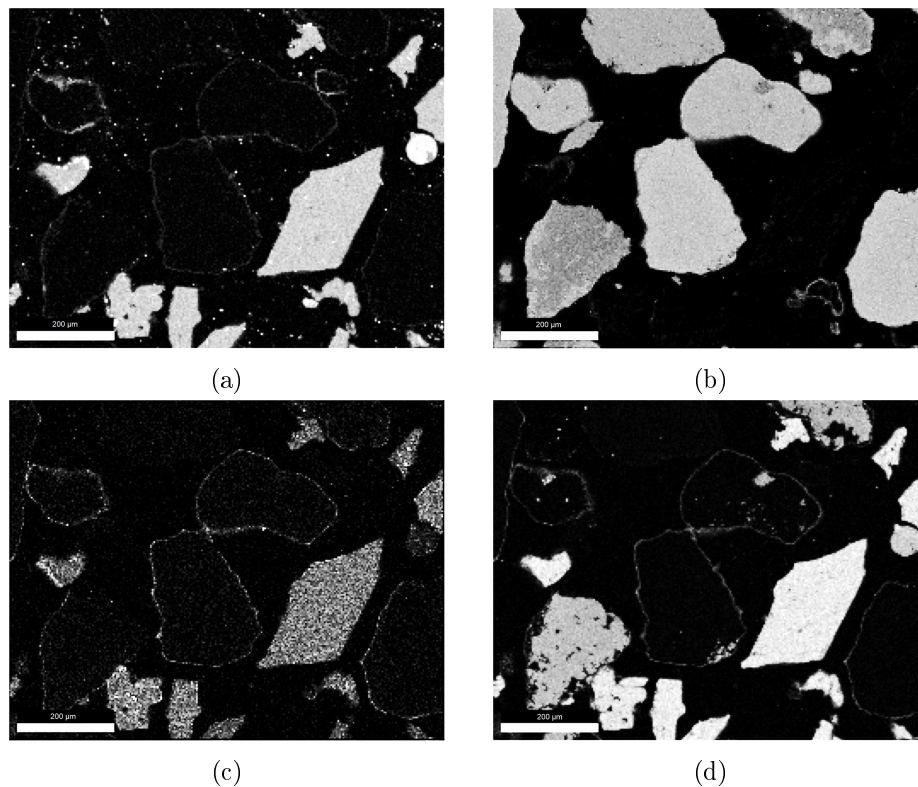


Figure 41: EDS mapping of (a) Si, (b) Ca, (c) Fe and (d) Mg obtained from area 6 in Figure 38 of experiment DFB-03

The conducted mappings prove the observations made in the line scans to be valuable and are able to verify the layer formation results. A detection of layers on the lime particles was possible, the mappings indicate an enrichment of Si, Mg, Fe, and (the not shown, but qualitatively

detected) Al. Quantification of elements in the layer forming area surrounding the lime grains can only be obtained for Ca. On a C-free and O-free basis the average Ca atomic share in the layer forming area is approximately 66 %. The other qualitatively measured elements Mg, Al, Si, Na, and Fe in the layer forming zones make up an atomic share of approximately 33 %.

For the olivine particles layer formation is undetectable by mapping results. Neither the visualized results in Figure 41 nor the elemental quantification in olivine surface area indicates any layer formation phenomena.

The results obtained from area reports, line scans and mapping of the area depicted in Figure 38 do not show irregularities in layer formation processes and are consistent with additionally executed analyses. Intensive search on the sample surface brought up just one phenomenon of layer formation for olivine particles in this sample. This particle of special interest was investigated as well to obtain information about the causes of layer formation absence on the majority of olivine particles. The analysed area with the reported areas, line scan profiles and the (manually reduced) area for the map analysis is depicted in Figure 42.

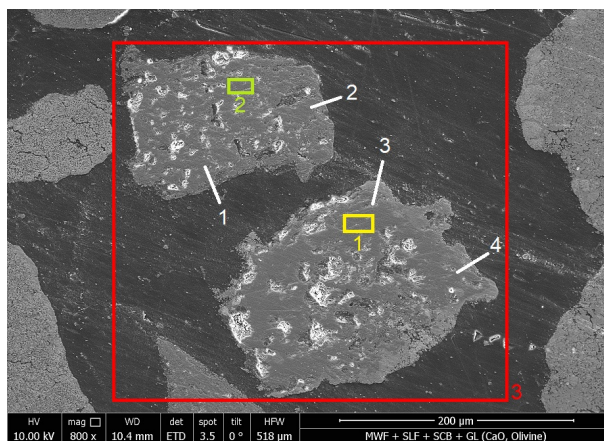


Figure 42: SEM image including the analysed areas for the area reports and the line scan profiles for experiment DFB-03. Visible are olivine particles.

Reports of the areas 1 and 2 proved the grains to be olivine particles with an approximate atomic ratio Mg:Si:O of 9:5:1. Impurities apart from C within the particle are not detected, on a C-free and O-free basis the atomic share of Mg, Si and Fe combined is 99 %. The area report 3 provided information about the entity of detected elements in the area and showed the dominance of C, O, Mg, Si, Ca, and Fe with detected amounts of Na, Al, and P. This list of elements represents the analysis input for the line scans and mappings.

Line scans conducted through the upper olivine grain in Figure 42 showed similar results as Line Scan 1 in the previously presented area, depicted in Figure 40. A detection of significant layer formation was unachieved. The results of both line scans executed are therefore not depicted separately but are represented by the olivine line scan in Figure 40.

Line Scan 4 as marked in Figure 42 and depicted in Figure 43 shows one of only two line scans conducted within the analysis of this bed material which indicated layer formation processes are happening. The peak of Ca in the line scan profile is significant and the trends of Si and Mg with the saddle point in their trend show the clear tendency of a layer formation process. It can also be seen that the count ratio of Mg:Si within the olivine particle is maintained in the layer

zone. The result of this line scan is representative for Line Scan 3 conducted through the surface of the very same olivine grain, but reflects a layer formation phenomenon which was detected just once within the whole sample.

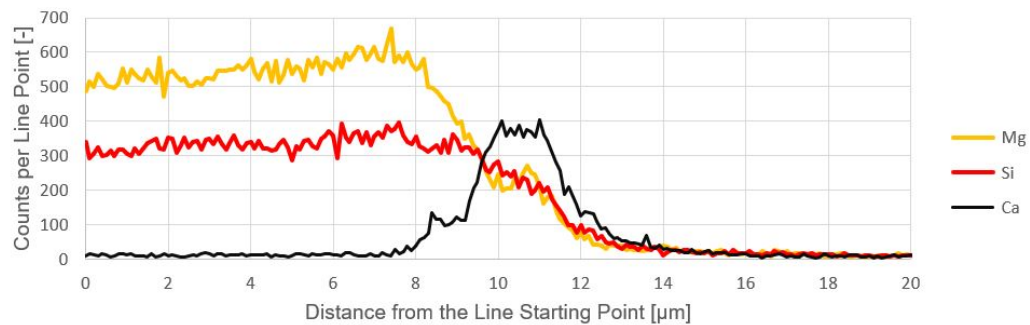


Figure 43: Line Scan 4 profile of Mg, Si, and Ca as marked in Figure 42 of experiment DFB-03 through a olivine particle surface

For verification and quantification a mapping of area 3 was made. The loss of information was minimized by doing the analysis in reference to all elements of slightest qualitative occurrence in the elemental report of area 3. The entity of elements analysed via mapping is: C, O, Na, Mg, Al, Si, P, K, Ca, and Fe. For reasons of manageability only the mapping results which presented valuable information are depicted in Figure 44.

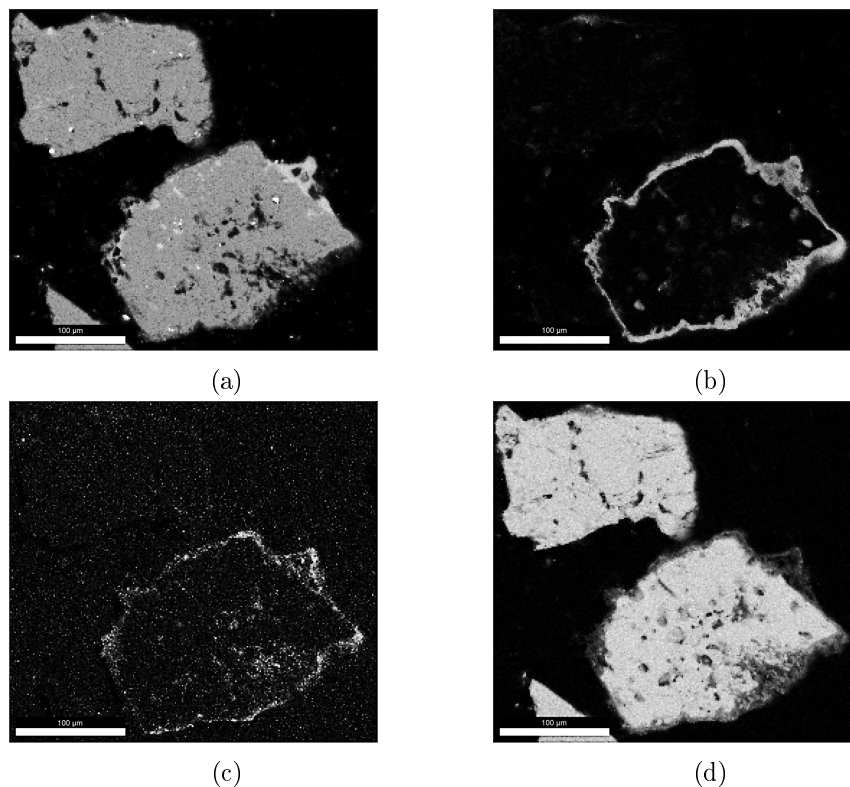


Figure 44: EDS mapping of (a) Si, (b) Ca, (c) Al and (d) Mg obtained from area 3 in Figure 42 of experiment DFB-03

The mapping results may again verify the observations seen in the line scan profiles. Where the upper olivine particle does not show any layer formation tendency, the lower olivine particle presents a clear layer. For the upper olivine particle no area for quantitative measurement could be obtained, therefore the analysis focuses on the layer area of the lower olivine particle.

Analysis of the layers observable on the lower olivine grain reflects a very complex composition distribution within these layers. The outer layer zones could be discriminated depending on the location on the referring olivine grain. Therefore the elemental analysis needs to focus on dominating elements and qualitatively detected elements in this zones.

Inner layer which resemble the composition of the olivine composition are detected. The intrusion of Ca can only be detected qualitatively for these areas and presence of any additional non-olivine element is undetected. The share of Fe and Si in this area is slightly elevated to create an atomic ratio Mg:Si:Fe of 6:4:1. Intrusion of Na and Al as depicted in Figure 44 is not reaching the inner zone area.

The outer layers formed on the olivine grain are not presenting a homogeneous set of results. Within the area of outer layers there are zones with dominance of Si over Ca and reverse. Dominance of Si is accompanied by enrichment of Na, whereas the Ca-dominating areas are richer in Fe.

The primary conclusion of the two area analyses conducted for this experiment in terms of obtained layer formation phenomena are:

- Layer formation on lime particles could be detected qualitatively within this experiment. The layer composition could be identified qualitatively and the layer formation potential of Mg, Al, Si, Na, and Fe on the lime grain was detected. The at least partially carbonated nature of the lime grains found in the analysis and the possible (positive) influence on layer formation mechanisms is discussed in Chapter 4.8.
- The overall layer classification for olivine particles in this experiment does not leave a clear picture of mechanisms taking place. In general, the formation of Ca-rich layers on olivine particles could not be detected. For the only particle where layer formation could be obtained, the layer composition showed high interaction with the ash forming fraction. Especially in outer layers Al and Na could be detected qualitatively. Since this particle is the only olivine grain demonstrating layer formation phenomena, it must be considered, that it is an exceptional particle and not representative for the process. A possibility is, that the particle was left in the system after a previous run. The possible influence of the consequent feedstock feeding and the SER processing for the absence of layers on the majority of olivine grains and the constitution of the individual layer detected is discussed in Chapter 4.8.

4.5 DFB-04 - HNS

The influence of high alkali-shares in the ash derived from HNS feedstock on pure lime bed material should be analysed through this experiment. Additionally the implementation of SER and its influence was investigated. The evaluation was prevented by major impurities in the system due to improper cleaning after the previous experiment. The results are mentioned nevertheless, since general observations could still be made.

4.5.1 Gasification Parameters

The key parameters of operation are summarized in Table 15. This is the only experiment executed with pure lime bed material. The original separating cut of lime (KSW) bed material was adapted through sieving. The used bed material represents a separating cut of $<500\ \mu\text{m}$. The approximate gasification temperature is applied for the DFB steam gasification without SER processing. For the SER process the temperature was decreased to approximately $700\ ^\circ\text{C}$.

Parameter	Unit	Value
Bed Material	kg	81.4 Lime (KSW)
Feedstock	kg DS	59.7 HNS
Feeding Rate	kg TS/hour	20.3
Theoretical Ash Load	kg/kg	1.1
Total Feeding Time	hours	3.17
Approx. Gasification Temperature (excl. SER)	$^\circ\text{C}$	750

Table 15: Key parameters for gasification of experiment DFB-04

The atomic shares of ash forming elements derived from the feedstock are depicted in Figure 45. The dominance of K and Ca can be observed clearly. Since interaction of ash and bed material is mainly analysed through element discrimination in superficial areas of the bed material grain, interaction of Ca from the ash with the lime particles can not be detected. The main focus therefore will be set on the influence of K.

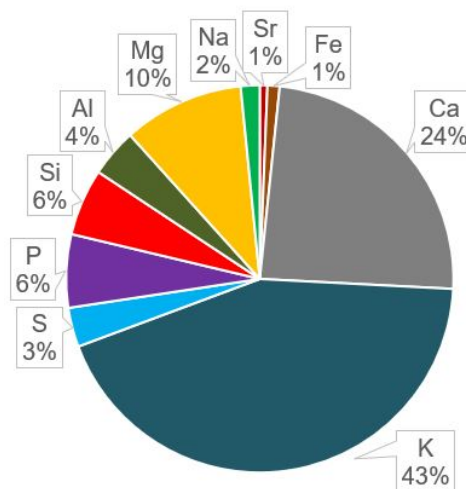


Figure 45: Atomic share of ash forming elements given in % during experiment DFB-04

A schematic timeline for the experimental operation is depicted in Figure 46. Intermediate destabilization of temperature parameters in the gasification zone required an interruption of the experiment. If this occurrence stands in any relation to the ash chemistry needs to be investigated through SEM and EDS analysis. Furthermore, the influence of the SER process implemented needs to be discussed.



Figure 46: Timeline for experiment DFB-04

4.5.2 SEM/EDS Analysis & Discussion

Layer formation possibilities in pure lime bed material during the gasification of K-rich feedstock was the focus of this analysis. HNS as feedstock provides a valuable source of K, while the ash yield is low which might prevent the formation of agglomeration initiating ash fractions. The influence of SW gasification as start-up and intermediate feedstock is not evaluated.

The bed material sample was found to be a homogeneous mass of lime bed material. Therefore two areas of investigation were chosen, one representing various lime particles and another one focussed on one single lime particle. To facilitate the depiction, the presented area and analysis focuses on the single lime particle analysis. Phenomena detected for this particle were compared to detected phenomena for the multitude of particles, to see if these phenomena occur generally.

The area depicted in Figure 47 reflects the central lime grain and edges of surrounding lime particles. Through reports of the marked areas the nature of depicted particles was verified. The EDS spectrum proved the main elements to be Ca, O, and C with unquantifiable impurities of Si. The entity of impurities and trace elements detected were approximately quantified (with significant error intervals) to be below 2 % of atomic share.

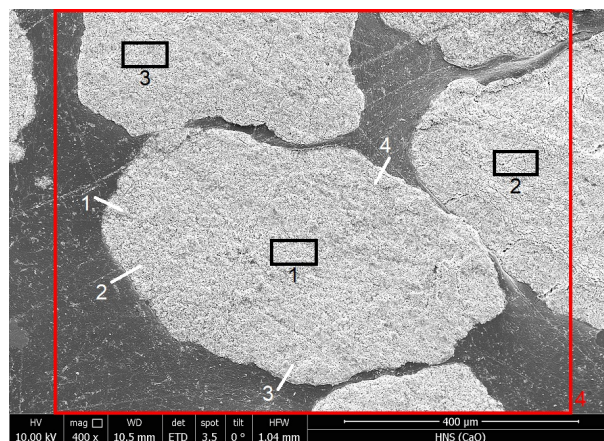


Figure 47: SEM image including the analysed areas for the area report and the line scan profiles for experiment DFB-04. Visible are lime particles.

Line scans through the surface of the lime particles were conducted to analyse the formation of layers and qualitative determination of the referring layer composition. The report of area 4 detected the major elements to be C, O, and Ca with trace amounts of Si, Mg, Mn. The line scan profiles depicted in Figure 47 were analysed additionally for Al, K, P, and Mg as these elements are main constituents of the ash fraction of HNS. The representative profile of Line Scan 1 is depicted in Figure 48 and just shows trends which provided valuable results.

Line Scan 1 delivers a trend which was obtained several times. The interaction of Ca and Si on the grain surface is almost undetectable even for qualitative analysis. The slight peak of Ca gives insufficient information about actual layer formation. The primary conclusion obtained from line scan analysis must be, that layer formation is unprovable by this method of analysis.

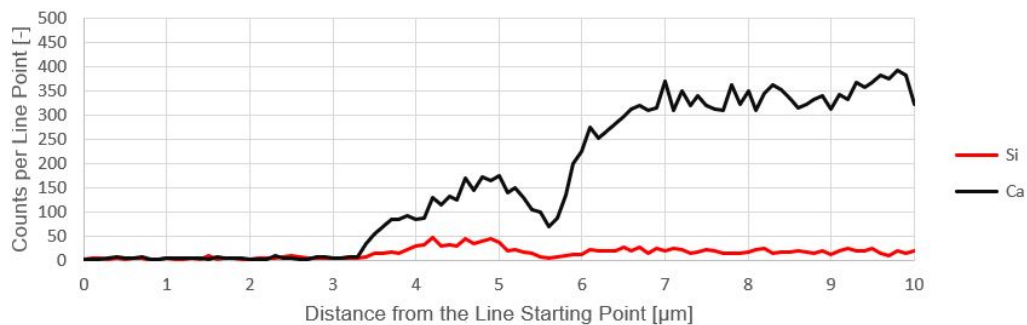


Figure 48: Line Scan 1 profile of Si and Ca as marked in Figure 47 of experiment DFB-04 through a lime particle surface

For quantitative analysis by mapping the whole set of mentioned elements was confirmed: C, O, Ca, Si, Mg, Mn, Al, K, and P. For reasons of manageability only the mapping results which presented valuable information are depicted in Figure 49.

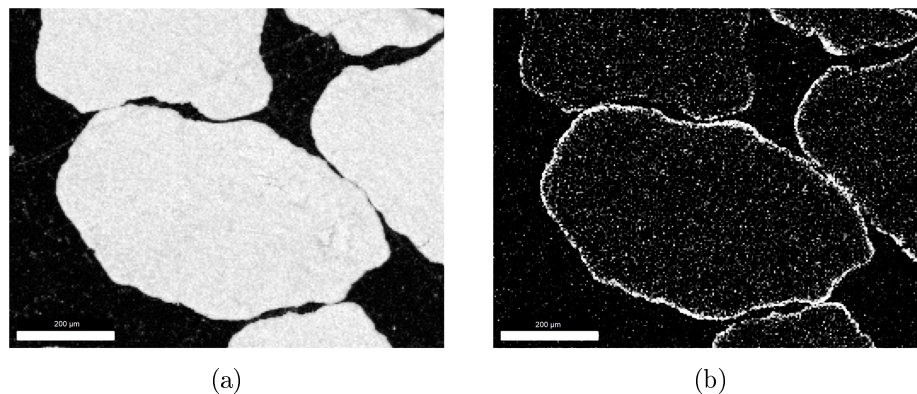


Figure 49: EDS mapping of (a) Ca and (b) Mn obtained from area 4 in Figure 47 of experiment DFB-04

Analysis of the mapping in this area provided clear absence of all the main elements present in the ash. Neither K, Mg, Si or P were found to interact in any way with the lime grains in the bed. Elemental mapping of Ca proves the particles to be lime. On a C-free and O-free basis the total impurities of other elements than Ca were almost unquantifiable. The main trace elements found was Si with an atomic share of approximately 2 %. Especially the absence of the main ash forming element K is interesting.

An interesting observation could be obtained for the mapping of Mn. Although being present in the ash fraction of HNS as trace element (0.5 %), Mn was the only element found to show any interaction with the lime bed material. Since Mn was not expected regarding the composition of the ash derived from HNS, line scan data for Mn is unavailable. The layer formation tendency can not be neglected by the mapping. Quantitative analysis as well as a profound explanation have to be made.

Quantitative analysis of the layer forming area on a C-free and O-free basis showed dominance of Ca in these layers which took shares in the range of 80 to 90 %. The remaining elements detected were Mn, Si and P. Quantitative analysis for the amounts detected was impossible.

Although the detection of Si failed, the qualitative analysis detected an approximate ratio of Si:Mn of 1. Since the analysis data of these trace elements needs to be seen in reference to the high error intervals, this ratio analysis can not be taken as a valuable result.

The origin of Mn in the gasification system could be identified by focussing on the operations executed prior to this experiment. The most recent operation conducted was a roasting process of manganese ore. Due to insufficient cleaning and preparation of the reactor for consequently conducted gasification processes, remains of Mn-rich matter were left in the reactor. Thereby the reproducibility and the ability to be validated is not guaranteed.

The capability of Mn to interact with lime particles might seem interesting, nevertheless the unknown compositional and interaction data makes a validation of seen results impossible. The possibility of catalytic deactivation of lime through layers of this kind should be considered for feedstocks of increased Mn-content. Altogether the probability of phenomena like the one seen in this analysis can not be quantified.

4.6 DFB-05 - EOP

The analysed sample of this experiment represents the only process within this work, which had to be terminated prematurely due to defluidization. Aim of this analysis was the identification of driving forces and main influencing parameters which cause defluidization and operation failure during the gasification of alkali-rich feedstocks. The connection between ash composition and agglomeration initiating processes was investigated, when a bed material mixture of olivine and lime is used.

4.6.1 Gasification Parameters

The key parameters of operation are summarized in Table 16. The EOP feedstock used for this experiment was pelletized with lime additive due to known disadvantageous ash melting behaviour. The additive takes a share of approximately 6 wt% of the feedstock mass and has to be regarded for the atomic balance in the ash fraction. The olivine used for this experiment consisted of 50 kg coarse olivine and 15 kg fine olivine particles.

Parameter	Unit	Value
Bed Material	kg	20 Lime (KSW) 50 Olivine coarse 15 Olivine fine
Feedstock	kg DS	58.2 EOP 3.8 Lime (KSW)
Feeding Rate	kg TS/hour	19.8
Theoretical Ash Load	kg/kg	3.4
Total Feeding Time	hours	3.5
Approx. Gasification Temperature	°C	750

Table 16: Key parameters for gasification of experiment DFB-05

The atomic shares of ash forming elements derived from the feedstock are depicted in Figure 50. The dominance of K and Ca over other typical ash elements like Si can be obtained clearly.

The influence of this dominance in the ash and thereby caused interaction with the bed material is investigated in the analysis. Through the addition of lime the atomic shares shift to elevated values of Ca in the ash fraction. In particular the share of Ca increases from 11 % to 46 % atomic share. Thereby the ash melting behaviour should be improved due to a higher Ca:K ratio. The increase of Ca and decrease of the other element shares through addition of lime is evident in Figure 50.

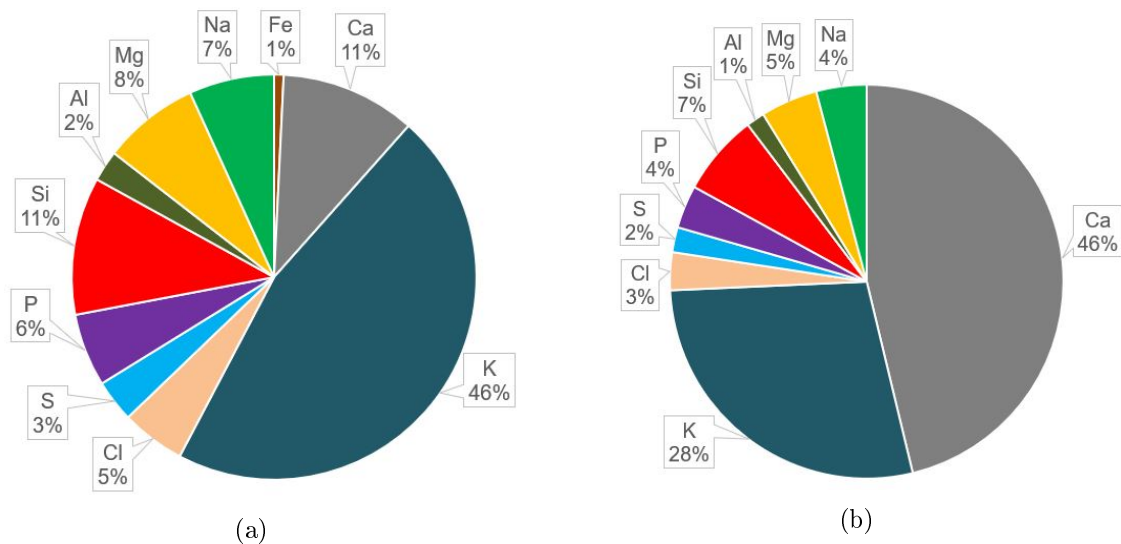


Figure 50: Atomic share of ash forming elements given in % during experiment DFB-05 (a) without the lime additive and (b) including the lime additive

A schematic timeline for the experimental operation is depicted in Figure 51. As mentioned the experiment could not be conducted as planned but had to be terminated early because of defluidization in the gasification reactor. The analysis via SEM and EDS mainly aimed on the determination of agglomeration mechanisms which caused the defluidization.



Figure 51: Timeline for experiment DFB-05

4.6.2 SEM/EDS Analysis & Discussion

The analysis conducted for this experiment mainly focussed on the occurring defluidization phenomena which caused the termination of the gasification process. To determine the entity of occurring layer formation phenomena separated from the agglomeration mechanisms, the analysis is conducted for two separate areas.

The area depicted in Figure 52 reflects every type of particles found in the sample through SEM imaging. Orange marked and numbered particles have been found by primary evaluation to be of different nature, the determination of composition and origin is done by mapping evaluation. Composition reports of the shown areas 1 to 5 were conducted to determine the composition

of the particles quantitatively and to obtain the total spectrum of occurring elements in the depicted area.

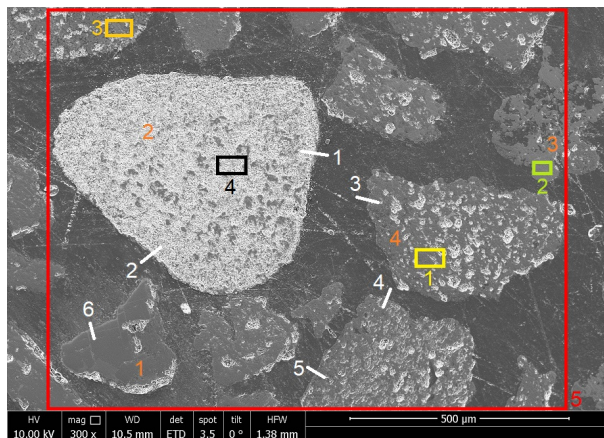


Figure 52: SEM image including the analysed areas for the area report and the line scan profiles for experiment DFB-05. Visible are various (mainly coarse) non-agglomerated olivine particles and one lime particle (2).

Area 1 was determined to be within an olivine particle with an atomic ratio Mg:Si:Fe of approximately 6:4:1. Area 2 was determined to be part of a grain directly derived from the ash forming matter and mainly consisted of Ca, Si, Mg, Al, P, and Fe on a C-free and O-free basis. Areas 3 and 4 are reflecting the composition of lime particles with qualitative amounts of Si and K as trace element. The finding of Si in the structure mainly is referred to the grinding process, the finding of K needs to be verified and analysed by line scans and mappings. In the total area 5 the dominance of C, O, Ca, Mg, Si, Fe and Al could be obtained.

For the qualitative proof of layer formation on the different types of particles, several line scans were conducted whose profiles are depicted in Figure 52. The expectation was, that Line Scans 1 and 2 should show possible layer formation on lime grains, Line Scan 3, 4, and 5 should show probable layer formation on olivine particles and Line Scan 6 was conducted to clearly identify the nature of the referring particle and layers. The set of elements applied for the line scans included the detected elements of area 5 as well as additional ash forming elements: C, O, Na, Mg, Al, Si, P, S, Cl, K, Ca, and Fe.

The elements profile of Line Scan 2 as marked in Figure 52 is depicted in Figure 53. It can be seen, that the Si signal does not provide any detection which would indicate layer formation through Si. The qualitative detection of Si within the lime grain may be seen as well. For the distribution of K through the surface of the lime grain the detection indicates presence of larger quantities. The analysis Line Scan 1 and line scans in other analysed areas reflected K-rich outer areas within the lime particles. As it is detected in the mappings, significant amounts of K are detected within the lime particle, with decreasing shares when running the line further to the centre of the particle.

Line Scan 5 as marked in Figure 52 is depicted in Figure 54 as representative for the line scans conducted through the surface of the olivine particles. The main compounds of olivine without including O can be detected (Mg, Si, Fe). The trend of a Ca-rich layer forming area is clearly visible in the line spectrum as well. Other ash forming elements could not be detected both quantitatively or qualitatively. Several line scans conducted into other olivine grains showed

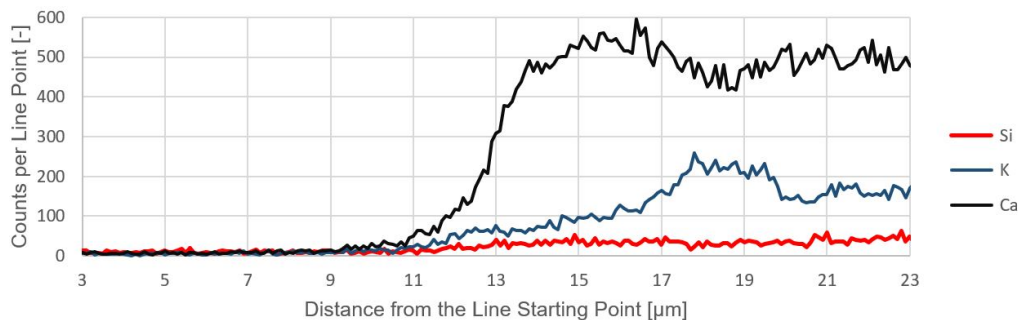


Figure 53: Line Scan 2 profile of Si, K, and Ca as marked in Figure 52 of experiment DFB-05 through a lime particle surface

similar trends for the layer thickness and composition.

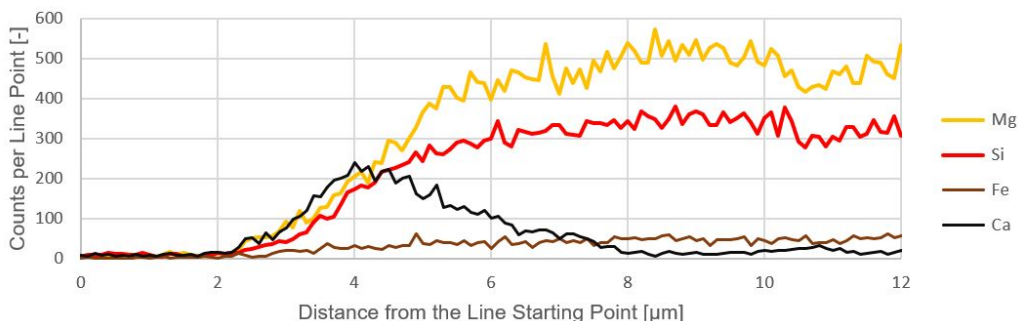


Figure 54: Line Scan 5 profile of Mg, Si, Fe, and Ca as marked in Figure 52 of experiment DFB-05 through an olivine particle surface

For verification and quantification a mapping of area 5 was made. The loss of information was minimized by doing the analysis in reference to all elements of slightest qualitative occurrence in the elemental report of area 5. The entity of elements analysed via mapping is: C, O, Na, Mg, Al, Si, P, S, Cl, K, Ca, and Fe. For reasons of manageability only the mapping results which presented valuable information are depicted in Figure 55.

Line scan results were verified by the mapping outcome. Layer formation through Si or other elements on the lime particles could not be detected. The enrichment of K in the lime particle which was detected via line scan analysis could be detected in the mappings as well. The mapping analysis shows zones of K-enrichment and zones without K-enrichment within the lime particle. By discrimination of these two areas the average composition on a C-free and O-free basis was determined. In the K-rich zones the average Ca:K ratio is 4:1. In the remaining fraction in the lime particle (the darker area in section (d) of Figure 55) the amount of K could not be detected quantitatively but only as trace element. Apart from Ca, K, C, and O, trace amounts of Si could be detected all over the sample surface area of lime. Other elements were quantitatively and qualitatively absent. The observations for particle 2 (as marked in Figure 52) were obtained through mappings of different areas as well. No lime particle without K intruded into the grain could be found.

For the olivine particles the mappings gave clear information about the composition and layer formation phenomena. Quantitative analysis of the layer composition could be conducted. The main compounds were Ca, Mg, Si, Fe and K. A discrimination between different layer zones

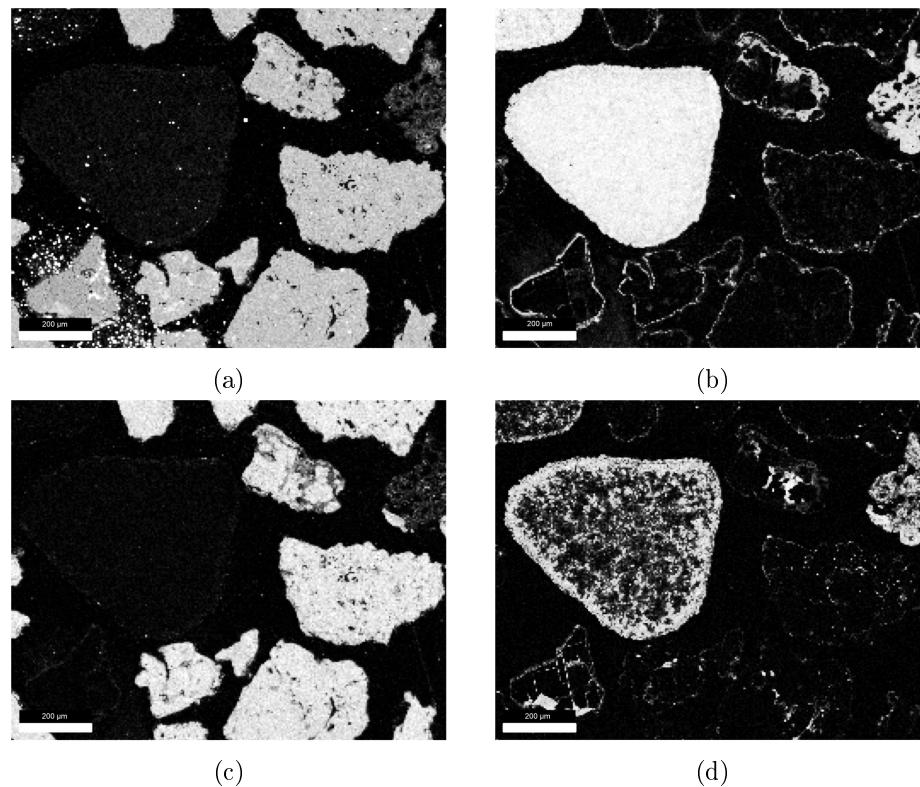


Figure 55: EDS mapping of (a) Si, (b) Ca, (c) Mg, and (d) K obtained from area 5 in Figure 52

could not be made. The average Ca:Si:Mg atomic ratio detected in the layers formed on the olivine particles was approximately 3:2:2. Fe and K could be detected only qualitatively in the olivine layers. The K spectrum visible in section (d) of Figure 55 does not show the continuity of the Ca spectrum in reference to the olivine particles.

The origin of particle 1 and 3 (as marked in Figure 52) is analysed and detected as neither lime nor olivine grain. The mappings shown in Figure 55 as well as additional not depicted line scans were taken for the determination of the composition of these two fractions.

Particle 1 was detected to be mainly consisting of O, Si and Al with qualitatively detected trace elements being K, Ca and C. The Al:Si ratio of approximately 2:1 and high content of oxygen leave the conclusion, that particle 1 represents an Al-silicate. The origin of this grain stays unknown. The most obvious possibilities would be through direct insertion with the bed material or feedstock.

The origin of particle 3 could be determined by evaluation of Mg, K and P mapping and quantitative analysis of the area. High contents of Ca and K in conjunction with qualitatively detected Mg, Si, Al, P and Fe lead to the initial conclusion, that particle 3 represents an ash particle. If there are bed material parts incorporated within the structure stays unknown.

For the valuable analysis of this sample the composition of particle 1 and 3 is not taken into account. Since the exact definition and determination of the origin of those particles is beyond recognition its occurrence is not discussed further.

Analysis results in reference to layer formation mechanisms and layer composition demonstrated the difference between lime and olivine. Where lime does not show quantitative or quali-

tative layer formation mechanisms at all on the original grain, olivine grains developed intensive Ca-rich layers which interact with the elements inherent in olivine. The phenomena obtained for olivine are of major importance for the following validation of agglomeration processes.

For the analysis of agglomeration processes an area with clear agglomeration phenomena was chosen. SEM analysis of the sample surface demonstrated, that agglomeration phenomena mainly occurred with the fine olivine particles. The previously analysed area focussed on the coarse olivine fraction and lime particles. Therefore the following analysis focusses on an area, which contains fine olivine fraction as well. Although being the minor share of olivine in the bed material (see Table 16, agglomeration phenomena could be found in the sample several times. The analysis results indicate, that fine olivine particles more readily interacted with ash particles and caused the agglomeration.

The area depicted in Figure 56 represents several olivine particles, some of them being connected through an agglomerated phase of different composition. An area report was executed for the agglomeration area of non-olivine nature, additionally several line scans in reference to the agglomeration area are conducted and analysed qualitatively. The quantification was achieved by mapping of area 2 as marked in Figure 56.

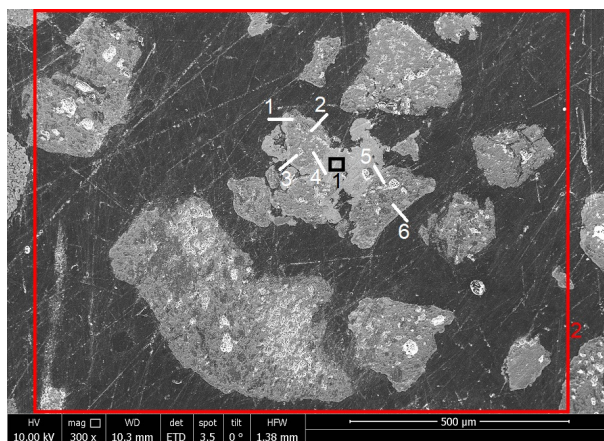


Figure 56: SEM image including the analysed area for the area report and the line scan profiles for experiment DFB-05. Visible are coarse (non-agglomerated) and fine (agglomerated) olivine particles.

The report of area 1 proved the intermediate phase between the olivine particles to be of a more complex composition than olivine. On a C-free and O-free basis the dominating elements were Ca (in the range of 47 to 53 At%) and K (in the range of 17 to 25 At%). The remaining qualitatively detected elements were Mg, Al, Si, P, and Fe. The elemental composition makes it very likely, that this fraction is derived from the ash fraction.

The analysed line scan profiles as depicted in Figure 56 proved to provide a whole set of information. Knowing the main compounds in the different investigated fraction the set of elements inserted for analysis includes C, O, Na, Mg, Al, Si, P, K, Ca, and Fe.

The profile of Line Scan 3 as depicted in Figure 57 stands as representative for the qualitative olivine layer composition. The layer profile indicates two different layers, discriminable by composition. An inner layer which is Ca-rich and Si-rich is detected in the distance of approximately 8 to 13 μm from the line starting point. An outer layer consisting mainly on K and Ca is de-

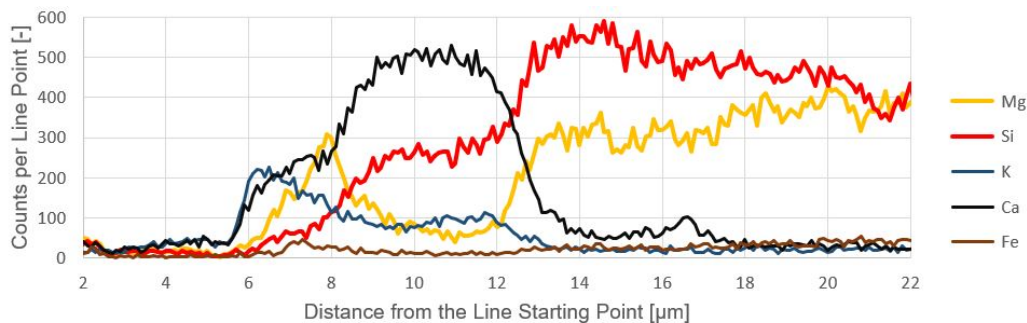


Figure 57: Line Scan 3 profile of Mg, Si, K, Ca, and Fe as marked in Figure 56 of experiment DFB-05 through a olivine particle surface

tected additionally. A peak of Mg appear in the transition zone from inner to outer layer at 8 μm .

The detected phenomena in the depicted line scan have to be put into reference with measurement errors and data manipulation through preparation methods. Therefore additional line scans were executed. These additional line scans conducted from the embedding material into the inner olivine grain demonstrated similar to almost identical information as depicted in Figure 57. The formation of two discriminable layers, K-enrichment in the outer layer, and also the Mg peak in the transition area in between was detected in Line Scan 1, 2, and 3. In comparison to the layers detected in the previous area on the coarse olivine particles (see Figure 52) the layers on the fine olivine particles contain outer and inner zones and develop (outer) layers with higher ash resemblance.

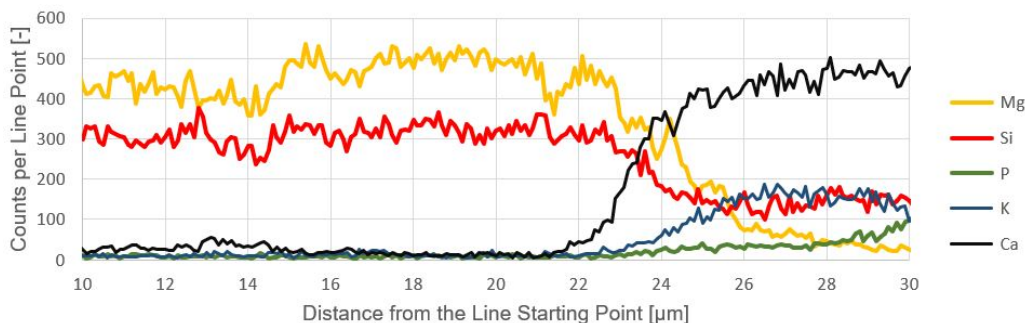


Figure 58: Line Scan 4 profile of Mg, Si, P, K, and Ca as marked in Figure 56 of experiment DFB-05 from a olivine particle into an agglomerated phase

Line Scan 4 as depicted in Figure 58 demonstrates the elemental composition along the line scan profile from the olivine grain into the bright agglomeration area in-between the olivine particles. Same as in Line Scan 5 the profile indicated an ash fraction with high Ca, K and Si contents. Additionally, qualitative detection of P could be achieved. A closer look on the trend verifies the observation seen through the layer forming area. On the olivine surface a sharp increase of Ca is detected. As soon as Ca is the dominant element, a rise in K takes place. Different layer forming mechanisms could not be detected.

The phenomena obtained from the line scans conducted in the area shown in Figure 56 showed different phenomena than for the area depicted in Figure 52. The layer formation mechanism seems to have shifted from clear Ca-rich layer formation to a more inhomogeneous composition.

Within the layers two discriminable layer zones exist. Major difference between these layers is the Ca:Si:K ratio. Closer to the olivine surface the amount of K decreases and a Ca-rich and Si-rich inner layer was formed. The phenomenon of Mg-enrichment in the transition area between outer and inner layer is detected multiple times. For the agglomeration area the formed layer seems to be running into the ash derived fraction continuously. Again, K is found to exist only in a certain distance from the surface.

For verification and quantification a mapping of area 2 was performed. The loss of information was minimized by doing the analysis in reference to all elements of slightest qualitative occurrence in the map report executed previously. The entity of elements analysed via mapping is: C, O, Na, Mg, Al, Si, P, S, Cl, K, Ca, and Fe. For reasons of manageability only the mapping results which presented valuable information are depicted in Figure 59.

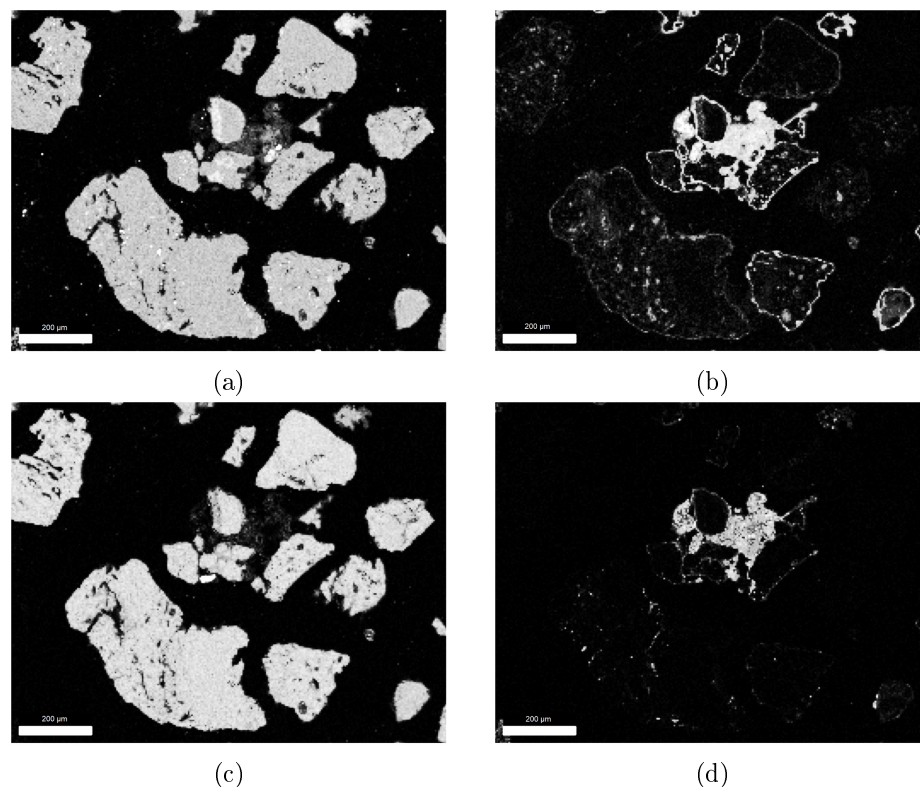


Figure 59: EDS mapping of (a) Si, (b) Ca, (c) Mg, and (d) K obtained from area 2 in Figure 56 of experiment DFB-05

As demonstrated in Figure 59 the mappings of Si and Mg as well as Ca and K demonstrate similar areas of occurrence, which indicates that both Si and Mg are the dominant elements in the bed material, but not in the agglomerated ash fraction, where Ca and K are dominant. For the Si and Mg mappings the main difference is the higher detected presence of Si in the agglomerated ash area, this has been proven by quantitative measurements. On a C-free and O-free basis the dominating elements are Ca with approximately 60 % atomic share and K with approximately 25 % atomic share. Quantitative amounts of Si around 5 % atomic share are detected in average in the ash fraction and the elements Mg, P and Fe can be detected qualitatively.

Quantitative analysis of the layer composition could be obtained only as mean value for the overall layers on the particles. As the mappings of Ca and K in Figure 59 show, the tendency of Ca to form a continuous layer on the olivine grains seems enhanced in comparison to the tendency

of K to be involved in the layer formation. Analysis of the Ca-rich inner layer zones detects K only as trace elements in unquantifiable amounts. The average atomic ratio of Ca:Si:Mg in these inner zones is approximately 2:1:1. Other trace elements detected in these areas are Fe and P. Analysis of the outer layer results in an elemental composition resembling the measurement for the agglomerated ash area. The amounts of Ca and K measured in average for the outer layer formation zones comply with the mean values from the ash fraction. Therefore the discontinuous detection of K in the layers of coarse and fine olivine particles reflects the difference of discriminable layer formation. Only for particle with sufficient interaction with ash derived matter the formation of two discriminable layers is probable.

4.7 DFB-06 - RH

The analysis of this experiment is conducted to investigate layer formation and agglomeration tendency, when little potential of Ca is provided by the ash fraction. A mixture of lime and olivine is used for the gasification of RH feedstock. The theoretical ash load is the highest within the experiments in this work.

4.7.1 Gasification Parameters

The key parameters of operation are summarized in Table 17. Especially the high theoretical ash load and its effect on layer formation and possible agglomeration phenomena are investigated. The approximate gasification temperature is applied for the DFB steam gasification without SER processing. For the SER process the temperature was decreased to approximately 700 °C.

Parameter	Unit	Value
Bed Material	kg	28.5 Lime (KSW) 28.5 Lime (KS01) 12.7 Olivine
Feedstock	kg DS	106.6 RH
Feeding Rate	kg TS/hour	25.6
Theoretical Ash Load	kg/kg	19.2
Total Feeding Time	hours	4.5
Approx. Gasification Temperature (excl. SER)	°C	750

Table 17: Key parameters for gasification of experiment DFB-06

The atomic shares of ash forming elements derived from the feedstock are depicted in Figure 60. The dominance of Si and the minor shares of other elements in the ash fraction are clearly visible.

A schematic timeline for the experimental operation is depicted in Figure 61. The individual steps indicate, that stabilization of the key parameters of gasification was the main problem during the process. For this purpose additional lime was introduced into the system when the gasification was halted. Temperature and fluidization could be stabilized through this method. Furthermore the influence of the implemented SER process needs to be discussed.

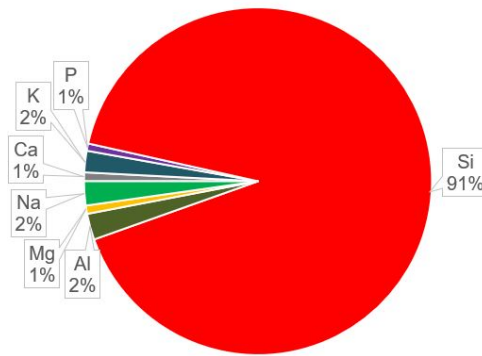


Figure 60: Atomic share of ash forming elements given in % during experiment DFB-06



Figure 61: Timeline for experiment DFB-06

4.7.2 SEM/EDS Analysis & Discussion

The analytical approach is made to focus on the influence of produced ash which is almost completely free of Ca. The dominance of Si with minor shares of Al, Na and K creates very little ash induced potential for the creation of catalytically active Ca-rich layers. To improve the visibility of detected phenomena and focus on both bed material fractions separately the analysis is conducted on two different areas.

The area for the analysis of layer formation and ash interaction of lime particles is depicted in Figure 62. Reports of marked areas and line scans on the marked profiles were obtained. The different particles are identified by the area reports 1 to 3 and an overall report is conducted for the entity of elements which need to be considered for the line scans and mappings.

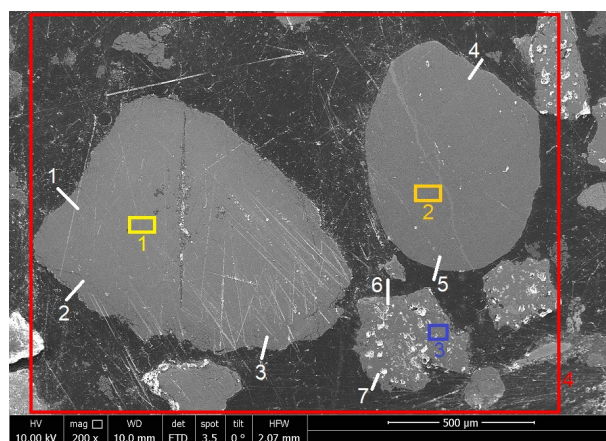


Figure 62: SEM image including the analysed areas for the area reports and the line scan profiles for experiment DFB-06. Visible are lime and olivine particles.

Report analyses of the areas 1 to 3 prove the particles to be of different compositions. Area 1 represents the composition of lime with little impurities of C. On a C-free and O-free basis the

atomic share of Ca in the particle cross section is approximately 98 %. Si is detected qualitatively as trace element.

Area 2 represents the composition of lime with high impurity of Mg and little impurity of C. On a C-free and O-free basis the detected atomic share of Ca and Mg combined is 99 %, and the Ca:Mg atomic ratio is approximately 8:5. Knowing that MgO and Mg-Ca-oxides (dolomite) are a major impurity of the lime used as bed material the origin of the high Mg share seems plausible.

Area 3 represents the composition of olivine with a Mg:Si atomic ratio of approximately 2:1. The qualitative detection of Fe and C is obtained from the area report as well.

Analysis of area 4 for the entity of present elements on the sample surface shows dominance of C, O, and Ca. The additionally detected elements are Mg, Si, and Fe.

The line scan profiles marked in Figure 62 are mainly focussing on the pure lime particle and the lime particle with elevated Mg share. To gather a maximum of information about the layer formation on olivine grain, Line Scan 6 and 7 are conducted through the particle surface of olivine as well. For the evaluation of olivine layer formation an analysis of a different area is conducted as well. The set of elements inserted for analysis of the line scan profiles is: C, O, Na, Mg, Al, Si, K, Ca and Fe.

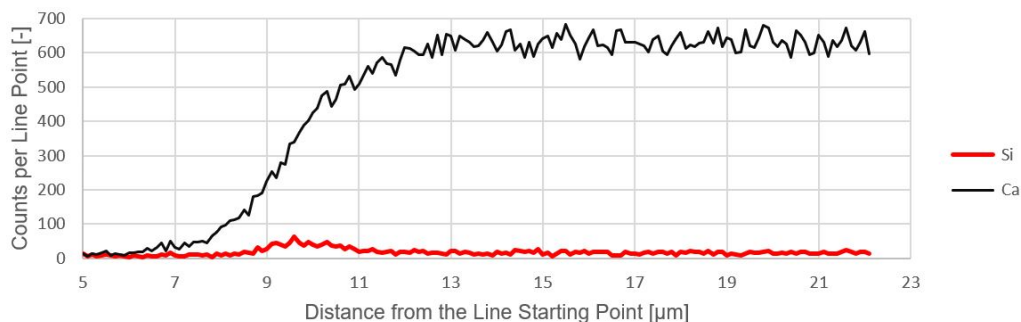


Figure 63: Line Scan 1 profile of Si and Ca as marked in Figure 62 of experiment DFB-06 through a lime particle surface

Line Scan 1 as depicted in Figure 63 shows the profile through the particle surface of pure lime. The data shows, that layer formation is not detectable on the particle surface. The slightly visible peak of Si does not provide enough intensity to conclude, that any layer formation process is taking place. Line Scans 2 and 3 had the same outcome as Line Scan 1, therefore Figure 63 is representative for the analysis of pure lime particles. To provide proof for the absence of layers on pure lime particles the mappings are taken into account as well.

Line Scan 4 through the lime/dolomite particle as depicted in Figure 64 shows analogous phenomena as the pure lime particle. The line scan data does not provide an intensity profile which indicates layer formation. The share of Mg within the particle structure is detected in significant amounts. An identical profile could be obtained through Line Scan 5.

For verification and quantification a mapping of area 4 was made. The loss of information was minimized by doing the analysis in reference to all elements of slightest qualitative occurrence in the elemental report of area 4. The entity of elements analysed via mapping is: C, O, Na, Mg, Al, Si, K, Ca, and Fe. For reasons of manageability only the mapping results which presented valuable information are depicted in Figure 65.

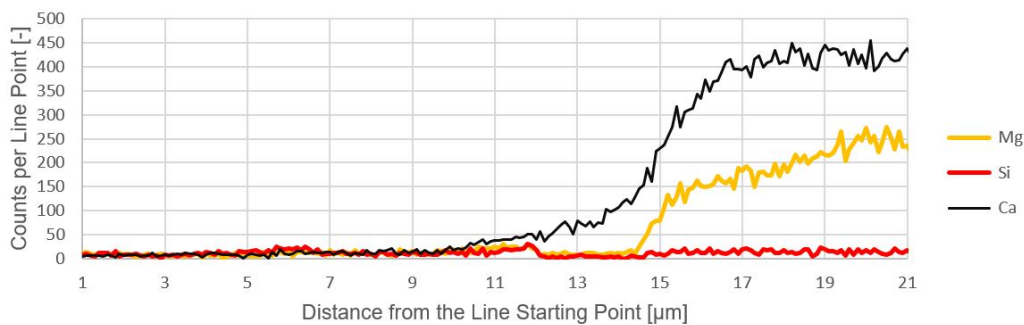


Figure 64: Line Scan 4 profile of Mg, Si and Ca as marked in Figure 62 of experiment DFB-06 through a lime/dolomite particle surface

The data and information obtained from the mapping analysis gives clear information about the particles within the analysed area. The particle analysed in area report 1 shows total dominance of Ca. For the lime/dolomite particle a homogeneous distribution of Mg and Ca is detected, with a crack through the cross section which is enriched in Ca and absolutely Mg-free. Particle 3, as it is an olivine grain, may be identified as such by the mapping. For the layer formation analysis of olivine an additional area of investigation is taken, to facilitate the recognizability and depiction. Qualitatively a layer formation by Ca can be seen in section (b) of Figure 65.

The quantitative mapping results for the pure lime particle indicated an average Ca atomic share of 99 % on a C-free and O-free basis. Impurities could not even be qualitatively identified. In the superficial area of the lime particle Si can be detected qualitatively, as Line Scan 1 in Figure 64 already indicated. Nevertheless, the layer formation is neither continuous nor quantitatively measurable.

The quantitative mapping results for the lime/dolomite particle indicates an average combined atomic share of Ca and Mg of 99 % on a C-free and O-free basis (which was already detected via area report). In comparison to the area report result for the Ca:Mg atomic ratio (8:5) the average Ca:Mg ratio detected by mapping is approximately 2:1. For the particle surface area the results are exactly the same as for the pure lime particle. Layer formation was discontinuous and of too little intensity to be verified.

For the analysis of layer formation on the olivine particles an area without lime grains was taken. This was made for reasons of contrast on the mapping images and to provide the layer signal of multiple olivine particles. The area analysed is depicted in Figure 66. To obtain initial data about the olivine cross section a report of area 1 was obtained. The entity of occurring elements was measured by report analysis of area 2. Qualitative analysis of layer formation on the olivine is executed through line scans.

The analysis of area 1 proved the particle to be an olivine grain with an atomic ratio Mg:Si:Fe of approximately 10:6:1. Apart from these three elements any additional elements could not be detected on a C-free and O-free basis. The analysis of area 2 reflected the dominance of C-rich embedding material and O. For the most important inorganic bed material and ash elements the report could only detect Mg, Si, Ca, Fe, Al and Na qualitatively.

The analysis by line scanning in this area focuses on the layers on the olivine particles. Therefore Line Scans 1 to 4 were conducted as marked in Figure 66. The set of elements which was applied for this purpose is: C, O, Na, Mg, Al, Si, P, K, Ca, Fe.

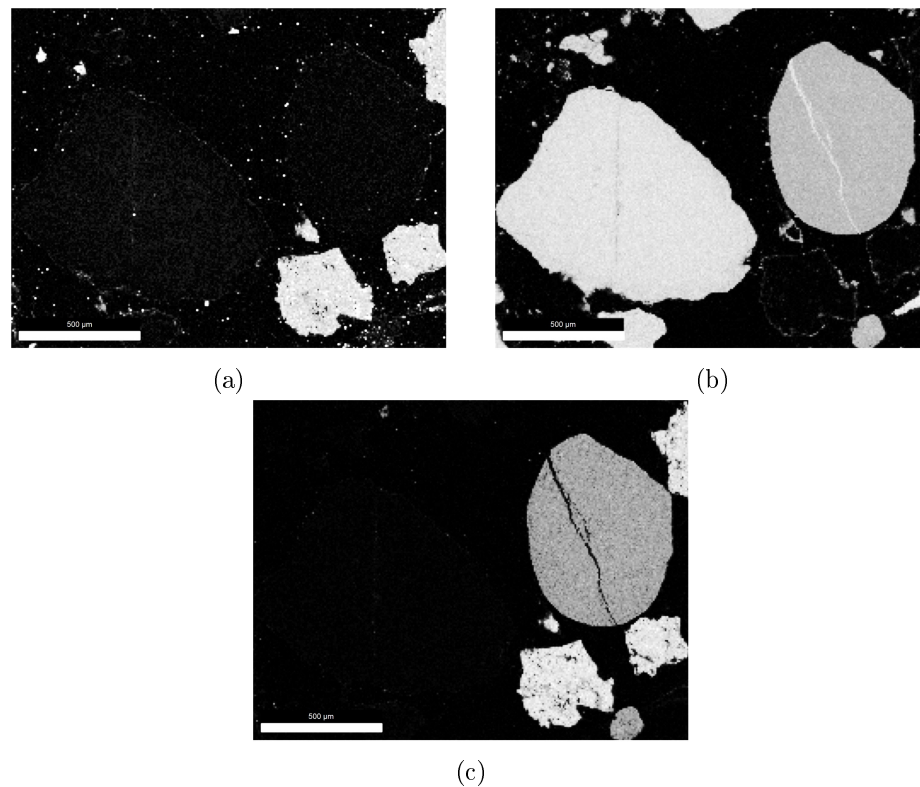


Figure 65: EDS mapping of (a) Si, (b) Ca, and (c) Mg obtained from area 4 in Figure 62 of experiment DFB-06

Line Scan 1, as depicted in Figure 67, is representative for the 4 line profiles conducted in this area and also the Line Scans 6 and 7 in the previously analysed area (as marked in Figure 62). Every line scan indicated significant peaks of Ca in the transition area from bed to embedding material. In 5 out of 6 cases the counts profile of Ca could outpace the counts of Mg and Si in the layer forming zone. This does not directly lead to the conclusion of higher quantitative Ca shares. The profile of the corresponding Si and Mg trends leave the opportunity of layer discrimination open for the mapping quantification.

For verification and quantification a mapping of area 2 was made. The loss of information was minimized by doing the analysis in reference to all elements of slightest qualitative occurrence in the elemental report of area 2. The entity of elements analysed via mapping was: C, O, Na, Mg, Al, Si, P, K, Ca, and Fe. For reasons of manageability only the mapping results which presented valuable information are depicted in Figure 68.

The mapping results depicted in Figure 68 detect all the grains in the area to be of olivine nature. The layer formation of Ca on these particles is clearly visible as well. Apart from Si, Mg, Ca, and Fe no other elements could be detected via mapping on a C-free and O-free basis. A blurring effect on the mapping of Si in section (a) of Figure 68 can be observed. If the origin is from the grinding process or from the ash fraction is undetectable, due to the fine particle distribution it is most likely an intrusion of abrasive material.

Quantitative analysis of the layers on olivine grains were conducted and a discrimination of layers could be made. Since the line between inner and outer layer is not drawn clearly the discrimination can only be executed through average measurement of area composition. This

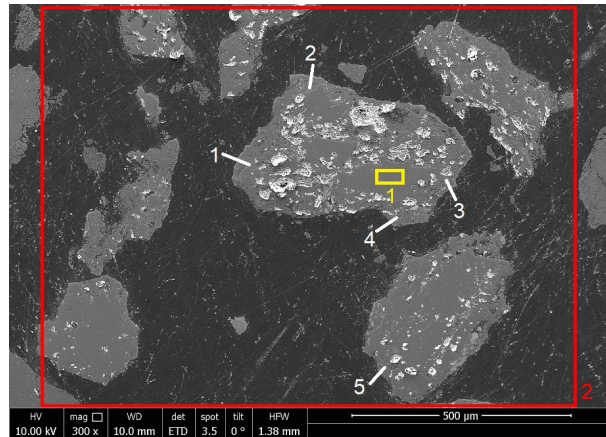


Figure 66: SEM image including the analysed areas for the area reports and the line scan profiles for experiment DFB-06. Visible are olivine particles.

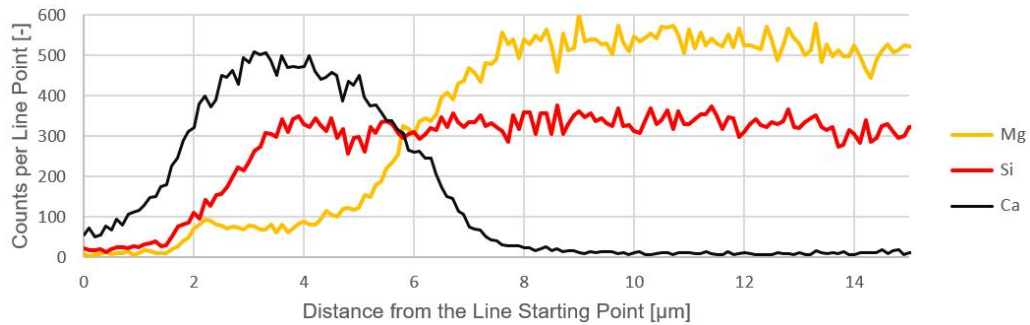


Figure 67: Line Scan 1 profile of Mg, Si and Ca as marked in Figure 66 of experiment DFB-06 through a olivine particle surface

leads to the results of outer layers on the olivine particle with Si:Ca ratios in the range of 5:6 to 5:11. The detection of Mg in the outer layers was only possible qualitatively.

In the inner layers the Ca share could be detected, but was unquantifiable. As already seen in the line scans the share of Mg in the layer forming zones is sub-stoichiometric to the olivine share. As Mg is only detectable qualitatively in the outer layer the detection via mapping verifies the phenomenon obtained through line scanning. For the areas of inner layers the average Mg share equals the share of Si, which still is sub-stoichiometric to the inner olivine shares. While the Si:Mg shares increase from the inner olivine through the layers, the share of Si:Fe shows a different trend. It decreases from approximately 10:1 to 5:1 in the inner layers. For the outer layers a ratio is unavailable since Fe can only be detected qualitatively in the outer layer areas.

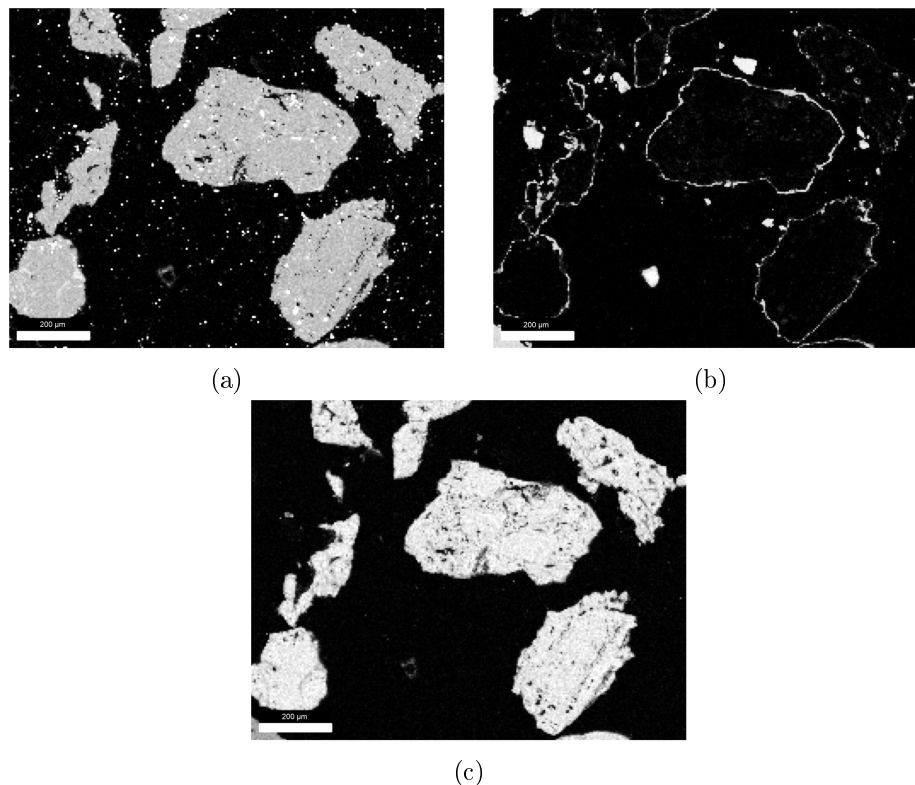


Figure 68: EDS mapping of (a) Si, (b) Ca, and (c) Mg obtained from area 4 in Figure 62 of experiment DFB-06

4.8 Identified Ash-Bed Material-Interactions

The following discussion is divided into several chapters, which are dedicated to the different types of bed material used in the DFB steam gasification system.

4.8.1 Quartz

Layer formation and agglomeration tendencies of quartz have been investigated for two experiments, which are part of a set including three operational runs with partial exchange of bed material. Of these three consecutive processes the last two were analysed (DFB-01 & DFB-02). Almost all of the bed material was exchanged previously to experiment DFB-01, the consecutive operation DFB-02 utilized approximately 80 wt% bed material from DFB-01.

Layer Formation:

Layer formation on quartz particles was generally observed to be dominated by interaction of Ca and Si. The low ash yield and ash content of SW in experiment DFB-01, with a mixture of quartz (SiO_2) and lime (CaO) as bed material, raises reasonable doubts on the influence of ash forming matter in this process. Since Ca and Si are the only elements detected in the quartz layers and both these elements are main elements of the bed materials, the origin of Ca may stem from lime derived material. Especially the total absence of other ash forming elements in the layers indicates the layer formation to be driven by a different source. This source might be a lime fraction derived from the bed material lime by attrition. In comparison to literature data the absence of alkali elements, which are a significant part of woody biomass ash, in the formed

layers is noticeable [107, 119].

Results from experiment DFB-02 point into a similar direction. The mostly recycled quartz particles developed layers on its surface which could be distinguished by EDS analysis. With the higher theoretical ash load during this experiment, the layers still consisted mainly of Ca and Si but main ash forming elements could be detected qualitatively (e.g. Mg, Al, Fe, Ti). To which extent the Ca in these layers is derived by lime bed material or the ash fraction is undetectable.

It seems, that higher ash yields increase the influence of ash forming matter in the layer formation process. Lower ash yields on the other hand decrease the influence, nevertheless layer formation can be promoted through application of lime bed material mixtures. To prove this assumption it was impossible to obtain enough information from the executed analysis. Specially designed operations without feedstock could be made to measure the influence of lime additive in the bed material. The applicability evaluation of the bench-scale FBC reactor demonstrated it to be a possible device for this investigation. Apart from the influence of the lime bed material, the basic layer formation on quartz particles during DFB steam gasification does not provide new findings to literature.

Agglomeration:

Agglomeration processes for quartz particles have only been observed in experiment DFB-02. Detected agglomeration could be identified to occur in conjunction with qualitative amounts of Na. These high amounts could only be measured in areas where agglomeration occurred. Based on the ash composition the main part of Na is introduced into the system through the MWF feedstock. Apart from the occurrence of Na, the composition of the agglomerated area resembles the composition of the layers on the quartz particles. The composition of the agglomerated area and the shares of elements suggest, that agglomeration is initiated by a fraction, which is derived from the produced ash, but does not reflect the ash fraction itself. Especially the share of Al in the agglomerated area is far below the share in the original ash fraction derived from the MWF/GL-mixture feedstock.

The assumption extracted from the analysis data is, that agglomeration of the quartz particles is not induced directly by the ash fraction or by direct attack of alkali compounds. High shares of Al in the feedstock seem to be no major factor in the creation of layers and agglomeration. Apart from the Al share the feedstock of experiment DFB-02 demonstrates high resemblance to woody biomass. Therefore the suggested mechanism for agglomeration would be the coating induced agglomeration through adhesion of alkali silicates and diffusion of Ca [107, 113]. With the information obtained from the EDS analysis the mechanism can not be determined exactly.

4.8.2 Olivine

Layer formation and agglomeration tendencies of olivine have been investigated for three experiments, which were conducted independently. The experiments were executed with highly varying feedstocks and olivine was used as dominant bed material component (DFB-05: 76 wt%) and as minor bed material component (DFB-03: 7 wt%, DFB-06: 18 wt%). The main assumed influences on layer formation and agglomeration mechanisms were ash composition and SER processing.

Layer Formation:

Layer formation detected on olivine particles provides an inconsistent set of data. Although operational time, theoretical ash load and significant shares of Ca in the ash should promote layer formation, it was undetected on the majority of olivine particles from experiment DFB-03. This ob-

ervation stands in contrast to the other experiments analysed and literature data [109,125,127]. Theoretical expectation would suggest, that this experiment provides the best data for Ca-rich layer formation, due to the long operational time and the high theoretical ash load. In conjunction with the theoretical ash load the atomic share of Ca (13 %) in the successively inserted feedstock (MWF, SLF, SCB, GL) provides a high potential of interaction. The influence of SER processing needs to be discussed, but can not be measured quantitatively. If formed layers are dissolved by this SER process, it is an important point of research for future experiments. Contrary to this observation stands the result from experiment DFB-06, where layers are detected clearly although SER processing was applied at the end.

The overall results of layers formed on olivine particles reflect, that direct interaction with the particle surface is only made by Ca. Within the layers significant shares of K (DFB-05) and other ash forming elements can be detected, if the potential provided by the ash is high. Nevertheless direct interaction with the olivine surface was limited to Ca in the observations made. Outer layer zones were detected, which resembled the ash fraction. These outer layers are distinguishable through decreased Si:Ca atomic ratios and presence of ash derived elements such as K and P. The assumption, that layer formation is initialized by solid-solid reaction between CaO and olivine and outer layers might be formed through adhesion of molten K-silicates as proposed by Kuba et al. can be confirmed with the obtained results [127].

Results from experiment DFB-06 show the influence of Ca potential of lime bed material in accordance with the results of experiment DFB-01. Although feedstock (RH) derived ash is almost Ca-free, layers enriched in Ca are formed. The ash composition seemed to be irrelevant for the formation of layers. The only major source of Ca in the DFB system during this experiment is the lime bed material. The most plausible conclusion is, that layers on the olivine particles are created through interaction with lime derived fragments. This assumption is discussed in detail in Chapter 4.8.3.

In summary, the layer composition on olivine particles complies with the literature data described in Chapter 2.5.4. Initial inner layers formed on the particles demonstrate high resemblance with olivine particles composition with significant shares of Ca. Inner layer formation with other elements than Ca stays undetected [127]. In outer layers alkali elements could be measured. The phenomenon of Fe and Mg migration through substitution by Ca could be detected only insufficiently. A preference for Fe migration prior to Mg migration as stated by Kuba et al. could not be measured [127]. The most probable explanation for the absence of this phenomenon is the short operational time.

The layer formation on olivine by lime derived Ca needs further research. The obtained results leave the assumption, that bed material mixtures are a suitable way to promote the formation of Ca-rich layers.

Agglomeration:

Agglomeration processes including olivine were strongly dependent on the ash forming matter. Olivine and its layers did not agglomerate directly, but were connected through ash matter. This ash matter mainly contained Ca, K, and Si shares. The agglomeration through this low melting ash particles complies with previously detected mechanisms [109]. Where ash consists of significant K or Na shares, agglomeration was found to be promoted. Especially in experiment DFB-05, which was terminated by defluidization, the agglomeration of various olivine particles through K-rich ash fraction was detected. The low melting ash fraction seems to be the driving force for the agglomeration happening. Similar observations were obtained for the agglomeration of olivine and quartz in experiment DFB-02, where agglomeration areas showed qualitative amounts of Na. In comparison to the overall ash composition the agglomeration area in experiment DFB-05 showed higher contents of K.

The agglomeration phenomena detected for olivine particles demonstrates the mechanisms,

which may take place. Direct agglomeration through layers on olivine particles stays undetected. The agglomeration process required an alkali-enriched fraction, which was only found in the ash fraction [109]. The problem of defluidization during experiment DFB-05 demonstrated the initiation through ash particles enriched in alkali compounds [137,138]. Literature showed agglomeration initiated by alkali-rich outer layers on olivine [109]. This agglomeration mechanism was not detected even though alkali-rich outer layers were present. Longer operational times might be necessary.

4.8.3 Lime

Little layer formation and no agglomeration phenomena could be detected for lime particles in the entity of experiments analysed. Nevertheless the influence of attrition and fragmentation for this rather soft material needs to be discussed.

Layer Formation:

The only significant detection of layers on lime particles could be achieved for experiment DFB-03 and DFB-04. The layers in experiment DFB-03 showed qualitative detection of main ash forming elements on carbonated particles. If carbonation or SER processing has an influence on these layers stays unknown. Overall the detection of these layers is too imprecise to identify mechanisms or driving forces. Layers in experiment DFB-04 have to be neglected to a great extent, because they are formed by impurities of Mn, which are unquantifiable.

An interesting observation, which does not clearly correspond with usual layer formation was detected for experiment DFB-05. Quantitative amounts of K are found within the structure of lime particles. The mapping results indicate this mechanism is not a layer formation process but an intrusion of K into the particle structure. Taking the unused bed material composition into account, this phenomenon had to be occurring after the insertion into the DFB steam gasification reactor. This observation was unexpected and comparable literature data is unavailable. If K-enrichment within these particles is caused by sample adulteration (e.g. sampling, grinding) or an occurrence, which can be obtained in general for the operational modes of experiment DFB-05 can not be stated clearly at the moment. A possible explanation may be the interaction of lime with gaseous K-compounds, which are formed during the process [1,114]. For a detailed analysis, the thermodynamics of CaO-K interaction have to be studied.

Attrition:

Multiple indicators for significant attrition of lime particles are found all through the experiments. In experiments with little Ca potential provided by the produced ash fraction, layer formation on olivine and quartz particles could still be detected. In these experiments the general influence of ash elements was hardly detectable. This observation promotes the assumption, that attrited lime (which is almost pure CaO) causes the layer formation and not the ash fraction.

Since influences of Ca from the ash and derived from lime bed material can not be discriminated within this work, especially designed experiments for the determination of attrition induced layer formation need to be conducted. The processes should be adapted to guarantee temperature profiles of typical combustion/gasification operations without using feedstock. A suitable option for experimental runs is the bench-scale FBC reactor, since external heating up to approximately 850 °C through heating shells can be applied [132]. The electrical heating system in the DFB reactor is not designed for stable temperature operation at gasification/combustion temperatures, but only has to provide enough thermal energy for the ignition of the feedstock (approx. 400 °C for wood pellets) [133].

5 Conclusion

A short overview of the results and literature data leaves the following conclusion:

- The utilization of the bench-scale FBC reactor for layer formation and agglomeration analysis requires an adaptation of the feeding system and additional flue gas cleaning devices.
- Lime Attrition is a significant parameter during DFB operation. This finding is in accordance with literature data [129, 130, 139, 140]. The obtained results indicate significant influences of attrited lime on layer formation.
- Quartz particle layers are dominated by Si, Ca, and K when woody biomass with sufficient potential of these elements is thermally converted. This finding is in accordance with literature data [116, 118].

For low theoretical ash loads the creation of Ca-rich layers is promoted by bed material mixture with lime. Results indicated the behaviour of Na to be similar to K in interaction with quartz. The share of Na+K combined has been found previously to be a key parameter for the ash chemistry, which implies both elements act similar [114, 116]. Discriminable outer and inner layers are detected.

- Olivine particle layers are dominated by Si, Ca, and Mg. Alkali elements in the ash fraction only have limited interaction with the olivine particle. This finding is in accordance with literature data [109, 127].

The results indicate interaction with Ca derived from lime bed material, when the ash fraction provides little potential of Ca. The influence and potential of lime derived Ca requires adapted operations.

- Alkali-rich feedstock ash initiates and promotes agglomeration processes [44, 108, 141]. The detection of defluidization causing processes taking place during DFB steam gasification could be achieved by SEM and EDS analysis.
- The influence of SER processing on layer formation and agglomeration processes could not be identified.
- Quantitative layer formation or agglomeration for lime particles could not be identified.

6 Outlook

For future research and experiments some highly interesting phenomena, which could be indicated but not verified in this work, should be taken into account.

- The resemblance in ash chemistry between several waste feedstocks (MWF, SLF) and woody biomass was indicated but unverified. Further research should focus on longer operational times to develop thicker layers to better understand the exact mechanisms occurring.
- The interaction of attrited lime with other bed material types needs to be analysed. The proposed way of research is through external heating without using feedstock, to determine if Ca, originated from lime, interacts with other bed materials to form layers.
- For additional research of lime layer formation mechanisms, operational times need to be elevated and the different layer formation on CaO and CaCO₃ needs to be investigated.
- For the evaluation of SER processes and its influence on layer formation mechanisms, bed material samples should be taken before and after conducting the SER process to obtain the effects more clearly.

Nomenclature

ΔG^0	Gibbs Free Standard Enthalpy
λ	Air-Fuel Ratio
CB	Coniferous Bark
CFB	Circulating Fluidized Bed
CHP	Combined Heat and Power
DAF	Dry and Ash Free
DDGS	Distillers Dried Grain with Solubles
DFB	Dual-Fluidized Bed
DS	Dry Substance
EDS	Energy-Dispersive X-Ray Spectroscopy
EFB	Entrained Fluidized Bed
EOP	Exhausted Olive Pomace
FB	Fluidized Bed
FBC	Fluidized Bed Combustion
FBG	Fluidized Bed Gasification
GF	Grate Firing
GL	German Lignite
HNS	Hazelnut Shells
IAT	Initial Agglomeration Temperature
IDT	Initial Defluidization Temperature
LHV	Lower Heating Value
LOI	Loss on Ignition
MSS	Municipal Sewage Sludge
MSW	Municipal Solid Waste
MWF	Municipal Waste Fraction
NL	Norm Litres
PF	Pulverized Fuel
RH	Rice Husks
SCB	Sugar Cane Bagasse
SEM	Scanning Electron Microscopy

SER Sorption Enhanced Reforming

SFB Stationary Fluidized Bed

SLF Shredder Light Fraction

SRCW Short Rotation Coppice Willow

SW Softwood

TS Total Substance

Wt% Mass Percentage

References

- [1] Martin Kaltschmitt, Hans Hartmann, and Hermann Hofbauer, editors. *Energie aus Biomasse: Grundlagen, Techniken und Verfahren*. Springer Vieweg, Berlin Heidelberg, 3., aktualisierte und erweiterte auflage edition, 2016. OCLC: 948486478.
- [2] D. M. Etheridge, L. P. Steele, R. L. Langenfelds, R. J. Francey, J.-M. Barnola, and V. I. Morgan. Natural and anthropogenic changes in atmospheric CO₂ over the last 1000 years from air in Antarctic ice and firn. *Journal of Geophysical Research: Atmospheres*, 101(D2):4115–4128, February 1996.
- [3] Lasse Rosendahl, editor. *Biomass combustion science, technology and engineering*. Number 40 in Woodhead publishing series in energy. Woodhead Publ, Oxford, 2013. OCLC: 813394494.
- [4] Martin Kranert and Klaus Cord-Landwehr, editors. *Einführung in die Abfallwirtschaft: mit 131 Tabellen*. Studium. Vieweg + Teubner, Wiesbaden, 4., vollst. aktualisierte und erw. aufl edition, 2010. OCLC: 643059968.
- [5] Hans Martens and Daniel Goldmann. *Recyclingtechnik*. Springer Fachmedien Wiesbaden, Wiesbaden, 2016.
- [6] Morten Ingerslev, Simon Skov, Lisbeth Sevel, and Lars Bo Pedersen. Element budgets of forest biomass combustion and ash fertilisation – A Danish case-study. *Biomass and Bioenergy*, 35(7):2697–2704, July 2011.
- [7] Noora Huotari, Eila Tillman-Sutela, Mikko Moilanen, and Raija Laiho. Recycling of ash – For the good of the environment? *Forest Ecology and Management*, 348:226–240, July 2015.
- [8] Hans van der Sloot and International Ash Working Group, editors. *Municipal solid waste incinerator residues*. Number 67 in Studies in environmental science. Elsevier, Amsterdam ; New York, 1997.
- [9] Andreas Hornung, editor. *Transformation of Biomass: Theory to Practice*. John Wiley & Sons, Ltd, Chichester, UK, August 2014.
- [10] James H. Clark and Fabien E. I. Deswarte, editors. *Introduction to Chemicals from Biomass: Clark/Introduction to Chemicals from Biomass*. John Wiley & Sons, Ltd, Chichester, UK, August 2008.
- [11] Naomi B. Klinghoffer and Marco J. Castaldi, editors. *Waste to energy conversion technology*. Number number 29 in Woodhead publishing series in energy. Woodhead Publishing Limited, Oxford, UK, 2013. OCLC: ocn808413468.
- [12] Michael E Himmel. *Direct microbial conversion of biomass to advanced biofuels*. Elsevier, Amsterdam, 2015. OCLC: 908620677.
- [13] Michael Cox, Henk Nugteren, and Maria Janssen-Jurkovicova, editors. *Combustion residues: current, novel and renewable applications*. John Wiley & Sons, Chichester, England ; Hoboken, NJ, 2008. OCLC: ocn181368841.
- [14] Adrian James, Ronald Thring, Steve Helle, and Harpuneet Ghuman. Ash Management Review-Applications of Biomass Bottom Ash. *Energies*, 5(12):3856–3873, October 2012.

- [15] R.C.E. Modolo, T. Silva, L. Senff, L.A.C. Tarelho, J.A. Labrincha, V.M. Ferreira, and L. Silva. Bottom ash from biomass combustion in BFB and its use in adhesive-mortars. *Fuel Processing Technology*, 129:192–202, January 2015.
- [16] G.C.H. Doudart de la Grée, M.V.A. Florea, A. Keulen, and H.J.H. Brouwers. Contaminated biomass fly ashes – Characterization and treatment optimization for reuse as building materials. *Waste Management*, 49:96–109, March 2016.
- [17] A. Maresca, J. Hyks, and T.F. Astrup. Recirculation of biomass ashes onto forest soils: ash composition, mineralogy and leaching properties. *Waste Management*, September 2017.
- [18] Márcia Freire, Helena Lopes, and Luís A.C. Tarelho. Critical aspects of biomass ashes utilization in soils: Composition, leachability, PAH and PCDD/F. *Waste Management*, 46:304–315, December 2015.
- [19] I Obernberger, T Brunner, and G Barnthaler. Chemical properties of solid biofuels—significance and impact. *Biomass and Bioenergy*, 30(11):973–982, November 2006.
- [20] Mahad Baawain, Abdullah Al-Mamun, Hamid Omidvarborna, and Wala Al-Amri. Ultimate composition analysis of municipal solid waste in Muscat. *Journal of Cleaner Production*, 148:355–362, April 2017.
- [21] Emilia den Boer, Andrzej Jędrzak, Zygmunt Kowalski, Joanna Kulczycka, and Ryszard Szpadt. A review of municipal solid waste composition and quantities in Poland. *Waste Management*, 30(3):369–377, March 2010.
- [22] M. Liikanen, O. Sahimaa, M. Hupponen, J. Havukainen, J. Sorvari, and M. Horttanainen. Updating and testing of a Finnish method for mixed municipal solid waste composition studies. *Waste Management*, 52:25–33, June 2016.
- [23] Stanislav V. Vassilev, David Baxter, Lars K. Andersen, and Christina G. Vassileva. An overview of the chemical composition of biomass. *Fuel*, 89(5):913–933, May 2010.
- [24] Matthew J. Aylott, E. Casella, I. Tubby, N. R. Street, P. Smith, and Gail Taylor. Yield and spatial supply of bioenergy poplar and willow short-rotation coppice in the UK. *New Phytologist*, 178(2):358–370, April 2008.
- [25] Blas Mola-Yudego and José Ramón González-Olabarria. Mapping the expansion and distribution of willow plantations for bioenergy in Sweden: Lessons to be learned about the spread of energy crops. *Biomass and Bioenergy*, 34(4):442–448, April 2010.
- [26] Blas Mola-Yudego and Pär Aronsson. Yield models for commercial willow biomass plantations in Sweden. *Biomass and Bioenergy*, 32(9):829–837, September 2008.
- [27] Ingwald Obernberger and Gerold Thek. Physical characterisation and chemical composition of densified biomass fuels with regard to their combustion behaviour. *Biomass and Bioenergy*, 27(6):653–669, December 2004.
- [28] M. Mandø. Direct combustion of biomass. In *Biomass Combustion Science, Technology and Engineering*, pages 61–83. Elsevier, 2013.
- [29] Robert C. Brown, editor. *Thermochemical Processing of Biomass: Conversion into Fuels, Chemicals and Power*. John Wiley & Sons, Ltd, Chichester, UK, March 2011.
- [30] Prabir Basu. *Biomass gasification, pyrolysis, and torrefaction: practical design and theory*. Academic Press is and imprint of Elsevier, Amsterdam ; Boston, second edition edition, 2013. OCLC: ocn852806063.

- [31] J.P. Wolf and Dong. Biomass combustion for power generation: an introduction. In Biomass Combustion Science, Technology and Engineering, pages 3–8. Elsevier, 2013.
- [32] Walter R. Niessen. Combustion and incineration processes: applications in environmental engineering. CRC Press/Taylor & Francis, Boca Raton, 4th ed edition, 2010. OCLC: ocn318875286.
- [33] Chungun Yin, Lasse A. Rosendahl, and Søren K. Kær. Grate-firing of biomass for heat and power production. Progress in Energy and Combustion Science, 34(6):725–754, December 2008.
- [34] Albino Reis and European Conference on Industrial Furnaces and Boilers, editors. Industrial furnaces and boilers: proceedings of the 4th European conference, 1 - 4 April 97, Espinho-Porto, Portugal. INFUB, Rio Tinto, Portugal, 1. ed edition, 1997.
- [35] Hermann Hofbauer. Unterlagen zur Vorlesung Wirbelschichttechnik, 1995.
- [36] Thomas Brunner. Aerosols and coarse fly ashes in fixed-bed biomass combustion: formation, characterisation and emissions. Number 7 in Series thermal biomass utilization. BIOS Bioenergiesysteme, Graz, 1. ed edition, 2006. OCLC: 934064406.
- [37] J. Porteiro, D. Patiño, J. Moran, and E. Granada. Study of a Fixed-Bed Biomass Combustor: Influential Parameters on Ignition Front Propagation Using Parametric Analysis. Energy & Fuels, 24(7):3890–3897, July 2010.
- [38] Nguyen Dinh Tung, Dieter Steinbrecht, and Tristan Vincent. Experimental Investigations of Extracted Rapeseed Combustion Emissions in a Small Scale Stationary Fluidized Bed Combustor. Energies, 2(1):57–70, February 2009.
- [39] Lianming Li, Chunjiang Yu, Fang Huang, Jisong Bai, Mengxiang Fang, and Zhongyang Luo. Study on the Deposits Derived from a Biomass Circulating Fluidized-Bed Boiler. Energy & Fuels, 26(9):6008–6014, September 2012.
- [40] Lianming Li, Chunjiang Yu, Jisong Bai, Qinhui Wang, and Zhongyang Luo. Heavy metal characterization of circulating fluidized bed derived biomass ash. Journal of Hazardous Materials, 233-234:41–47, September 2012.
- [41] Wan-Xi Peng, Sheng-Bo Ge, Abdol Ghaffar Ebadi, Hikmat Hisoriev, and Mohammad Javad Esfahani. Syngas production by catalytic co-gasification of coal-biomass blends in a circulating fluidized bed gasifier. Journal of Cleaner Production, 168:1513–1517, December 2017.
- [42] Stefan Kern, Christoph Pfeifer, and Hermann Hofbauer. Gasification of wood in a dual fluidized bed gasifier: Influence of fuel feeding on process performance. Chemical Engineering Science, 90:284–298, March 2013.
- [43] Friedrich Kirnbauer and Hermann Hofbauer. The mechanism of bed material coating in dual fluidized bed biomass steam gasification plants and its impact on plant optimization. Powder Technology, 245:94–104, September 2013.
- [44] Marcus Öhman, Linda Pommer, and Anders Nordin. Bed Agglomeration Characteristics and Mechanisms during Gasification and Combustion of Biomass Fuels. Energy & Fuels, 19(4):1742–1748, July 2005.

- [45] Maria Zevenhoven-Onderwater, Rainer Backman, Bengt-Johan Skrifvars, and Mikko Hupa. The ash chemistry in fluidised bed gasification of biomass fuels. Part I: predicting the chemistry of melting ashes and ash-bed material interaction. *Fuel*, 80(10):1489–1502, August 2001.
- [46] Stanislav V. Vassilev, David Baxter, Lars K. Andersen, Christina G. Vassileva, and Trevor J. Morgan. An overview of the organic and inorganic phase composition of biomass. *Fuel*, 94:1–33, April 2012.
- [47] Margaret E. Farago, editor. *Plants and the Chemical Elements*. Wiley-VCH Verlag GmbH, Weinheim, Germany, June 1994.
- [48] B.M Jenkins, L.L Baxter, T.R Miles, and T.R Miles. Combustion properties of biomass. *Fuel Processing Technology*, 54(1-3):17–46, March 1998.
- [49] Thomas R. Miles, Thomas R. Miles, Larry L. Baxter, Richard W. Bryers, Bryan M. Jenkins, and Laurance L. Oden. Boiler deposits from firing biomass fuels. *Biomass and Bioenergy*, 10(2-3):125–138, January 1996.
- [50] A.A. Tortosa Masiá, B.J.P. Buhre, R.P. Gupta, and T.F. Wall. Characterising ash of biomass and waste. *Fuel Processing Technology*, 88(11-12):1071–1081, December 2007.
- [51] David T. Clarkson. Calcium transport between tissues and its distribution in the plant. *Plant, Cell and Environment*, 7(6):449–456, August 1984.
- [52] A. J. M. Baker and J. Proctor. The influence of cadmium, copper, lead, and zinc on the distribution and evolution of metallophytes in the British Isles. *Plant Systematics and Evolution*, 173(1-2):91–108, 1990.
- [53] D. A. Robb and W. S. Pierpoint, editors. *Metals and micronutrients: uptake and utilization by plants*. Number no. 21 in *Annual proceedings of the Phytochemical Society of Europe*. Academic Press, London ; New York, 1983.
- [54] Eric John Hewitt and Terence Athur Smith. *Plant mineral nutrition*. English U. P, London, 1975. OCLC: 1278598.
- [55] Anna Hwang, Wonhyun Ji, and Jeehyeong Khim. Characteristics of phosphorus containing waste-bones. *Materials Letters*, 61(3):677–679, February 2007.
- [56] Charlotte Poschenrieder, Benet Gunsé, Isabel Corrales, and Juan Barceló. A glance into aluminum toxicity and resistance in plants. *Science of The Total Environment*, 400(1-3):356–368, August 2008.
- [57] Hideaki Matsumoto. Cell biology of aluminum toxicity and tolerance in higher plants. In *International Review of Cytology*, volume 200, pages 1–46. Elsevier, 2000.
- [58] R. B. Clark. Effect of aluminum on growth and mineral elements of al-tolerant and Al-intolerant corn. *Plant and Soil*, 47(3):653–662, August 1977.
- [59] Merle Tränkner, Bálint Jákli, Ershad Tavakol, Christoph-Martin Geilfus, Ismail Cakmak, Klaus Dittert, and Mehmet Senbayram. Magnesium deficiency decreases biomass water-use efficiency and increases leaf water-use efficiency and oxidative stress in barley plants. *Plant and Soil*, 406(1-2):409–423, September 2016.
- [60] Waite Agricultural Research Institute, D. J. D. Nicholas, and Adrian R. Egan, editors. *Trace elements in soil-plant-animal systems*. Academic Press, New York, 1975.

- [61] Richard W. Bryers. Fireside slagging, fouling, and high-temperature corrosion of heat-transfer surface due to impurities in steam-raising fuels. *Progress in Energy and Combustion Science*, 22(1):29–120, January 1996.
- [62] G. R. Cramer, A. Lauchli, and V. S. Polito. Displacement of Ca^{2+} by Na^{+} from the Plasmalemma of Root Cells : A Primary Response to Salt Stress? *PLANT PHYSIOLOGY*, 79(1):207–211, September 1985.
- [63] F. P. W. Winteringham. Soil and fertilizer nitrogen. Number 244) in (Technical reports series. International Atomic Energy Agency. IAEA, Vienna, 1984. OCLC: 252376671.
- [64] Pavel Tlustoš, Petr Cigler, M Hrubý, Stanislav Kužel, Jirina Száková, and J Balík. The role of titanium in biomass production and its influence on essential elements' contents in field growing crops. *Plant, Soil and Environment*, 51, 2005.
- [65] Claire L. Carlson, Domy C. Adriano, and Philip M. Dixon. Effects of Soil-Applied Selenium on the Growth and Selenium Content of a Forage Species. *Journal of Environment Quality*, 20(2):363, 1991.
- [66] J.C. Dawson and J.W. Anderson. Comparative enzymology of cystathionine and selenocystathionine synthesis of selenium-accumulator and non-accumulator plants. *Phytochemistry*, 28(1):51–55, 1989.
- [67] Karaj S. Dhillon and Surjit K. Dhillon. Accumulation of selenium in sugarcane (*Sachharum officinarum* Linn.) in seleniferous areas of Punjab, India. *Environmental Geochemistry and Health*, 13(3):165–170, September 1991.
- [68] R. Macholz. Trace Element Analytical Chemistry in Medicine and Biology. Vol. 4. Proceedings of the Fourth International Workshop Neuherberg, Federal Republic of Germany, April 1986. Herausgegeben von P. Brätter und P. Schramel. 629 Seiten, zahlr. Abb. und Tab. Walter de Gruyter, New York 1987, Preis: 295,—DM. *Food / Nahrung*, 31(8):808–808, 1987.
- [69] Alina Kabata-Pendias and Henryk Pendias. Trace elements in soils and plants. CRC Press, Boca Raton, Fla, 1984.
- [70] F. M. Rhoads, S. M. Olson, and A. Manning. Copper Toxicity in Tomato Plants. *Journal of Environment Quality*, 18(2):195, 1989.
- [71] Manuela D. Machado, Eduardo V. Soares, and Helena M.V.M. Soares. Selective recovery of copper, nickel and zinc from ashes produced from *Saccharomyces cerevisiae* contaminated biomass used in the treatment of real electroplating effluents. *Journal of Hazardous Materials*, 184(1-3):357–363, December 2010.
- [72] L. M. Mugwira and B. D. Knezek. Navy bean responses to zinc fertilizers. *Communications in Soil Science and Plant Analysis*, 2(5):337–343, January 1971.
- [73] A.W. Gardner and P.K. Hall-Patch. An outbreak of industrial molybdenosis. *Veterinary Record*, Vol. 74:113–115, 1962.
- [74] D.D. Hemphill, University of Missouri-Columbia Environmental Health Center, and University of Missouri Extension Division. Trace Substances in Environmental Health, IV: Proceedings. University of Missouri, 1971.
- [75] T. Wallace. The Diagnosis of Mineral Deficiencies of Plants by Visual Symptoms. *Soil Science*, 74(5), 1952.

- [76] Thomas N. Cooley, Marina H. Gonzalez, and Dean F. Martin. Radio-Manganese, -Iron, and -Phosphorus Uptake by Water Hyacinth and Economic Implications. *Economic Botany*, 32(4):371–378, 1978.
- [77] S.B. Wilson and D.J.D. Nicholas. A cobalt requirement for non-nodulated legumes and for wheat. *Phytochemistry*, 6(8):1057–1066, August 1967.
- [78] André Läuchli and Roderick Leon Bielecki, editors. *Inorganic Plant Nutrition*. Springer Berlin Heidelberg, Berlin, Heidelberg, 1983.
- [79] N. W. Lepp, editor. *Effect of Heavy Metal Pollution on Plants*. Springer Netherlands, Dordrecht, 1981.
- [80] Barry G. Morrell, Nicholas W. Lepp, and David A. Phipps. Vanadium uptake by higher plants. *Minerals and the Environment*, 5(2-3):79–81, September 1983.
- [81] Helen L. Cannon. The Biogeochemistry of Vanadium. *Soil Science*, 96(3), 1963.
- [82] Giovainni Micera and Alessandro Dessì. Chromium adsorption by plant roots and formation of long-lived Cr(V) species: An ecological hazard? *Journal of Inorganic Biochemistry*, 34(3):157–166, November 1988.
- [83] R. A. Skeffington, P. R. Shewry, and P. J. Peterson. Chromium uptake and transport in barley seedlings (*Hordeum vulgare* L.). *Planta*, 132(3):209–214, 1976.
- [84] P. R. Shewry and P. J. Peterson. The Uptake and Transport of Chromium by Barley Seedlings. *Journal of Experimental Botany*, 25(4):785–797, 1974.
- [85] Helmut Sigel and Astrid Sigel, editors. Nickel and its role in biology. Number v. 23 in *Metal ions in biological systems*. M. Dekker, New York, 1988.
- [86] J. C. Bartley and E. F. Reber. Toxic effects of stable strontium in young pigs. *The Journal of Nutrition*, 75:21–28, September 1961.
- [87] J. F. Lembrechts, J. H. van Ginkel, and G. M. Desmet. Comparative study on the uptake of strontium-85 from nutrient solutions and potted soils by lettuce. *Plant and Soil*, 125(1):63–69, June 1990.
- [88] B. A. Markert, editor. *Plants as biomonitors: indicators for heavy metals in the terrestrial environment*. VCH, Weinheim ; New York, 1993.
- [89] Domy C. Adriano. *Trace Elements in Terrestrial Environments*. Springer New York, New York, NY, 2001.
- [90] B. J. Alloway, editor. *Heavy metals in soils*. Blackie ; Halsted Press, Glasgow : New York, 1990.
- [91] Zahra Atafar, Alireza Mesdaghinia, Jafar Nouri, Mehdi Homaei, Masoud Yunesian, Mehdi Ahmadimoghaddam, and Amir Hossein Mahvi. Effect of fertilizer application on soil heavy metal concentration. *Environmental Monitoring and Assessment*, 160(1-4):83–89, January 2010.
- [92] Andrew P. Jackson and Brian J. Alloway. The bioavailability of cadmium to lettuce and cabbage in soils previously treated with sewage sludges. *Plant and Soil*, 132(2):179–186, April 1991.

- [93] J. V. Lagerwerff. Uptake Of Cadmium, Lead And Zinc By Radish From Soil And Air. *Soil Science*, 111(2), 1971.
- [94] Norbert Medlitsch. Untersuchungen zur Interaktion von Biomasseasche und Bettmaterial in Wirbelschichtverbrennung und -vergasung. Diplomarbeit, Technische Universität Wien, Vienna, 2017.
- [95] Robert S. Anderson and Suzanne P. Anderson. *Geomorphology: the mechanics and chemistry of landscapes*. Cambridge University Press, Cambridge ; New York, 2010. OCLC: ocn466341136.
- [96] Gregor Markl. *Minerale und Gesteine*. Springer Berlin Heidelberg, Berlin, Heidelberg, 2015.
- [97] Kurt Bucher and Rodney Grapes. *Petrogenesis of Metamorphic Rocks*. Springer Berlin Heidelberg, Berlin, Heidelberg, 2011.
- [98] Stefan Koppatz. Outlining active bed materials for dual fluidised bed biomass gasification : in-bed catalysts and oxygen/carbonate looping behaviour. Dissertation, Technische Universität Wien, Wien, 2012.
- [99] Mónica Martin. Gasification of alternative biomass feedstock in a dual fluidized bed gasification. Diplomarbeit, Technische Universität Wien, Wien, 2017.
- [100] Eberhart Schiele and Leo W. Berens. *Kalk: Herstellung, Eigenschaften, Verwendung*. Verl. Stahleisen, Düsseldorf, 1972. OCLC: 3323431.
- [101] Bing-Shun Huang, Hsin-Yi Chen, Kui-Hao Chuang, Ren-Xuan Yang, and Ming-Yen Wey. Hydrogen production by biomass gasification in a fluidized-bed reactor promoted by an Fe/CaO catalyst. *International Journal of Hydrogen Energy*, 37(8):6511–6518, April 2012.
- [102] Florian Benedikt, Josef Fuchs, Johannes Christian Schmid, Stefan Müller, and Hermann Hofbauer. Advanced dual fluidized bed steam gasification of wood and lignite with calcite as bed material. *Korean Journal of Chemical Engineering*, 34(9):2548–2558, September 2017.
- [103] Paul Fennell. *Calcium and chemical looping technology for power generation and carbon dioxide (CO₂) capture*. Elsevier, Boston, MA, 2015.
- [104] Mook Tzeng Lim and Zainal Alimuddin. Bubbling fluidized bed biomass gasification—Performance, process findings and energy analysis. *Renewable Energy*, 33(10):2339–2343, October 2008.
- [105] Qiangqiang Ren and Linna Li. Co-combustion of Agricultural Straw with Municipal Sewage Sludge in a Fluidized Bed: Role of Phosphorus in Potassium Behavior. *Energy & Fuels*, 29(7):4321–4327, July 2015.
- [106] A. Schabauer. Co-gasification of sewage sludge and wood in a dual fluidized bed steam gasifier. Master’s thesis, Wien, Techn. Univ., Dipl.-Arb., 2009, Wien, 2009.
- [107] Elisabet Brus, Marcus Öhman, and Anders Nordin. Mechanisms of Bed Agglomeration during Fluidized-Bed Combustion of Biomass Fuels. *Energy & Fuels*, 19(3):825–832, May 2005.
- [108] Alejandro Grimm, Nils Skoglund, Dan Boström, and Marcus Öhman. Bed Agglomeration Characteristics in Fluidized Quartz Bed Combustion of Phosphorus-Rich Biomass Fuels. *Energy & Fuels*, 25(3):937–947, March 2011.

- [109] Alejandro Grimm, Marcus Öhman, Therése Lindberg, Andreas Fredriksson, and Dan Boström. Bed Agglomeration Characteristics in Fluidized-Bed Combustion of Biomass Fuels Using Olivine as Bed Material. *Energy & Fuels*, 26(7):4550–4559, July 2012.
- [110] J. R. Curray and J. C. Griffiths. Sphericity and roundness of quartz grains in sediments. *Geological Society of America Bulletin*, 66(9):1075, 1955.
- [111] Daizo Kunii and Octave Levenspiel. *Fluidization engineering*. Butterworth-Heinemann, Boston, 1991. OCLC: 606321366.
- [112] Willard D. Pye, Margaret Hurst Pye. Sphericity Determinations of Pebbles and Sand Grains. *SEPM Journal of Sedimentary Research*, Vol. 13, 1943.
- [113] Nils Skoglund. Ash chemistry and fuel design focusing on combustion of phosphorus-rich biomass. PhD thesis, Department of applied physics and electronics, Umeå universitet, Umeå, 2014. OCLC: 941603896.
- [114] Dan Boström, Nils Skoglund, Alejandro Grimm, Christoffer Boman, Marcus Öhman, Markus Broström, and Rainer Backman. Ash Transformation Chemistry during Combustion of Biomass. *Energy & Fuels*, 26(1):85–93, January 2012.
- [115] Alejandro Grimm, Nils Skoglund, Dan Boström, Christoffer Boman, and Marcus Öhman. Influence of Phosphorus on Alkali Distribution during Combustion of Logging Residues and Wheat Straw in a Bench-Scale Fluidized Bed. *Energy & Fuels*, 26(5):3012–3023, May 2012.
- [116] Patrycja Piotrowska, Alejandro Grimm, Nils Skoglund, Christoffer Boman, Marcus Öhman, Maria Zevenhoven, Dan Boström, and Mikko Hupa. Fluidized-Bed Combustion of Mixtures of Rapeseed Cake and Bark: The Resulting Bed Agglomeration Characteristics. *Energy & Fuels*, 26(4):2028–2037, April 2012.
- [117] Nils Skoglund, Alejandro Grimm, Marcus Öhman, and Dan Boström. Effects on Ash Chemistry when Co-firing Municipal Sewage Sludge and Wheat Straw in a Fluidized Bed: Influence on the Ash Chemistry by Fuel Mixing. *Energy & Fuels*, 27(10):5725–5732, October 2013.
- [118] Hanbing He, Xiaoyan Ji, Dan Boström, Rainer Backman, and Marcus Öhman. Mechanism of Quartz Bed Particle Layer Formation in Fluidized Bed Combustion of Wood-Derived Fuels. *Energy & Fuels*, 30(3):2227–2232, March 2016.
- [119] Hanbing He, Nils Skoglund, and Marcus Öhman. Time Dependent Crack Layer Formation in Quartz Bed Particles during Fluidized Bed Combustion of Woody Biomass. *Energy & Fuels*, 31(2):1672–1677, February 2017.
- [120] Hanbing He, Nils Skoglund, and Marcus Öhman. Time-Dependent Layer Formation on K-Feldspar Bed Particles during Fluidized Bed Combustion of Woody Fuels. *Energy & Fuels*, 31(11):12848–12856, November 2017.
- [121] Seán T. Mac an Bhaird, Eilín Walsh, Phil Hemmingway, Amado L. Maglinao, Sergio C. Capareda, and Kevin P. McDonnell. Analysis of bed agglomeration during gasification of wheat straw in a bubbling fluidised bed gasifier using mullite as bed material. *Powder Technology*, 254:448–459, March 2014.
- [122] Fabrizio Scala and Riccardo Chirone. An SEM/EDX study of bed agglomerates formed during fluidized bed combustion of three biomass fuels. *Biomass and Bioenergy*, 32(3):252–266, March 2008.

- [123] Nicolas Berguerand and Teresa Berdugo Vilches. Alkali-Feldspar as a Catalyst for Biomass Gasification in a 2-MW Indirect Gasifier. *Energy & Fuels*, 31(2):1583–1592, February 2017.
- [124] Matthias Kuba, Hanbing He, Friedrich Kirnbauer, Dan Boström, Marcus Öhman, and Hermann Hofbauer. Deposit build-up and ash behavior in dual fluid bed steam gasification of logging residues in an industrial power plant. *Fuel Processing Technology*, 139:33–41, November 2015.
- [125] Friedrich Kirnbauer and Hermann Hofbauer. Investigations on Bed Material Changes in a Dual Fluidized Bed Steam Gasification Plant in Güssing, Austria. *Energy & Fuels*, 25(8):3793–3798, August 2011.
- [126] Lopamudra Devi, Menno Craje, Peter Thüne, Krzysztof J. Ptasinski, and Frans J.J.G. Janssen. Olivine as tar removal catalyst for biomass gasifiers: Catalyst characterization. *Applied Catalysis A: General*, 294(1):68–79, October 2005.
- [127] Matthias Kuba, Hanbing He, Friedrich Kirnbauer, Nils Skoglund, Dan Boström, Marcus Öhman, and Hermann Hofbauer. Mechanism of Layer Formation on Olivine Bed Particles in Industrial-Scale Dual Fluid Bed Gasification of Wood. *Energy & Fuels*, 30(9):7410–7418, September 2016.
- [128] Jesús Delgado, María P. Aznar, and José Corella. Biomass Gasification with Steam in Fluidized Bed: Effectiveness of CaO, MgO, and CaO-MgO for Hot Raw Gas Cleaning. *Industrial & Engineering Chemistry Research*, 36(5):1535–1543, May 1997.
- [129] Xuan Yao, Hai Zhang, Hairui Yang, Qing Liu, Jinwei Wang, and Guangxi Yue. An experimental study on the primary fragmentation and attrition of limestones in a fluidized bed. *Fuel Processing Technology*, 91(9):1119–1124, September 2010.
- [130] Zhongxiang Chen, John R. Grace, and C. Jim Lim. Limestone particle attrition and size distribution in a small circulating fluidized bed. *Fuel*, 87(7):1360–1371, June 2008.
- [131] Yuanyuan Shao, Chunbao (Charles) Xu, Jesse Zhu, Fernando Preto, Jinsheng Wang, Han-ning Li, and Chadi Badour. Ash Deposition in Co-firing Three-Fuel Blends Consisting of Woody Biomass, Peat, and Lignite in a Pilot-Scale Fluidized-Bed Reactor. *Energy & Fuels*, 25(7):2841–2849, July 2011.
- [132] Daniel Essletzbichler. Design, set-up and commissioning of a fluidized bed reactor in laboratory scale for thermal-conversion of biomass. Diploma Thesis, Technische Universität Wien, Vienna, 2017.
- [133] Maximilian Kolbitsch. First fuel tests at a novel 100 kWth dual fluidized bed steam gasification pilot plant. Dissertation, Technische Universität Wien, Vienna, 2016.
- [134] Stefan Koppatz, Christoph Pfeifer, Reinhard Rauch, Hermann Hofbauer, Tonja Marquard-Moellenstedt, and Michael Specht. H₂ rich product gas by steam gasification of biomass with in situ CO₂ absorption in a dual fluidized bed system of 8 MW fuel input. *Fuel Processing Technology*, 90(7-8):914–921, July 2009.
- [135] Joseph Goldstein. Scanning electron microscopy and x-ray microanalysis. Springer Science+Business Media, LLC, New York, NY, 4th edition edition, 2017.
- [136] Marcus Öhman and Anders Nordin. A New Method for Quantification of Fluidized Bed Agglomeration Tendencies: A Sensitivity Analysis. *Energy & Fuels*, 12(1):90–94, January 1998.

-
- [137] Weigang Lin, Kim Dam-Johansen, and Flemming Frandsen. Agglomeration in bio-fuel fired fluidized bed combustors. *Chemical Engineering Journal*, 96(1-3):171–185, December 2003.
- [138] Pawin Chaivatamaset and Suvit Tia. The characteristics of bed agglomeration during fluidized bed combustion of eucalyptus bark. *Applied Thermal Engineering*, 75:1134–1146, January 2015.
- [139] Fabrizio Scala and Piero Salatino. Attrition of limestones by impact loading in fluidized beds: The influence of reaction conditions. *Fuel Processing Technology*, 91(9):1022–1027, September 2010.
- [140] Zhongxiang Chen, John R. Grace, and C. Jim Lim. Development of particle size distribution during limestone impact attrition. *Powder Technology*, 207(1-3):55–64, February 2011.
- [141] Sigrid De Geyter, Marcus Öhman, Dan Boström, Morgan Eriksson, and Anders Nordin. Effects of Non-Quartz Minerals in Natural Bed Sand on Agglomeration Characteristics during Fluidized Bed Combustion of Biomass Fuels. *Energy & Fuels*, 21(5):2663–2668, September 2007.

List of Figures

1	Schematic structures and morphology of α -Quartz (left) and β -Quartz (right) [95]	14
2	Idealistic structure of Felspars in a matrix of TO_4 -tetrahedrons with changing orientation and cations (A) in structural hollow spaces [95]	15
3	The orthorhombic crystal structure of olivine [96]	16
4	Ellingham-diagram of thermodynamic stability of main oxides and products of combustion systems with 1 mol O_2 [113]	19
5	Cross sections of K-feldspar bed grain samples taken from the BFB process after (a) 3 days, (b) 5 days, (c) 13 days, (d) 23 days [119]	23
6	Cross sections of quartz bed grain samples taken from the CFB process after (a) 5 days, (b) 11 days, (c) 13 days [119]	23
7	Schematic mechanisms of crack layer formation on quartz particles in FBC of woody biomass fuels [119]	24
8	Cross sections of K-feldspar bed grain samples taken from the BFB process after (a) 1 day, (b) 3 days, (c) 5 days, (d) 13 days, (e) 23 days [120]	25
9	Cross sections of K-feldspar bed grain samples taken from the CFB process after (a) 1 day, (b) 5 days, (c) 11 days [120]	25
10	Schematic mechanisms of layer formation on K-feldspar in FBC of woody biomass fuels [120]	26
11	Proposed substitution mechanism to create CaMgSiO_4 from olivine ($\text{Mg}_{1.8}\text{Fe}_{0.2}\text{SiO}_4$) through intrusion of Ca^{+2} [127]	28
12	Flat die pelletizer by Cissonius GmbH [94]	32
13	Particle-size distribution of the original bed materials CaO-KSW, CaO-KS01, quartz (H31), olivine coarse (OC), and olivine fine (OF)	34
14	Design of the bench-scale fluidized bed reactor for the conversion of biomass at TU Wien; figure adapted from [132]	35
15	Design of the novel 100kW DFB steam gasification pilot plant at TU Wien [133]	37
16	Schematic principle of Sorption Enhanced Reforming (SER) [134]	40
17	Key parameters for combustion and atomic shares of ash forming elements given in % during experiment FBC	47
18	Temperature and pressure drop profile for the FBC experiment in the bench-scale reactor	48
19	SEM image including the analysed area for mapping of experiment FBC. Visible are K-feldspar (left), quartz (right), and ash fraction (below).	48
20	EDS mapping of (a) Si, (b) Ca, (c) K, (d) Na, (e) Al, (f) Mg, (g) P, and (h) Fe, obtained from the red marked area in Figure 19 for experiment FBC	49
21	Atomic share of ash forming elements given in % during experiment DFB-01	51
22	Timeline for experiment DFB-01	52
23	SEM image including the analysed areas for the area report and the line scan profiles of experiment DFB-01. Visible are lime and quartz particles.	52
24	Line Scan 1 profile of Si and Ca as marked in Figure 23 of experiment DFB-01 through a lime particle surface	53
25	Line Scan 4 profile of Si and Ca as marked in Figure 23 of experiment DFB-01 through a quartz particle surface	53
26	EDS mapping of (a) Si and (b) Ca obtained from area 4 in Figure 23 for experiment DFB-01	54
27	Atomic share of ash forming elements given in % during experiment DFB-02	55
28	Timeline for experiment DFB-02	56

29	SEM image including the analysed areas for the area report and the line scan profiles for experiment DFB-02. Visible are various quartz particles and one lime particle (center)	56
30	Line Scan 1 profile of Si and Ca as marked in Figure 29 of experiment DFB-02 through a quartz particle surface	57
31	EDS mapping of (a) Si and (b) Ca obtained from area 4 in Figure 29 of experiment DFB-02	58
32	SEM image of agglomerated particles including the line scan profiles, the mapped area and a particle numeration for references for experiment DFB-02. Visible are various quartz particles and one olivine particle (3)	58
33	Line Scan 1 profile of Mg, Si and Ca as marked in Figure 32 of experiment DFB-02 between two quartz particles	59
34	Line Scan 2 profile of Na, Mg, Si, and Ca as marked in Figure 32 of experiment DFB-02 through a quartz particle surface into the agglomerated phase	59
35	EDS mapping of (a) Si, (b) Ca, (c) Na and (d) Mg obtained from area 1 in Figure 32 of experiment DFB-02	60
36	Atomic share of ash forming elements given in % during experiment DFB-03 . . .	62
37	Timeline for experiment DFB-03	63
38	SEM image including the analysed areas for the area reports and the line scan profiles for experiment DFB-03. Visible are lime and olivine particles.	63
39	Line Scan 5 profile of Mg, Al, Si, Ca as marked in Figure 38 of experiment DFB-03 through a lime particle surface	64
40	Line Scan 1 profile of Mg, Si, Fe, and Ca as marked in Figure 38 of experiment DFB-03 through a olivine particle surface	65
41	EDS mapping of (a) Si, (b) Ca, (c) Fe and (d) Mg obtained from area 6 in Figure 38 of experiment DFB-03	65
42	SEM image including the analysed areas for the area reports and the line scan profiles for experiment DFB-03. Visible are olivine particles.	66
43	Line Scan 4 profile of Mg, Si, and Ca as marked in Figure 42 of experiment DFB-03 through a olivine particle surface	67
44	EDS mapping of (a) Si, (b) Ca, (c) Al and (d) Mg obtained from area 3 in Figure 42 of experiment DFB-03	67
45	Atomic share of ash forming elements given in % during experiment DFB-04 . . .	69
46	Timeline for experiment DFB-04	70
47	SEM image including the analysed areas for the area report and the line scan profiles for experiment DFB-04. Visible are lime particles.	70
48	Line Scan 1 profile of Si and Ca as marked in Figure 47 of experiment DFB-04 through a lime particle surface	71
49	EDS mapping of (a) Ca and (b) Mn obtained from area 4 in Figure 47 of experiment DFB-04	71
50	Atomic share of ash forming elements given in % during experiment DFB-05 (a) without the lime additive and (b) including the lime additive	73
51	Timeline for experiment DFB-05	73
52	SEM image including the analysed areas for the area report and the line scan profiles for experiment DFB-05. Visible are various (mainly coarse) non-agglomerated olivine particles and one lime particle (2).	74
53	Line Scan 2 profile of Si, K, and Ca as marked in Figure 52 of experiment DFB-05 through a lime particle surface	75
54	Line Scan 5 profile of Mg, Si, Fe, and Ca as marked in Figure 52 of experiment DFB-05 through a olivine particle surface	75

55	EDS mapping of (a) Si, (b) Ca, (c) Mg, and (d) K obtained from area 5 in Figure 52	76
56	SEM image including the analysed area for the area report and the line scan profiles for experiment DFB-05. Visible are coarse (non-agglomerated) and fine (agglomerated) olivine particles.	77
57	Line Scan 3 profile of Mg, Si, K, Ca, and Fe as marked in Figure 56 of experiment DFB-05 through a olivine particle surface	78
58	Line Scan 4 profile of Mg, Si, P, K, and Ca as marked in Figure 56 of experiment DFB-05 from a olivine particle into an agglomerated phase	78
59	EDS mapping of (a) Si, (b) Ca, (c) Mg, and (d) K obtained from area 2 in Figure 56 of experiment DFB-05	79
60	Atomic share of ash forming elements given in % during experiment DFB-06 . . .	81
61	Timeline for experiment DFB-06	81
62	SEM image including the analysed areas for the area reports and the line scan profiles for experiment DFB-06. Visible are lime and olivine particles.	81
63	Line Scan 1 profile of Si and Ca as marked in Figure 62 of experiment DFB-06 through a lime particle surface	82
64	Line Scan 4 profile of Mg, Si and Ca as marked in Figure 62 of experiment DFB-06 through a lime/dolomite particle surface	83
65	EDS mapping of (a) Si, (b) Ca, and (c) Mg obtained from area 4 in Figure 62 of experiment DFB-06	84
66	SEM image including the analysed areas for the area reports and the line scan profiles for experiment DFB-06. Visible are olivine particles.	85
67	Line Scan 1 profile of Mg, Si and Ca as marked in Figure 66 of experiment DFB-06 through a olivine particle surface	85
68	EDS mapping of (a) Si, (b) Ca, and (c) Mg obtained from area 4 in Figure 62 of experiment DFB-06	86

List of Tables

1	Typical mean values for the elemental composition of woody biomass adapted from [19]	4
2	Typical mean values for the elemental composition of herbaceous and fruity biomass adapted from [19]	4
3	Maxima, minima and mean values of C, O and H in wt% with the representing biomass [23]	5
4	Maxima, minima and mean values of N and S in wt% with the representing biomass [23]	6
5	Simplified classification of primary ash transformation products referring to their reactivity as acidic or basic compound adapted from [114]	20
6	Ultimate analysis of the feedstocks used for the experiments	30
7	Ash fraction analysis of the used feedstocks regarding the occurring oxides - marks values below the detection limit; * marks unmeasured values	31
8	Amount of total feedstock mass combusted/gasified in every experiment	31
9	Chemical composition of the bed materials used, given in oxides	33
10	Bed material masses and mixtures used for every experiment	33
11	Applied settings for the generation of SEM images	43
12	Key parameters for gasification of experiment DFB-01	51
13	Key parameters for gasification of experiment DFB-02	55
14	Key parameters for gasification of experiment DFB-03	62
15	Key parameters for gasification of experiment DFB-04	69
16	Key parameters for gasification of experiment DFB-05	72
17	Key parameters for gasification of experiment DFB-06	80